Materials Science & Engineering R 144 (2021) 100606

Contents lists available at ScienceDirect

Materials Science & Engineering R

journal homepage: www.elsevier.com/locate/mser

Architected cellular materials: A review on their mechanical properties towards fatigue-tolerant design and fabrication

M. Benedetti [a], A. du Plessis [b,c], R.O. Ritchie [d], M. Dallago [a], S.M.J. Razavi [e], F. Berto [e,*]

[a] Department of Industrial Engineering, DII, University of Trento, Trento, Italy
[b] Research Group 3D Innovation, Stellenbosch University, Stellenbosch, South Africa
[c] Faculty of Engineering, Nelson Mandela University, Port Elizabeth, South Africa
[d] Department of Materials Science & Engineering and Department of Mechanical Engineering, University of California, Berkeley, CA, USA
[e] Department of Mechanical and Industrial Engineering, NTNU – Norwegian University of Science and Technology, Trondheim, Norway

ARTICLE INFO

Keywords:
Architected cellular materials
Cellular structures
Lattice structures
Porous materials
Metamaterials
Additive manufacturing
Fatigue-tolerant

ABSTRACT

Additive manufacturing of industrially-relevant high-performance parts and products is today a reality, especially for metal additive manufacturing technologies. The design complexity that is now possible makes it particularly useful to improve product performance in a variety of applications. Metal additive manufacturing is especially well matured and is being used for production of end-use mission-critical parts. The next level of this development includes the use of intentionally designed porous metals - architected cellular or lattice structures. Cellular structures can be designed or tailored for specific mechanical or other performance characteristics and have numerous advantages due to their large surface area, low mass, regular repeated structure and open interconnected pore spaces. This is considered particularly useful for medical implants and for lightweight automotive and aerospace components, which are the main industry drivers at present. Architected cellular structures behave similar to open cell foams, which have found many other industrial applications to date, such as sandwich panels for impact absorption, radiators for thermal management, filters or catalyst materials, sound insulation, amongst others. The advantage of additively manufactured cellular structures is the precise control of the micro-architecture which becomes possible. The huge potential of these porous architected cellular materials manufactured by additive manufacturing is currently limited by concerns over their structural integrity. This is a valid concern, when considering the complexity of the manufacturing process, and the only recent maturation of metal additive manufacturing technologies. Many potential manufacturing errors can occur, which have so far resulted in a widely disparate set of results in the literature for these types of structures, with especially poor fatigue properties often found. These have improved over the years, matching the maturation and improvement of the metal additive manufacturing processes. As the causes of errors and effects of these on mechanical properties are now better understood, many of the underlying issues can be removed or mitigated. This makes additively manufactured cellular structures a highly valid option for disruptive new and improved industrial products. This review paper discusses the progress to date in the improvement of the fatigue performance of cellular structures manufactured by additive manufacturing, especially metal-based, providing insights and a glimpse to the future for fatigue-tolerant additively manufactured architected cellular materials.

1. Introduction

The necessity for highly reliable (fatigue tolerant), stiff, strong and lightweight materials is an important requirement in many industries, such as for automotive, aerospace, sports and the biomedical sectors [1–4]. In this regard, foams and architected cellular materials can provide exactly these properties. The light-weighting of structural components has many advantages in lower fuel consumption, better mechanical and other performance exactly tuned to the application. The main distinction is that foams have a random (stochastic) structure (see, for instance, Figs. 1A, 1B) generally obtained by a manufacturing process that allows limited control on the cell size and cell-wall thickness, while architected cellular materials (Fig. 1C) have a well determined periodic geometry which can be completely determined by a small

* Corresponding author.
E-mail address: filippo.berto@ntnu.no (F. Berto).

https://doi.org/10.1016/j.mser.2021.100606
Received 3 December 2020; Received in revised form 2 January 2021; Accepted 4 January 2021

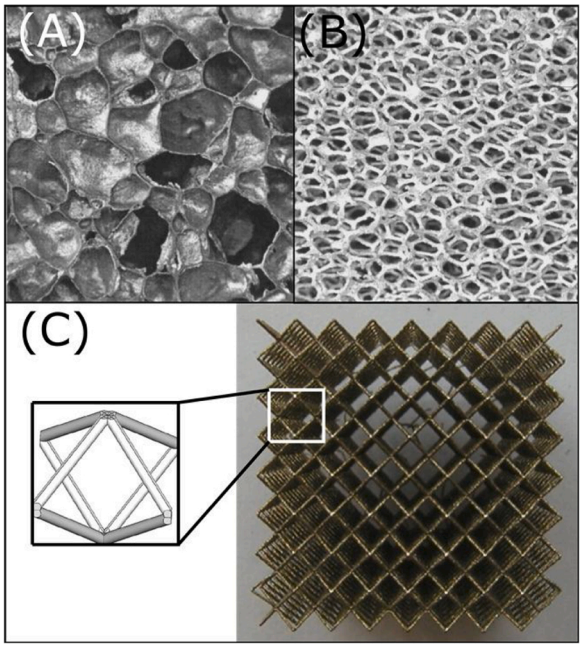

Fig. 1. Examples of cellular materials: (A) closed cell foam [8]. (B) open cell foam [8]. (C) regular cellular material (body cubic centered BCC unit cell) [9].

number of design parameters. In principle, a more controllable structure leads to more controllable mechanical properties and this makes architected cellular materials very versatile, as their properties can be varied over a wide range by simply modifying the geometrical design parameters [5–7]. Both stochastic foams and architected cellular structures can be referred to as "cellular"; hence, in the literature, the two terms are sometimes used interchangeably. Architected cellular materials are also often referred to as lattice structures (or lattices), especially when they are comprised of struts and nodes. Other forms of architected cellular materials are minimal surfaces, comprising of curved sheets or connected curved structures without clear nodes. The micro-architecture of cellular materials provides the designer with an additional level of control, besides the material of the struts (often called *base material* which can be metallic, ceramic, polymeric or composites) and the shape of the macroscopic part (for instance, a femoral stem). Cellular materials behave as structures on the small scale and as homogeneous materials on the macroscopic scale. In other words, there is a length-scale separation between the lattice scale and the macroscopic scale. Consequently, their behaviour on the macroscopic scale can be described in terms of effective homogeneous properties (with an effective elastic modulus, for instance) that depend on the base material and the unit cell design parameters. By only tailoring the geometry of the unit cell, while keeping constant the base material, it is possible to range between far extremes of the material properties space, such as stiffness, strength, density, permeability and thermal conductivity, to name a few. This ability to tune the effective material properties prompted the terminology "meta-materials" for all architected cellular materials. Cells can be open or closed, depending on whether both edges and faces are solid (Fig. 1A), or only the cell edges are solid (Fig. 1B). Open-celled cellular materials are permeable to the flow of fluids, which is normally a necessary requirement in biomedical applications, and thus constitute the totality of the lattice materials found in load bearing biomedical implants. On the other hand, closed cell cellular materials are more common where insulating (thermal, acoustic) properties are required.

Architected cellular structures have a particularly promising potential in the biomedical field because, compared to traditional fully dense metallic implants, orthopedic prostheses with a porous structure can show reduced stress shielding and improved osseointegration [10,11]. An example is shown in Fig. 2A of knee and hip implants additively manufactured with Ti-6Al-4 V, incorporating architected cellular structures. Fig. 2B depicts a lightweight bracket for an experimental vehicle also manufactured by the same process and material; this is described in more detail in [12]. Another application of lightweight structures includes spaceflight hardware; numerous topology optimized brackets have been successfully demonstrated and some examples are described in [13,14], although these do not yet include cellular structures. Cellular structures allow extreme light-weighting, in addition to higher local tailorability to the required properties, by varying the local density and other parameters. Light-weighting design principles, including cellular design, were reviewed recently in [15–18]. In principle, additional functions can be incorporated and multi-functionality brings new benefits yet to be revealed, as discussed in [12]. The benefits of high-energy absorption make cellular structures suitable as protective materials and for providing an additional protective role to their structural properties. There is currently a large drive towards developing protective headgear in sports, using lattice structure designs for their impact-absorption ability; an example is found in [19]. Other industrially relevant applications of cellular structures include heat exchangers and thermal management, due to the high surface area and high permeability properties of the open-porous structure [20,21]; related to this are applications in liquid-fuel rocket engines [22,23]. Such industrial applications as these require effective material properties that are extremely reliable, before the potential of these new designs can be unleashed at a larger scale.

The intricate geometric characteristics and associated manufacturing challenges of cellular structures has relegated them, until recently, to mere academic curiosity. Only the current impetuous development and maturing of additive manufacturing (AM) technologies has made their production with good quality possible in the last few years. The layer-wise fabrication process in additive manufacturing allows customized products of virtually any geometry to be manufactured [24–26]. Cellular materials have been manufactured in all additive manufacturing process categories and in a wide variety of materials including metals, polymers, ceramics and polymer-composite materials [27]. Since in fatigue-relevant applications, the material class of choice is metals, the present article will mainly review metallic cellular materials. Nevertheless, much of the present discussion is relevant to other material classes as well. According to the recent review presented in [27], 90 % of metallic cellular materials have been fabricated using a powder bed fusion (PBF) process. In essence, the powder is spread to a controlled thickness over the build platform (or over the previously built layers). Powder is melted and solidified using a fast-moving laser or electron beam. After powder consolidation, the build platform is lowered, and a new layer is spread. The process repeats until the entire model is created. When a laser is used, the process is called Laser Powder Bed Fusion (L-PBF), and in the case of an electron beam it is called Electron Beam Powder Bed Fusion (EB-PBF). In all cases, the heat input is intense and highly localized so that the final metallic components generally show unique properties including high surface roughness, porosity, heterogeneous microstructure, and residual stresses [28–30].

The above-mentioned characteristics of metallic additively manufactured components negatively affect the mechanical properties, especially the fatigue strength [31]. This is a critical aspect in all structures exposed to time-varying loads. A meaningful example in this regard are load-bearing orthopedic implants, particularly in view of the periodic nature of human gait for hip implants [32]. Nevertheless, in comparison to the wide number of papers published on the static mechanical behaviour of architected cellular materials, few studies on their fatigue resistance have been published to date [33]. Metallic materials, in general, have high notch sensitivity, so the fatigue resistance is strongly influenced by defects that act as stress raisers. Fatigue is in fact caused by the accumulation of damage at regions, *e.g.*, notches and imperfections, which act as local stress concentrations; accordingly, to be able to accurately predict the fatigue resistance of a structure, the

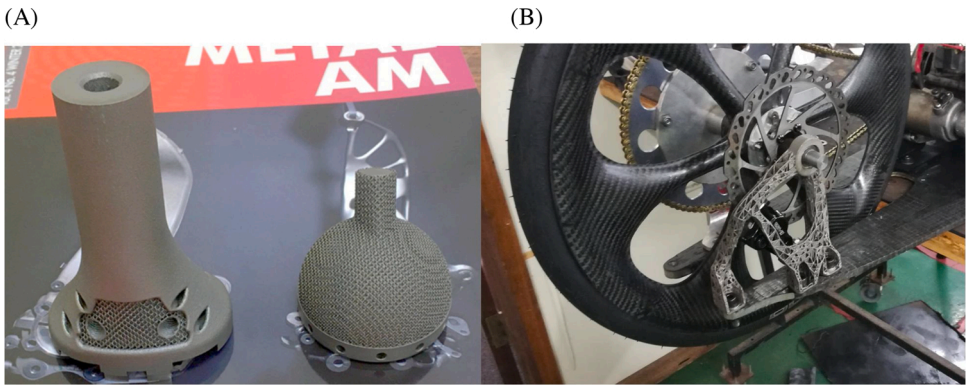

Fig. 2. Examples of architected cellular (lattice) structures in (A) implants, and (B) a lightweight bracket for an experimental vehicle. Examples courtesy of (A) LRS implants Pty Ltd & Executive Engineering Pty Ltd and (B) Nelson Mandela University.

focus must be shifted to the local details in geometry [34]. Additively manufactured architected cellular materials (or lattice structures) are particularly prone to fatigue damage, mainly for the following four reasons:

- the architecture of cellular materials is an intrinsic factor of structural weakening since a full geometry is replaced by a porous architecture consisting of struts joined at particular points termed nodes, reducing the load bearing area and increasing stress concentrations;
- as-built AM products are often characterized by poor geometrical accuracy and complex surface morphology, which leads to differences between the as-built and designed parts [35,36];
- there are technological limitations that pose lower limits on the size of the minimum printable geometrical details, such as truss thickness and fillet radii [37]; for fine feature sizes, the inevitable discrepancy between desired and actual geometry frustrates any attempt to attenuate local stress concentration through classical mechanical design measures; such as a gradual transition in strut sizes, smoothing of edges between struts, or stress relief grooves.
- The strut inclination angle relative to the printing direction is a factor that must also be considered [38,39]. Inclined struts are supported by loose powder which has lower thermal conductivity than the solid and thus a higher fraction of the powder is partially or completely melted compared to a vertical strut; as such, different thermal conditions may create unique microstructures and highly irregular surface morphology.
- Fatigue, more than any other mechanical property, is strongly affected by the manufacturing process; indeed, the critical importance of defects has been highlighted in many publications [31,40,41].

As a result, despite undeniable advancement in the design and fabrication of lattice structures, there is still a widespread concern about their structural integrity, especially under fatigue loading. Industry is still mistrusting of their widespread use in critically loaded mechanical components and is waiting for solid answers and guidance in this regard. The main issue in the study of the fatigue behaviour of architected cellular (lattice) materials is that no standards are available for the mechanical testing; the only available standard is the ISO 13,314, which prescribes a procedure for the monotonic compression testing of metallic porous structures that exhibit a ductile plateau behaviour. As a consequence, no guidelines are available for monotonic tests of lattice materials that do not display necessarily this specific behaviour and, in addition, no guidelines are available at all yet for their fatigue testing.

For this reason, we propose the present article as a review of the most recent and relevant contributions to understanding the fundamental concepts underpinning the fatigue behaviour of architected cellular (lattice) structures fabricated via metal additive manufacturing. For this purpose, fatigue design of lattice architectures, including recent advances in artificial intelligence-based design, fatigue testing methodologies, experimental assessment of fatigue related issues, such as defects, surface morphology and geometrical inaccuracies, will be analysed. Careful understanding of the state-of-the-art knowledge will permit us to suggest guidelines and methods to increase the success and improve the performance and reliability. We will also describe what remains to be improved and where research is still urgently needed. This review combines engineering and fundamental science from different fields of endeavour relevant to the design, mechanistic understanding and fabrication of architected cellular materials of the future.

The review is based on an extensive literature review of articles indexed in Scopus and Web of Science databases. As shown in Figure 3a, 65 papers specifically dealing with fatigue behaviour of cellular (lattice) materials were chosen and analysed. They span over the last ten years, with the majority of them concentrated in the last 4 years. Additional papers, bringing the overall amount of citations up to 291, are examined in order to widen the discussion to all the topics relevant to the article scope. The fatigue behaviour of 24 cell types (Fig. 3b) was investigated in the analysed literature; nevertheless, the first three cover about 50 % of all the reported investigations. To the best of our knowledge, the reviewed lattice materials were tested only under uniaxial fatigue, in 80 % of the papers by means of compression-compression fatigue tests (Fig. 3c). While several metallic materials were explored, the bulk of them (60 %) focused on the biomedical grade Ti-6Al-4 V, thus suggesting that the current interest in fatigue-related applications of cellular materials primarily stems from the biomedical sector.

The present review paper is organized in the following form: Section 2 provides the reader with the background on the most important AM techniques, on the architecture and static mechanical behaviour of architected cellular (lattice) materials as well as on the general aspects of fatigue behaviour in metallic materials. Section 3 examines the results of fatigue experiments undertaken on architected cellular materials, emphasizing the main factors influencing their fatigue response. Section 4 illustrates the experimental techniques that can be used to assess the fatigue-related characteristics of cellular materials. This will enable the identification in Section 5 of all the design and technological measures suitable for improving fatigue resistance. Section 6 is aimed at translating this state-of-art-knowledge into guidelines for a robust fatigue design and verification of architected cellular (lattice) materials. An insight into the design and architecture of fatigue-resistant cellular materials of the future is provided in Section 7, prior to final concluding remarks in Section 8.

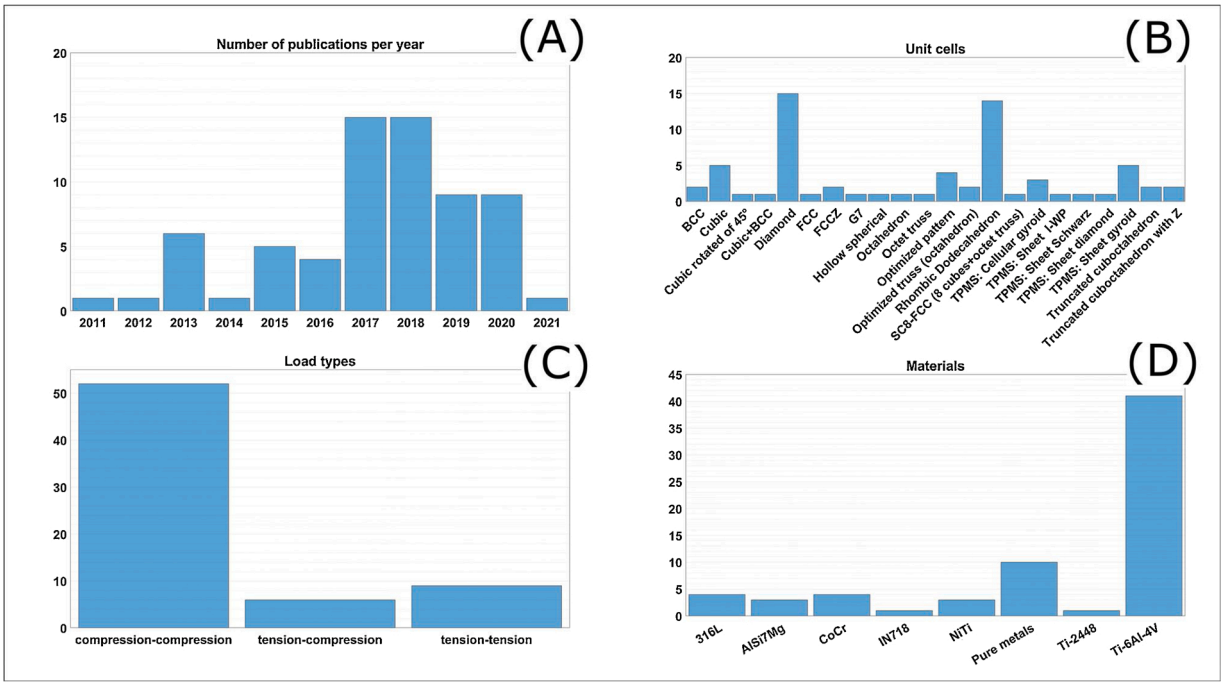

Fig. 3. Main features of the articles reviewed in this work. (A) number of publications pertinent to fatigue of cellular materials per year. (B) unit cell architectures, (C) fatigue load configuration and (D) materials analysed in the reviewed literature.

2. Background

2.1. Powder bed fusion additive manufacturing techniques

A recent and complete literature review dealing with additive manufacturing techniques has been published in *Progress in Material Science* [26]. In this paper, a clear and critical review of additive manufacturing of metallic components has been carried out underlining the advantages and main drawbacks of all the available processes.

According to ASTM Standard F2792 [42], AM processes can be classified into the two main categories of Directed Energy Deposition (DED) and Powder Bed Fusion (PBF). DED includes all the AM processes where focused energy from the heat source generates a melt pool into which feedstock in form of wire or powder is deposited (Fig. 4). DED processes (Fig. 4A) are also used for the production of large rough blank morphologies, but with extensive machining required to manufacture the final desirable geometry of the part.

In PBF processes (Fig. 4B), a layer-wise material feed in the form of a powder bed is used. Considering the complex geometry of lattice structures and the supporting role of the powder bed during the fabrication of these structures, PBF techniques have received most attention from researchers and engineering working in this field. Depending on the primary heat source, PBF technique can be divided into two main categories of laser PBF (L-PBF) and electron beam PBF (EB-PBF). A critical understanding of the capabilities and complications of these two PBF processes is needed for the selection of the right technique for a target application.

L-PBF [43] process begins with slicing the input computer-aided design (CAD) model in form of solid or surface, defining the scanning pattern and establishing a build-file based on a material dependent set of process parameters (Fig. 4C). A layer-wise fabrication of the part then takes place by spreading thin layers of powder with a controlled thickness. Subsequently, the powder is fused according to the slice geometry pass-by-pass and layer-upon-layer within an inert chamber, with the z-axis incrementally decreased after each produced layer.

EB-PBF uses a similar sequence of actions to L-PBF but with an electron beam heat. The fabrication process, which takes place within a vacuum chamber, includes a two-step sequence for each layer. First each layer of powder is sintered to prevent electro-static charging and repulsion of the powder particles; then the region defined by the slice geometry is fused using an additional pass. Due to the lightly sintered alloy powder on the bed, a faster scanning speed of the beam can usually be employed in the EB-PBF process. Comparative characteristics of two PBF machines based on laser and electron beam heat source are summarized in Table 1.

In both PBF processes, various scanning strategies can be implemented to scan each layer of the sliced geometry. Unidirectional, bidirectional, spiral, zigzag and cross-wise are among the most common scanning patterns in these processes; in all cases adjacent tracks are overlapped with a hatch spacing value less than the track width to ensure full melting (See Fig. 4C). The interior of a part is usually scanned first (termed the hatch scanning), followed by one or more contour scan tracks (termed contour scanning)(See Fig. 4D). Contour tracks follow the external geometry of the part and improve the surface quality, and must also overlap the hatch pattern. Subsequent layers usually include a rotation of the hatch directional strategy, for example by rotation of 67°. In addition, these hatch patterns can be implemented in islands or stripes – larger regions which are scanned separately and randomly to ensure homogenous thermal input and to minimize residual stress.

2.2. Architecture and static mechanical properties of lattice materials

According to Gibson and Ashby's fundamental work [47], only a few unit cells can be packed together in a regular and undistorted periodic pattern of identical cells to fill space. They are illustrated in Fig. 5, specifically the triangular, rhombic and hexagonal prisms, the rhombic dodecahedron and the tetrakaidecahedron. In addition, if distorted, the tetrahedron, the icosahedron and the pentagonal dodecahedron can also fill space. Accordingly, lattice cellular materials are built starting from these elementary unit cells.

In strut-based lattices, nodes located at the vertices or edges of the unit cells (and sometimes also in the interior of the cell) are connected by slender straight members usually called struts (or beams). The most important results from the present literature survey are illustrated in the

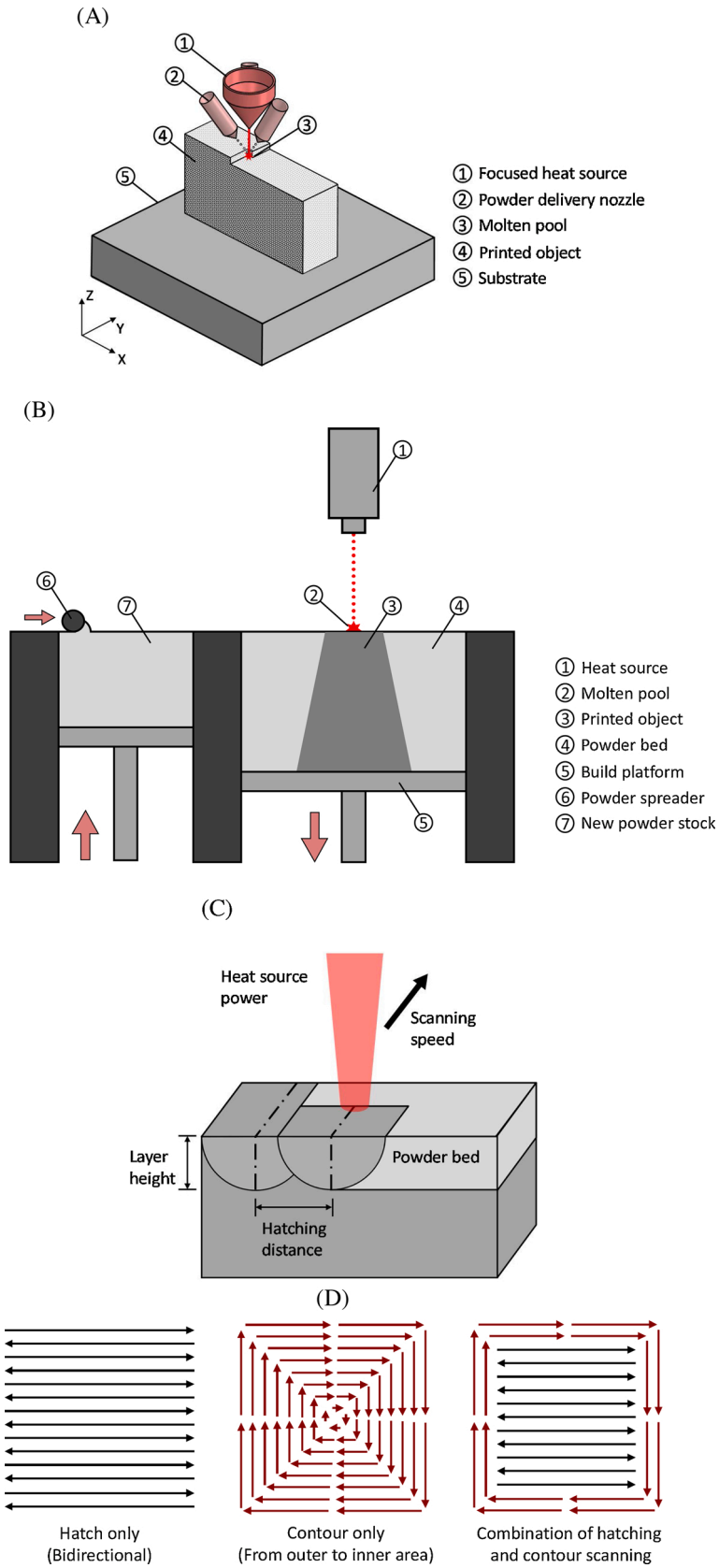

Fig. 4. Schematic illustration of (A) DED [44] and (B) PBF processes; (C) process parameters in PBF [45]; (D) various scanning strategies.

Table 1
A comparison between two laser and electron beam based PBF machines [46].

Parameter	L-PBF (Realizer SLM50)	EB-PBF (Arcam EBM S12)
Environment	Argon	Vacuum 10^{-4} - 10^{-5} (mbar)
Preheating (°C)	200 (building table resistive heating)	700 (powder bed heating by defocused electron beam)
Maximum beam power (W)	120	3500
Laser/electron beam spot (μm)	30–250	200–1000
Average powder layer thickness (μm)	20–100	50–200
Beam scan speed (m/s)	0.3–1.0	>1000

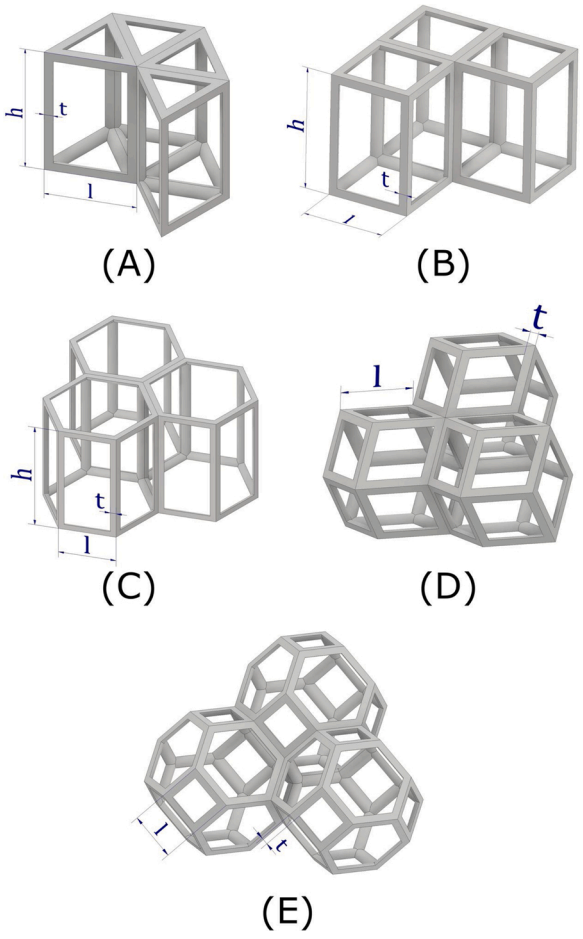

Fig. 5. Space-filling unit cells that can be packed without distortion. (A) Triangular, (B) rhombic and (C) hexagonal prism. (D) rhombic dodecahedron. (E) tetrakaidecahedron. *l* and *h* indicate characteristic unit cell dimensions, *t* is the thickness of the strut connecting nodes co-located on the edges of the unit cell. Adapted from [47].

first three rows of Fig. 6. They are mainly based on the elementary cubic cell, wherein the number of nodes and struts is modulated to confer the desired density and mechanical properties.

A very useful classification criterion, which has important consequences on the mechanical behaviour of the strut-based lattices, distinguishes between *bending-* and *stretching-* dominated structures by analyzing the nodal connectivity. If we imagine replacing the rigid (well-connected) junctions between the struts with pins, depending on the nodal connectivity of the lattice, when compressed, the structure can collapse due to the rotation of the struts about the joints (*i.e.*, it becomes a mechanism) or not (*i.e.*, it becomes simply a truss frame) (compare Figs. 7A and 7B, C). The former structure is defined as bending-dominated, because the struts of the frame with connected joints *bend* when loaded externally (the joint resists rotation), while the latter structure is defined as stretching-dominated because the struts are loaded mainly axially even with connected joints, with some struts experiencing tensile forces. An example of the two types of unit cells is shown in Fig. 7D-F. This classification is expressed mathematically by the Maxwell stability criterion, which is based on the sign of the coefficient *M*, which is negative for bending-dominated and positive for stretched dominated structures, respectively [48]. For 2D lattices, $M = b - 2j + 3$, where b is the number of struts and j is the number of nodes (Fig. 6a-c). For 3D lattices, $M = b - 3j + 6$, as shown in Fig. 7D-F. Stretching-dominated structures are structurally more efficient than bending-dominated structures because struts are loaded almost exclusively in tension or compression [5,6,48].

Other cell architectures that are gaining interest as cellular materials are based on triply periodic minimal surfaces (TPMS), some of them sketched in the last two rows of Fig. 6. These materials have many topological properties that have been proved to be beneficial for manufacturability due to their continuous curved surface geometries [39,49,50]. The first reference to a TPMS was made in the 19th Century by Schwarz, who introduced the Primitive and Diamond surfaces [51]. TPMS are surfaces created mathematically such that they have no self-intersecting or enfolded surfaces. “Triply periodic” means that the structure can be packed together in a periodic 3D pattern and “minimal surface” means that it locally minimizes surface area for a given boundary such that the mean surface curvature at each point is zero [51]. The complex and intertwined minimal surface divides the volume into two or more entangled convoluted domains, such that each domain is a single connected and infinite component. TPMS can be described mathematically using the level-set approximation technique based on harmonic functions of the spatial cartesian coordinates and the desired level of density [52]. There are several TPMS shapes available; the most investigated ones are illustrated in Fig. 6. Two different strategies are adopted to create TPMS cellular structures from the mathematical formulation [53]. In the first one, the TPMS is thickened to create a solid structure known as the “sheet TPMS”; in the second approach, the volume separated by the TPMS is filled to create a solid structure known as the “skeletal" or "cellular" TPMS. The lack of nodes and points of curvature-discontinuity ensured by these architectures is expected to reduce the stress concentration and ultimately to enhance the fatigue strength [50].

The single most important parameter of cellular materials, that any property can be related to, is the relative density $\overline{\rho}$ [47], defined as the ratio of the density of the cellular material ρ to the density of the base (solid) material ρ_0:

$$\overline{\rho} = \frac{\rho}{\rho_0} \tag{1}$$

The relative density essentially defines how much solid material is present in the overall volume occupied by the cellular material. The complement to unity of the relative density is porosity, calculated as $p = 1 - \overline{\rho}$. This parameter can be calculated with geometrical considerations: models to calculate the relative density of several different types of cellular materials as a function of the strut length and diameter are discussed in [47]. Despite being a powerful concept, the relative density alone is not sufficient to characterize the morphology of a cellular material. As an example, bending- and stretching-dominated structures will have different mechanical properties and failure mechanisms even with the same relative density; this will be discussed in the following sections.

The mechanical behaviour of cellular materials is illustrated by the compressive stress-strain curves in Fig. 8 along with photographs in [54]. The curves can be divided into three parts as in the figure: a linear elastic regime (1) until the struts yield due to bending or stretching, a plateau regime (2) during which the cells start to progressively collapse because of buckling, brittle crushing or yielding depending on the base

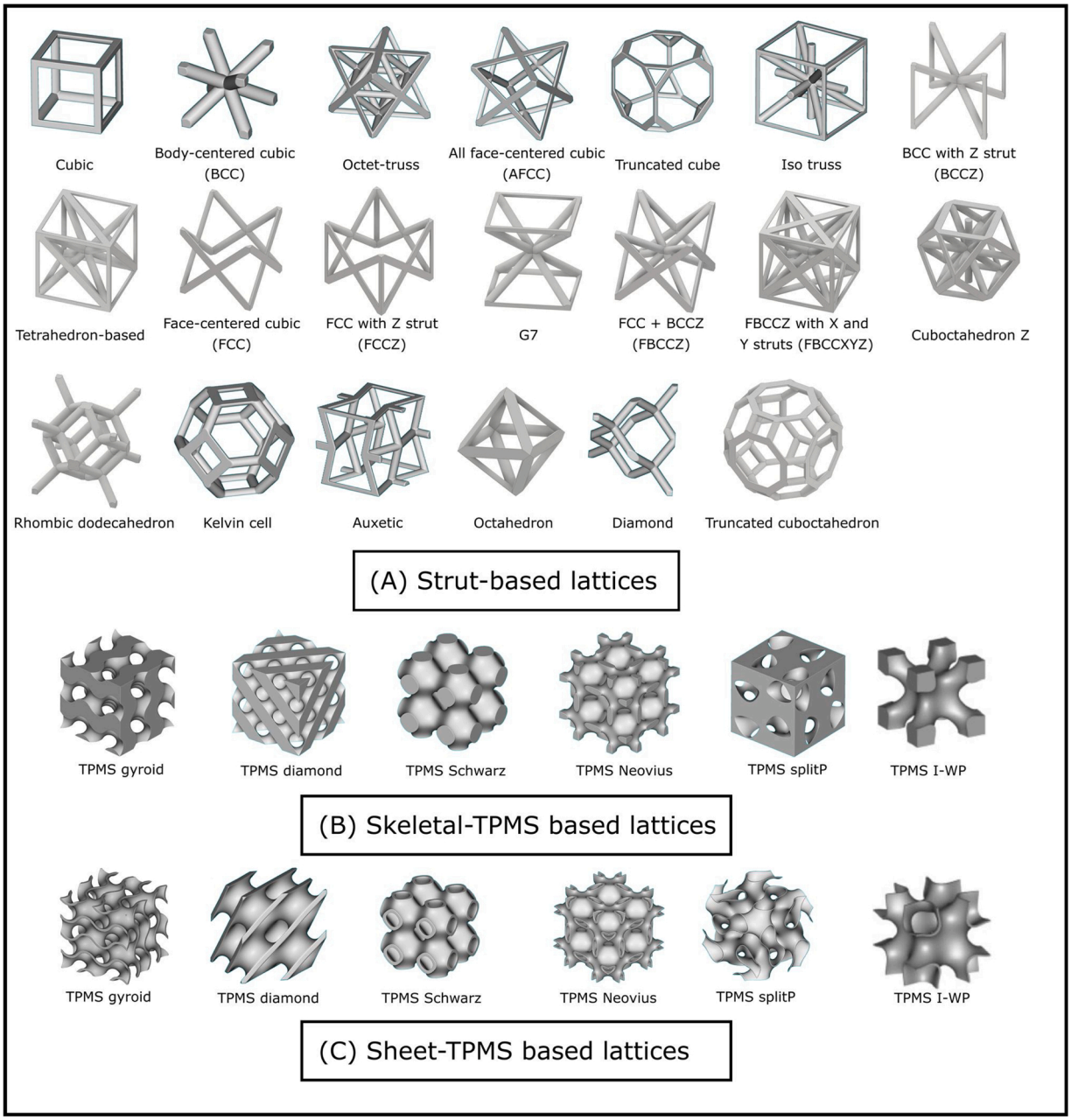

Fig. 6. Various architectures of lattice structures (A) Strut-based lattice cells are shown in the first three rows. (B) Skeletal- and (C) sheet-triply periodic minimal surfaces (TPMS).

material and the morphology, and finally a densification phase (3) that corresponds to the collapse of the cells one against the other (the struts reach contact). The stress-strain curves of the stretching-dominated lattices are generally characterized by higher initial stiffness and yield strength (prior to the first yield) than a bending-dominated lattice of the same relative density. Moreover, post-yield softening is also observed, due to the sudden failure by buckling or brittle crush of a layer of cells, with the subsequent plateau consisting of peaks and valleys that indicate the progressive failure of the layers. Stretching-dominated structures are therefore more structurally efficient but are prone to sudden failures and are not effective at dissipating deformation energy. On the other hand, bending-dominated structures are more compliant, have a more progressive transition to the stress plateau due to the bending of the struts, and have a relatively flat plateau [6,55]. In their numerical study, Kadkhodapur et al. [56] correlated the stress-strain curve with the failure mechanism for bending- and stretching-dominated lattices. They observed that stretching-dominated lattices tend to fail layer-by-layer for their investigated architectures (the failure of the first layer is indicated by post-yield softening), while bending-dominated lattices fail in shear bands, matched by a smaller fluctuations in the stress-strain curve. Several experimental studies have confirmed these results, as for example in [57,58]. Elastic-plastic materials, after yielding, can display a short plateau until all struts are yielded, followed by densification. Tensile stress-strain curves are the same as compressive curves in the elastic region, but after yielding the struts tend to progressively align along the loading direction, without any buckling, until failure [59]. In tension, cellular materials fail by ductile or brittle fracture, depending on the plastic resources of the base material [47].

The high number of cells in a lattice structure often makes it practically impossible to model the entire cellular component in full detail, even by using advanced finite element software combined with powerful processing hardware. Consequently, over the last decades, several

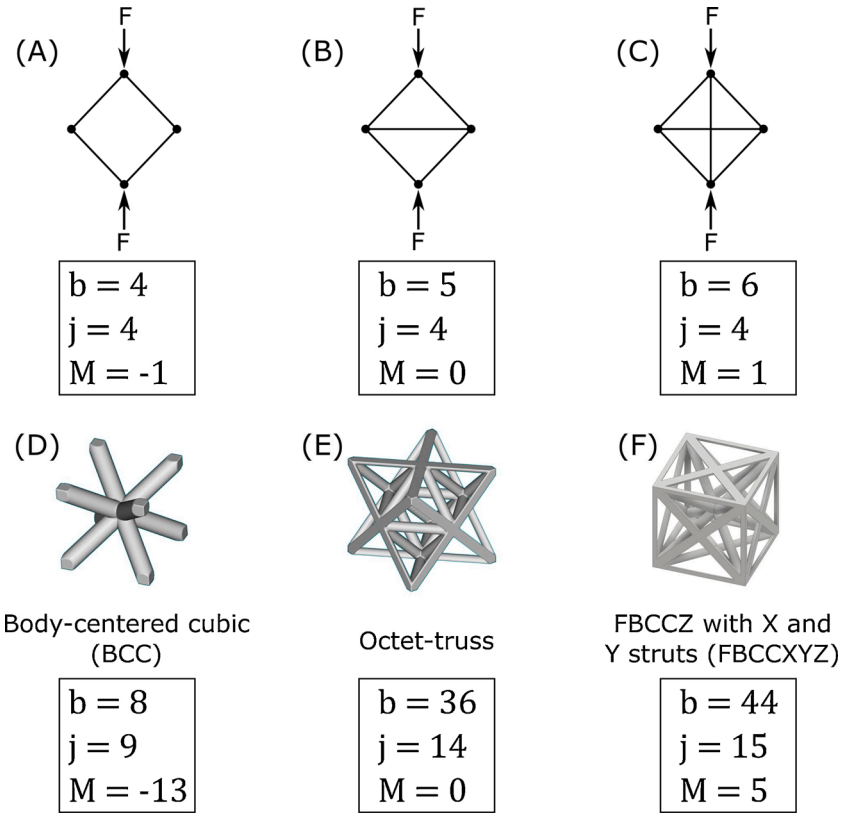

Fig. 7. (A) A bending-dominated structure becomes a mechanism if the joints are substituted by pins;(B) (C) a stretching-dominated structure stays a structure if the joints are substituted by pins. Examples of (D) bending dominated and (E) (F) stretching-dominated unit cells. *M* is the Maxwell number, *b* is the number of struts and *j* the number of nodes. FBCCZ is a unit cell obtained by combination of a face-centered cubic (FCC) and a body-centered cubic (BCC) with struts along X, Y and Z directions (see Fig. 6 for further details).

theoretical and numerical approaches have been specifically developed to model the mechanical properties of materials with a repetitive nature, which will be now very briefly reviewed. The aim of these approaches is to determine the effective properties of the lattice as a function of properties of the base material and the morphology of the cells. The effective properties can then be used as the properties of any regular material in the design process. A fundamental concept in the mechanical modelling of cellular materials is the Representative Volume Element (RVE), which is a fraction of the volume of the lattice that is representative of the properties of the entire structure. In other words, this element should be small enough to reduce the complexity of the problem, but big enough to approximate with the requested accuracy the behaviour of the lattice. In the case of regular periodic structures, the most logical choice for the RVE is the unit cell of the lattice. On the other hand, identifying the correct size of the RVE is not immediate in the case of cellular materials that are not regular periodic, such as, for instance, fully random foams, lattices affected by some degree of irregularity, or lattices with fabrication defects. In such cases, the simplest approach is to progressively increase the size of the RVE and choose the size at which the properties converge to a constant value [60–62].

Closed-form models for the effective elastic constants and the yield strength of 2D and 3D regular lattices made of simple unit cells were first devised by Gibson et al. [47,63], assuming the cell struts or walls behave like Euler-Bernoulli beams. The elastic constants were calculated from the stresses and strains produced by applying uniform loads to the unit cell. Moreover, they observed that it is possible to correlate the elastic modulus (sometimes regarded as quasi-elastic gradient) and yield strength of the lattice with its relative density $\bar{\rho}$ in the form of power laws, *viz*:

$$\frac{E}{E_0} = C_1\left(\frac{\rho}{\rho_0}\right)^n = C_1\bar{\rho}^n \tag{2a}$$

$$\frac{\sigma_y}{\sigma_{y0}} = C_2\left(\frac{\rho}{\rho_0}\right)^m = C_2\bar{\rho}^m \tag{2b}$$

in which σ_{y0} and E_0 are yield strength and elastic modulus of the base material and C_i ($i = 1,2$), m, and n are constants that depend on the type of unit cell and can be determined theoretically (closed form solution) or fitted to experimental data [38,64,65]. In particular, n (m) is equal to 1 (1) in an ideal stretch dominated structure and to 2 (3/2) in an ideal bending dominated structure. Figs. 9A, B display a collection of experimental data published in the literature [38,49,56,57,66–87] for relative quasi-elastic gradient and relative yield strength, respectively, for several cell architectures, all of which are sketched in Fig. 6.

It can be noted that the lattice materials display a decreasing trend in both elastic modulus and strength with decreasing relative density; this trend, apart from the large scatter displayed by the experimental data, is in better agreement with the Gibson-Ashby predictions for bending-dominated behaviour, even though some of the cell architectures are nominally categorized as stretched-dominated (*e.g.*, FCCZ or octet). This experimental evidence can be explained in terms of geometric inaccuracies affecting real manufactured cellular lattice material that can introduce spurious bending effects due to the misalignment of the struts axis with respect to the loading direction, among other possible reasons described later in this paper. This comparative analysis shows that closed-form equations based on classical beam theory have some limitations: (i) assuming the cell walls behave as beams provides good results only if they are sufficiently slender, *i.e.*, these models progressively lose accuracy as the relative density increases (generally it should be less than 0.3 [88]); (ii) the derivation of closed-form equations becomes impractical for very complex lattices; (iii) these models often assume a uniform section of the beam, which is not generally the case in real cellular lattices, although it is possible to derive closed-form equations also for cell walls of variable cross-section, provided the variation can be described by simple functions [89,90]; (iv) classical beam theory cannot accurately capture the stress-strain state at stress concentrators (such as

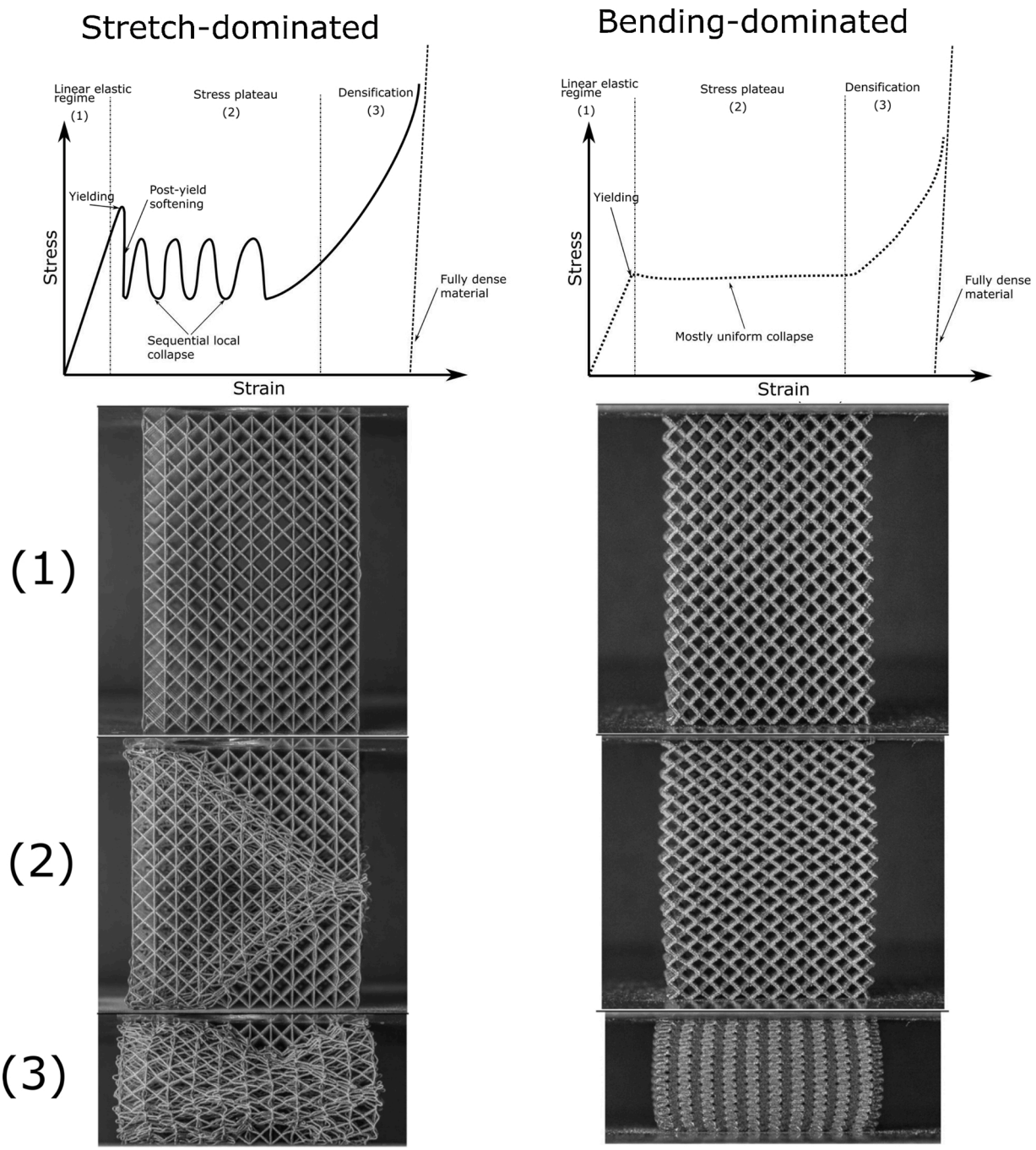

Fig. 8. Typical compressive strain-stress curves for bending- and stretching-dominated cellular materials with same relative density (curves adapted from [6]). (1) Linear-elastic regime. (2) Post-yield stress plateau. (3) Densification. Photographs were taken in [54] at the corresponding deformation regime on bending- (left) and stretching- (right) dominated lattice structures.

at cell nodes). More advanced numerical modelling techniques, however, such as numerical homogenization methods, are able to overcome these limitations [91]. Such homogenization techniques replace the cellular structure with the appropriate RVE; this can also include any possible irregularity of the lattice and does not have any limitation on the relative density value. The only two assumptions are that there exists a length-scale separation between the microstructure and the domain of interest and that there is a spatial periodicity in the lattice (*i.e.*, the field variables depend on multiple spatial scales and are periodic on the small scale and smooth on the macroscopic scale) [60,61]. Nevertheless, the homogenization method has some limitations, which are due to the assumptions that it is based on. Several situations arise in which, for instance, the length-scale separation is not verified due to the small number of unit cells that make up the domain considered, or the accurate stresses in some specific location need be known, or the effect of defects on the local stress state is investigated. The finite element (FE) method, on the other hand, does not have these limitations and it is thus a valid alternative in such situations. Indeed, potentially, with the FE method it is possible to study the mechanical behaviour of the most complex cellular materials including the finest details without the necessity of any simplifying assumption, the only limitation being the computational power of the computer. FE models of cellular lattices can be divided into two classes: models based on beam elements and models based on continuum elements [91]. The former are computationally

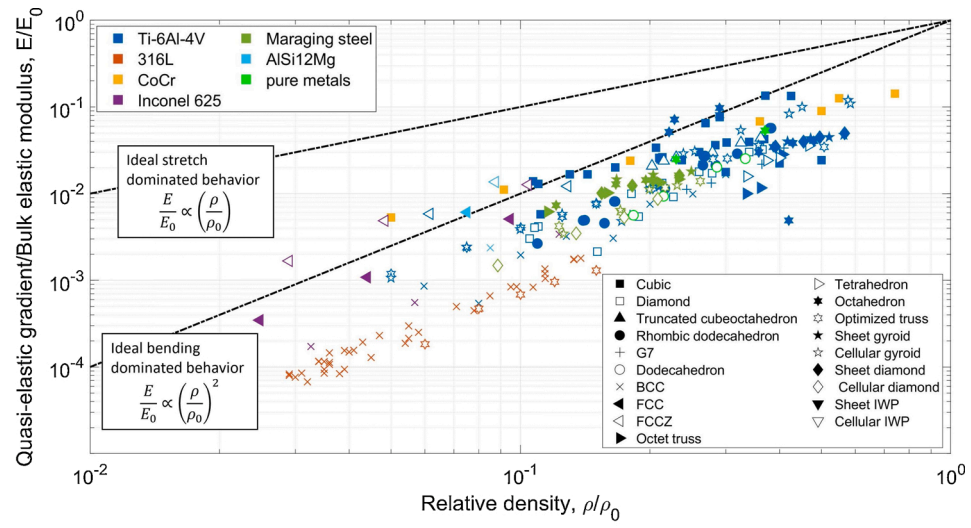

(A)

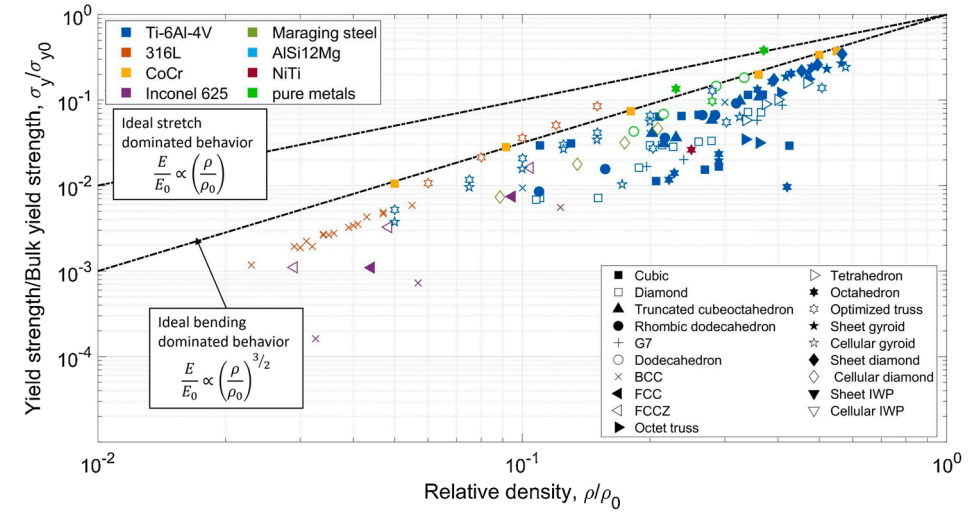

(B)

Fig. 9. Relative quasi static elastic gradient (A) and relative yield strength (B) as a function of relative density for cellular lattice materials investigated in the literature [38,49,56,57,66–87] with various unit cell architecture.

faster and are useful to calculate the effective properties of the lattice and can also correctly capture failure mechanisms [9,92]. Beam elements are quite versatile and can be used also to take into account material heterogeneities, irregularities in the strut cell wall thickness [35,93,94], and the effect of fillets at strut joints on the elastic properties [95]. Alkhader and Vural [96] used beam elements to show that the loss of periodicity in the structure of a stretching-dominated cell results into a shift towards a bending-dominated mechanical behaviour and thus a decrease in stiffness. Also, the study of the fatigue behaviour of cellular materials gained considerably from the use of beam elements; in [97] the effect of cell geometry and relative density on the fatigue behaviour was investigated, while in [98] a computational approach to predict the fatigue behaviour was proposed, including also manufacturing irregularities. On the downside, beam models are accurate only for low relative densities (slender cell walls) and they do not provide the local stress-strain state. Continuum models provide the highest accuracy and the most faithful reproduction of any morphological feature at the expense of long computation times [91]. Several examples of complex analyses carried out using 2D and 3D continuum elements can be found in the literature. In the recent literature, the failure mechanisms of stretching- and bending-dominated lattices were simulated using 3D continuum models and successfully compared with experimental tests in [56], while Cuadrado et al. [85] also investigated the effect of load orientation. Multi-material analyses can also be completed, for instance to study the effect of tissue ingrowth in L-PBF Ti6Al4V biomedical scaffolds [87]. The FE method and accurate geometrical measurement techniques, such as X-ray Computed Tomography (CT), form a very powerful set of tools to interpret experimental results because, for the first time, it becomes possible to simulate the mechanical behaviour of as-fabricated lattices [99,100]. This last topic will be further analysed in the following sections.

2.3. Fatigue of bulk metallic materials

Since the present review paper is intended for a broad, also non-specialistic, readership, the third part of this background section is aimed at introducing the reader to the fundamental aspects of metal fatigue. The peculiar characteristic of this damage mechanism is that structural components exposed to time-varying loads are prone to failure at stress levels well below a given material's ultimate strength. This repeated loading of the structure can lead to microscopic damage in the materials. If the loads are above a certain threshold, the accumulated microscopic damage in the material can result in nucleation and propagation of cracks or other macroscopic damage that leads to fatigue

failure of the component. Engineering metals are commonly composed of an aggregate of small crystal grains. These small crystal grains show a local anisotropic behaviour due to the presence of crystal planes and also small voids and particles of a different chemical composition than the bulk material. Due to the nonuniformity of the microstructure, the applied stress to the component is distributed in a non-uniform manner at the microstructural size scale [101].

Dealing with ductile engineering metals, crystal grains with an unfavourable orientation relative to the direction of the applied stress develop intense deformation due to shear motion between crystal planes. These regions with severe shear deformation are called slip bands. The continuation of the cyclic loading results in an increase in the number of slip bands and eventually some slip bands develop into cracks within the crystal grains and then propagate through the neighbouring grains, producing a large crack in the component that can lead to the final failure. The number of loading cycles associated with creation of a crack in the material is called fatigue initiation life, while the remaining number of cycles until final failure is known as fatigue crack growth life.

On the other hand, engineering metals with limited ductility, such as high strength metals, tend to show a more localized damage evolution in the vicinity of the defects within the material [101]. These initial defects can be voids, lack of fusion, inclusions, slip bands, weak grain boundaries, and surface defects such as scratches or surface roughness. This crack can grow from the mentioned defects and propagate through the section of the component in a plane perpendicular to the loading direction. Therefore, the fatigue damage process in materials with limited ductility is characterized by crack initiation and propagation from a few defects, while in ductile materials a more widespread damage intensification is the mechanism of fatigue failure.

Generally, depending on the applied stress level, the fatigue life of the component varies and can be categorized in one of two main regimes of low-cycle fatigue (LCF) and high-cycle fatigue (HCF), which respectively represent fatigue in the presence of, and in the absence of, plastic deformation. The transition between LCF and HCF can be determined by the stress levels indicating the level of plastic deformation in the material. This transition life depends on the ductility of the material and cannot be set to a constant number. On the one hand, the fatigue life at high stress levels (LCF) is shorter and is commonly characterized by repeated plastic deformation in each cycle. In this case, fatigue failure is mainly governed by crack propagation rather than crack initiation. On the other hand, the lower stress levels in HCF result in global elastic deformation of material. In this regime, the fatigue life is mainly governed by fatigue crack initiation, motivated by local plastic deformation, such that crack propagation stage is a smaller portion of the total life. LCF is mostly evaluated using strain-life fatigue models. From this perspective, LCF tests are performed in strain-controlled condition under different stain amplitudes, with the test data used to obtain the constants in the fatigue models. A commonly used fatigue model that describes the LCF behaviour is the Coffin-Manson relation [102] as given below:

$$\frac{\Delta\varepsilon_p}{2} = \varepsilon_f^{'}(2N)^c \tag{3}$$

where $\Delta\varepsilon_p/2$ is the plastic strain amplitude, $\varepsilon_f^{'}$ is an empirical constant known as fatigue ductility coefficient, $2N$ is the number of reversals to failure, and c is an empirical constant, of order -0.5, known as the fatigue ductility exponent.

HCF conversely is evaluated mostly using stress-based models. As an example, Basquin's equation can be used to represent the relation between the applied cyclic stress and the fatigue life. For this aim, test specimens are tested under fatigue loading with different stress levels and the Basquin's equation will represent a linear regression of fatigue life data in double logarithmic plot of stress-life (also known as *S-N* curve) [34].

$$\sigma_a = A(2N)^B \tag{4}$$

where σ_a is the applied stress amplitude to the test specimen, N is the number of cycles to failure ($2N$ is the number of reversals to failure), and A the fatigue stregth coefficient and B the fatigue strength exponent. Ideally, basic *S-N* fatigue data are generated under a fully reversed stress cycling meaning that the maximum and minimum stress have the same level but different signs (σ_{max}=-σ_{min}). In this condition, the mean stress is equal to zero (σ_m=(σ_{max}+σ_{min})/2 = 0). However, in real-life applications, the actual loading involves a mean stress on which the oscillatory stress is superimposed. In order to illustrate the mean stress effect on the fatigue behaviour of materials, the results of a fatigue test using a non-zero mean stress are often presented in a Haigh (or often referred to as Goodman) diagram (see Fig. 10). This diagram plots the oscillatory stress amplitude, σ_a as a function of the mean stress, σ_m using constant lifelines. The region below each curve represents infinite life ($N > 10^6$~10^7) and the finite life region is above the curve. Several empirical relationships have been proposed in the literature that relate alternating stress to mean stress level, some of which are represented below:

$$\frac{\sigma_a}{\sigma_e} + \frac{\sigma_m}{\sigma_u} = 1, \quad \text{Goodman(1899)} \tag{5a}$$

$$\frac{\sigma_a}{\sigma_e} + \left(\frac{\sigma_m}{\sigma_u}\right)^2 = 1, \quad \text{Gerber(1874)} \tag{5b}$$

$$\frac{\sigma_a}{\sigma_e} + \frac{\sigma_m}{\sigma_y} = 1 \quad \text{Soderberg(1930)} \tag{5c}$$

$$\frac{\sigma_a}{\sigma_e} + \frac{\sigma_m}{\sigma_f} = 1 \quad \text{Morrow(1960)} \tag{5d}$$

where σ_a is oscillatory stress amplitude, σ_e is the fully-reversed fatigue limit, which is the stress level representing a fatigue life of 10^6~10^7, σ_m is the mean stress, σ_u is the ultimate strength, σ_y is the yield strength, and

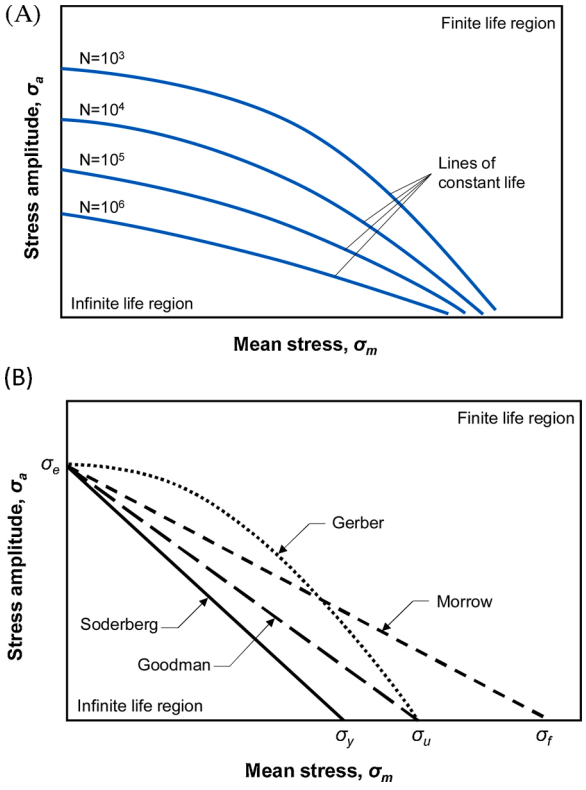

Fig. 10. Mean stress effect on fatigue properties; (A) Example of a Haigh diagram, (B) Comparative illustration of mean stress equations.

σ_f is the true fracture strength of the material. A comparative illustration of the mentioned equations is given in Fig. 10B. Among the mentioned equations, the ones proposed by Goodman and Gerber are the two most widely accepted methods due to their good agreement with the fatigue test data.

3. Experimental investigations on the fatigue behaviour of cellular materials

This section reviews experimental procedures and data collected in the literature about the fatigue behaviour of cellular materials. As shown in Fig. 3c, the majority of fatigue experiments have been carried out under uniaxial compression-compression, *viz.* the applied time-varying axial load is always comprised in the negative regime [103–119]. This testing configuration, even though not yet codified in specific standards, is mainly preferred due to its simplicity, as the testing machine needs only to be provided with compression plates and the specimen geometry does not necessitate specific interfaces with the machine. In general, fatigue specimens are designed according to the International Standard ISO 13,314 that codifies quasi-static mechanical tests on porous and cellular metals. The prescribed geometry is illustrated in Fig. 10a, wherein the linear dimensions of the specimen must be at least 10 times d_a, *viz.* the cell side or the average pore size, so as to minimize edge effects. In some cases [107], the specimen is provided with end solid plates build together with the central cellular part, as shown in Fig. 11b. This ensures a better parallelism and planarity of the specimen surfaces in contact with the machine compression plates.

Almost all the compression-compression fatigue tests reviewed in this paper were carried out in air at a frequency between 10 and 50 Hz and load ratio (ratio of the absolute maximum to minimum load) of $R = 0.1$. In general, fatigue tests are preceded by a quasi-static characterization of the cellular materials to estimate the yield and plateau stress. The maximum absolute global stress values adopted for the fatigue tests are generally between 10 and 80 % of the yield stress to explore fatigue lives ranging from a few thousands to 1–2 millions of cycles. In this way, S/N curves can be derived and fitted according to a power-law equation [120] or a modification thereof through the introduction of an asymptotic term [66].

In some cases, the specimen displacement field is acquired during the fatigue test through suitable experimental apparatus, such as mechanical [121] or optical non-contact [106] extensometers, a Linear Variable Displacement Transducer (LVDT) [122] or Digital Image Correlation (DIC) [123]. The knowledge of the evolution of the global strain during the fatigue tests allows valuable information to be acquired about the fatigue damage mechanisms of cellular materials. A qualitative plot of the total strain *vs.* the number of cycles is given in Fig. 12. This is a re-adaptation of similar plots proposed in [124,125], for cellular materials and originally developed for metal foams [126].

Accordingly, the fatigue life is subdivided into three stages. During the very early cycles of Stage I, there is a plastic redistribution of peak stresses at critical lattice locations characterized by high stress concentrations, followed by an elastic-shakedown. The largest part of stage I is dominated by ratcheting, *i.e.*, a progressive accumulation of inelastic strain, which is imputed in the literature to be viscous creep-like phenomena. Boniotti et al. [123] observed that ratcheting is characterized by a constant value of the strain amplitude ε_a and an increasing value of the mean strain ε_m (Fig. 13A). A sudden increase in the ratcheting rate is usually related to the damage initiation and propagation in one or a few critical locations of the lattice material. The number of cycles at damage initiation N_i is defined in [123] as a 1% increment - the dashed line in Fig. 13A - over the initial constant value of the strain amplitude - the solid line in Fig. 13A. Stage III is characterized by a sudden increase in the mean strain produced by the coalescence of several cracks leading to eventual failure. The number of cycles to failure is defined as the intersection point between the ratcheting line and the line fitting the last points of ε_m before the end of the test (Fig. 13B), as suggested in [109, 119,123,125–127]. Boniotti et al. [123] attempted to quantify the fraction of fatigue life spent in initiating the damage. Results are shown

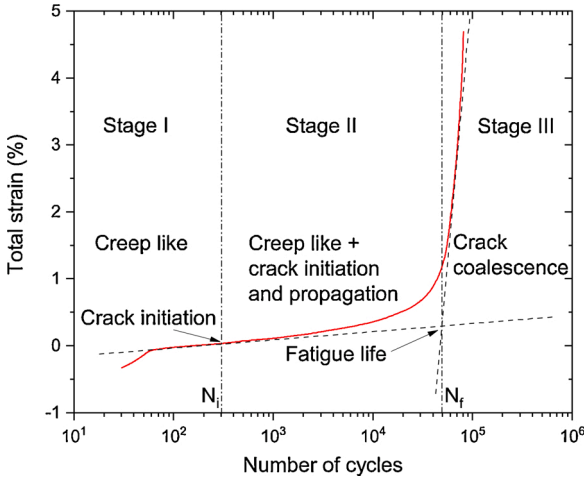

Fig. 12. Typical three stage evolution of fatigue damage in compression-compression fatigue tests of porous metallic materials. Adapted from [124,125].

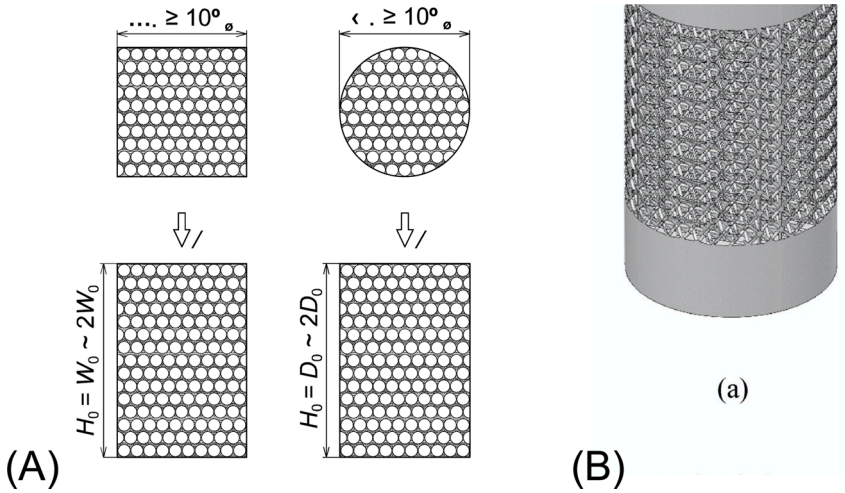

Fig. 11. (A) specimen geometry for compression-compression tests according to ISO 13314. (B) specimen geometry with solid end plates proposed in [107].

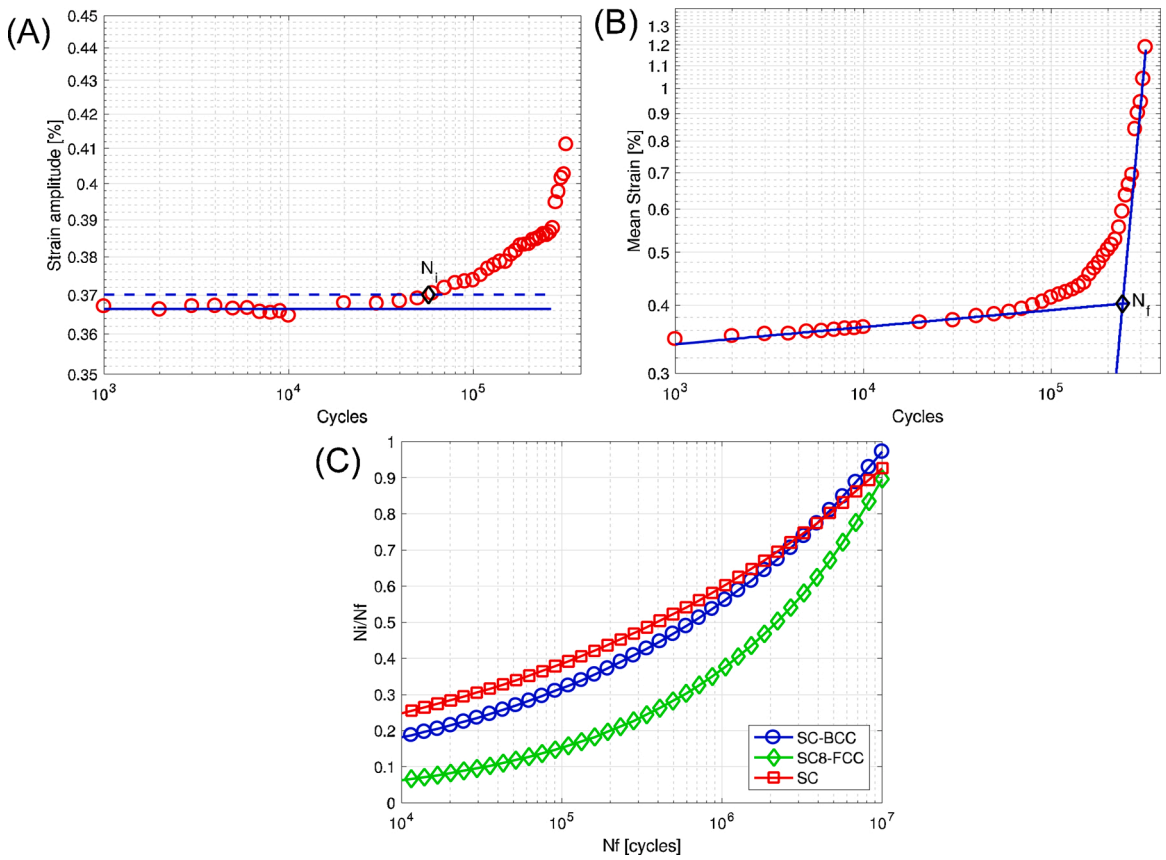

Fig. 13. Definition of (a) number of cycles at damage initiation N_i and (b) number of cycles at failure N_f according to [123]. (c) fraction of life spent in damage initiation, N_i/N_f *vs.* number of cycles to failure. SC: simple cubic cell. SC-BCC: BCC cubic cell. SC8-FCC: FCC cubic cell.

in Fig. 13C. Importantly, in the low-cycle fatigue regime, N_i takes a minor part of the total life, while in the high-cycle fatigue regime N_i contributes more than half of N_f. This suggests that different approaches must be adopted to assess the fatigue life of cellular materials. In the high-cycle fatigue regime, a damage initiation fatigue calculation approach is reasonable, while at short fatigue lives, a total fatigue life approach, including also the life spent to propagate damage and cracks until final failure, is preferable. This issue will be further addressed in Section 6.

The intensity of ratcheting occurring in stage I can be quantified in terms of the ratcheting rate, *i.e.*, the rate of accumulation of inelastic strain in the direction of the applied load. This can be defined as the slope of the line fitting the mean strain from the beginning of the tests up to the number of cycles at damage initiation. Several papers [103,104,119,128], attest that the ratcheting rate is linearly correlated with the applied stress amplitude in a double logarithmic scale. If the S/N curves are well fitted by a Basquin power law [120], then the ratcheting rate is still linearly correlated in a log-log scale with the number of cycles to failure N_f, as experimentally found in [123]. Fig. 14 summarizes the experimental ratcheting rate data collected in [103,104,119,123,128], as a function of N_f. Interestingly, the ratcheting rate is fairly independent of the cell architecture [123] (*i.e.*, cell type and porosity p) and mainly dictated by the metallic material which the lattices are made of. In particular, in terms of the ratcheting rate, the NiTi shape-memory alloy displays the lowest whereas titanium-alloys display the highest, with aluminium and stainless steel showing intermediate behaviour. Conversely, if the ratcheting rate is plotted as a function of the applied stress amplitude (as, for instance, in [105]), the effects of porosity and cell architecture are far more pronounced as they strongly affect the fatigue strength of the porous material.

In this regard, Zadpoor and collaborators [113] were among the first

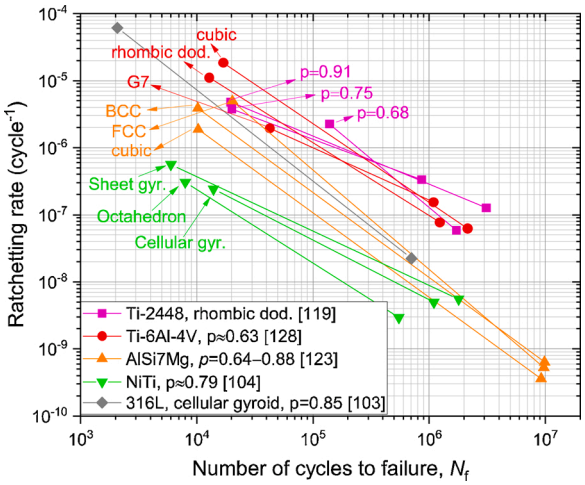

Fig. 14. Ratcheting rate *vs.* number of cycles to failure for several cell architectures investigated in the surveyed literature [103,104,119,123,128]. p indicates the open porosity.

to argue that the compression-compression fatigue strength of porous meta-materials is primarily influenced by cell type and porosity. Their idea was to eliminate the dependency upon the porosity by normalizing the fatigue strength with respect to the yield strength, which is a declining function of porosity as well (see Eq. (2b)). In this way, they demonstrated that the normalized fatigue strength is a function of the cell type only, even though the S/N curves obtained at different porosity values did not perfectly collapse into the same curve. Taking inspiration from this fundamental work, in the present review paper we show in

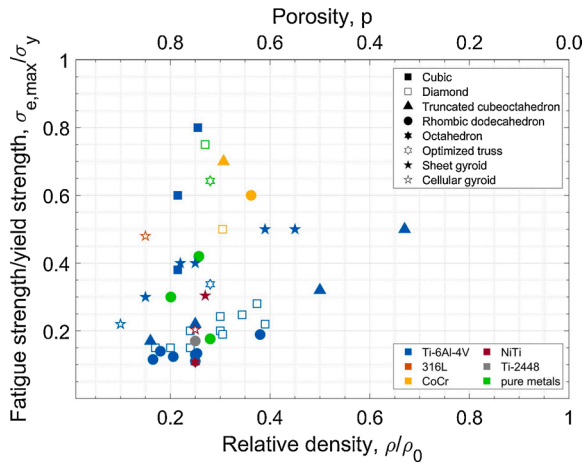

Fig. 15. Compression-compression fatigue strength normalized with respect to the yield strength as a function of the open porosity, *p*. $\sigma_{e,max}$ is the fatigue strength at 10^6 cycles to failure corresponding to the maximum compressive global stress applied to the sample. The data were taken from [103–119]. Where available, the measured porosity is used instead of the as-designed one. Fatigue experiments were carried out in air at load ratio $R = 0.1$. The vertical arrow indicates no failure for cubic cells tested at maximum stress up to 80 % of the yield strength.

Fig. 15 the fatigue data reported in [103–119]. Specifically, the normalized fatigue strength estimated at 10^6 cycles under compression-compression fatigue ($R = 0.1$) is plotted as a function of the porosity *p*. Polygonal symbols refer to strut-based cellular materials, while star and asterisk symbols denote cellular- and sheet-gyroid meta-materials, respectively. Symbol colours designate the metallic material used to additively manufacture the samples. Importantly, the majority of fatigue data available in the literature were obtained using Ti-6Al-4 V, mainly because such materials find applications in the biomedical field, where this alloy represents a "gold standard". Surprisingly, apart from the cubic cell (square symbol), strut-based cellular samples made up of this material (black polygonal symbols) lie in the lower band of Fig. 15. Despite the fact that the fatigue strength data are normalized with respect to the corresponding yield strength, the data still display a decreasing trend with increasing porosity. This demonstrates that the reduction in fatigue strength with increasing porosity is more pronounced than that in yield strength. As discussed in the Introduction, fatigue is a local damage phenomenon very different from yielding that affects the global mechanical response of the entire porous material. Therefore, the yield strength is not able to capture the entire detrimental effect of porosity on the high-cycle fatigue strength. Among the strut-based cellular materials, truncated cuboctahedron [107,113], and topology-optimized [108] cells proved to display the highest normalized fatigue strength. An important exception is represented by the cubic cell, which showed an exceptionally high compression-compression fatigue strength when the load axis is parallel to the struts printed orthogonally to the printing plane [113]. In this case, no fatigue damage is observed, even at a maximum compressive stress corresponding to 80 % of the yield strength. Yavari et al. [113] attributed such exceptionally high fatigue strength to the fact that, under this loading configuration, the cubic cell is the only one subjected only to compressive local stresses, while the remaining cell architectures undergo local bending stresses that are more dangerous to the fatigue strength. On the other hand, the cubic cell displays the highest anisotropic mechanical response in comparison with other strut-based cells; it is therefore of little practical interest for the manufacture of mechanical components which will be subjected to complex loading scenarios. Gyroid-based cellular materials tend to display better fatigue performance compared to their strut-based counterparts. This has been attributed to the absence of stress concentrations occurring at the nodes between struts and to the continuous curvature of their surfaces [49,104,112]. A particularly important issue that can be drawn from Fig. 15 is the remarkable influence exerted by the metallic material on the fatigue strength. Importantly, very ductile materials, such as pure metals (Ti, Fe, Ta), Co-Cr and 316 L stainless steel, exhibit a superior normalized fatigue strength with respect to their counterparts made up of titanium alloys or the shape-memory alloy NiTi. Apparently, a high ductility is required to accommodate stress peaks in the vicinity of stress raisers, such as nodes and geometric imperfections, which serve to reduce the notch sensitivity of the porous meta-material.

In more recent literature, there has been a growing awareness that a better understanding of the fatigue behaviour of cellular materials would be achieved if the experimental fatigue characterizations were also conducted under global tensile stresses. It is in fact known that tensile stresses are far more detrimental to the fatigue strength than compressive stresses as fatigue crack growth is favoured by stress states that tend to promote mode I type of loading (crack opening). This, however, poses a considerable experimental challenge as the specimen geometry must be designed to make possible to transfer tensile loading from the machine to the sample and to locate specimen failure in the sample's central gauge part where edge effects are minimized. Fig. 16 reviews the specimen geometries proposed so far in the literature to test cellular materials under tensile fatigue loading. In Fig. 16A, the specimen geometry proposed by [106] has a dog-bone shape, where the central part has a cellular structure and the ends are made up of solid metallic material. The geometry depicted in Fig. 16B was designed in [129]. The mechanical interface is composed of threaded solid ends, a stress relief groove and reinforced struts in the vicinity of the interface between solid and cellular parts, which are adopted to localize the specimen failure in the gauge part. Fig. 16C shows a cylindrical specimen [130], where a smooth transition from the solid ends to the porous central part is obtained through a continuous variation of the cell porosity. A similar specimen geometry was very recently adopted in [131]. The solution shown in Fig. 16D [132] resembles that depicted in Fig. 16C with the only difference that the threaded interface is replaced by solid smooth ends that are clamped by hydraulic grips. The specimen geometry illustrated in Fig. 16E adopts bolted flanges as mechanical interfaces with the testing machine [37]. The solid members are bell-shaped to make the load transfer more uniform from the bolts to the central porous part. The struts are reinforced in the vicinity of the members. Compared to the design solutions shown in Fig. 16A-D, this specimen geometry permits the central gauge part of the specimen to be much larger than the diameter of the testing machine grips, thereby allowing a much larger number of unit cells in the central part of the sample, which is then affected by lower edge effects. The specimen geometry shown in Fig. 16F was devised in [133] and consists of 4 stacked unit cells with a gradient of radius to ensure failure localization in the gauge part.

There have been a few investigations reported in the literature on the effect of mean stress on the fatigue behaviour of cellular materials. In this review paper, to eliminate the above-mentioned material induced variability in fatigue properties, we will focus on the most studied alloy, specifically Ti-6Al-4 V. The collected fatigue data are plotted in the Haigh diagram in Fig. 17, representing the stress amplitude as a function of mean stress for a fatigue life of 10^6 cycles to failure with both axes normalized by the yield strength. Interestingly, the sheet gyroid specimens (star symbol) [106] exhibited a dramatic decrement in the stress amplitude when the fatigue loading cycle is moved from compression-compression to tension-tension fatigue. The authors attributed this effect to the presence of internal defects (pores and lack-of-fusion defects), whose detrimental effect on the fatigue strength is much more pronounced under tensile stresses. de Krijger et al. [117] (square open symbol) investigated the mean stress effect in the compression-compression regime only. Importantly, in this regime, the diamond cell lattices showed a negligible effect of the load ratio. Lietaert et al. [130] investigated the same cell architecture (square half-solid

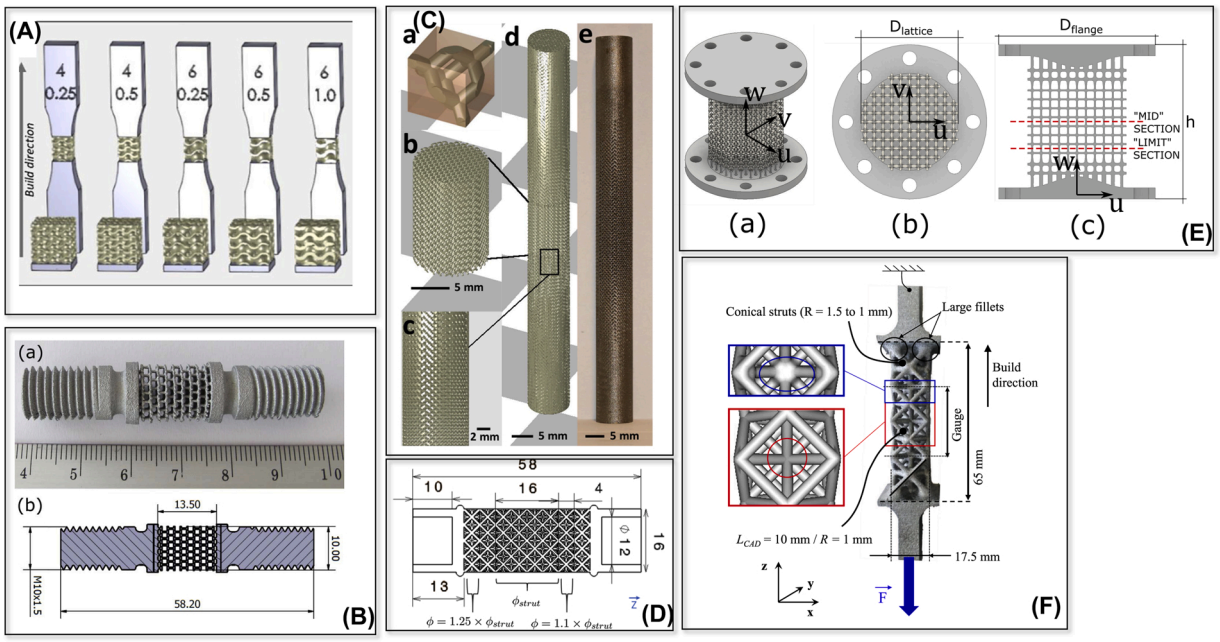

Fig. 16. Specimen geometries proposed in the literature to carry out uniaxial fatigue tests under tensile stresses. (A) Dog-bone specimen [106]. (B) Cylindrical specimen with threaded solid ends [129]. (C) Cylindrical specimen with continuous transition from solid to porous part [130]. (D) Cylindrical specimen with solid ends and strut diameter transition [132]. (E) Specimen with bolted bell-shaped flanges [37]. (F) Specimen with a gradient of strut radius [133].

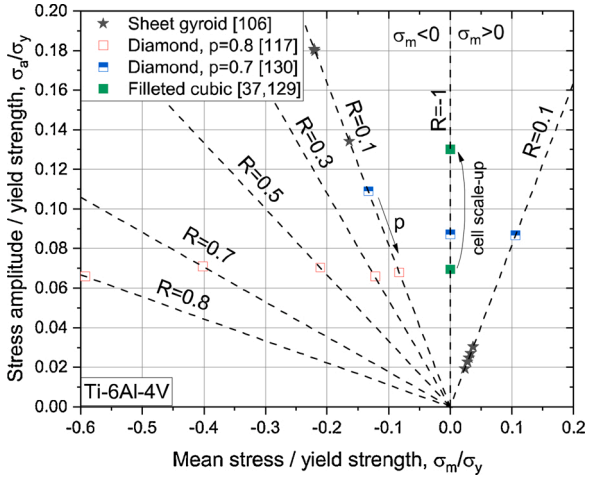

Fig. 17. Haigh diagram of cellular meta-materials made manufactured with Ti-6Al-4 V. The stress amplitude and mean stress are normalized with respect to the yield strength. The high-cycle fatigue data (at 10^6 cycles to failure) were taken from [106,117,129,130]. In [37], the effect of the cubic cell scale-up on the fatigue strength was specifically investigated.

symbol), but with lower open porosity (0.7 *vs.* 0.8) under compression-compression, compression-tension and tension-tension fatigue. As expected, the compression-compression fatigue strength was higher than that reported in [117] owing to the lower porosity. The application of tensile stresses resulted in a reduction of the fatigue strength, which was found to be nearly insensitive to the mean stress when passing from fully reversed (R=-1) to tension-tension ($R = 0.1$) fatigue loading. Even more pronounced was the fatigue decrement in the presence of tensile stresses for the cubic lattice tested in [129]. The normalized stress amplitude was in this case ~0.07, much lower than the value above 0.8 reported in [113] for compression-compression fatigue. The remarkably higher mean stress sensitivity of the cubic with respect to the diamond unit cell is linked to the fact that in the former the struts are subjected to axial loading, while the latter predominantly to bending loading. It is therefore clear that the cubic lattice is exposed to more detrimental tensile local stresses only when the external load becomes positive. Fig. 17 also displays the recent findings published in [37], wherein the cubic unit cell size was increased from the value 1.5 mm examined in [129] to 3 mm. The resulting improvement in fabrication accuracy was found to lessen any geometrical imperfections which served to enhance the fatigue strength. This fatigue improvement measure will be further discussed in Section 5. From the above discussion, it can be concluded that fatigue failure under tensile loading is directly correlated to the presence of defects and geometric imperfections, whose negative impact is naturally much more pronounced under tensile stresses [134].

From the vast literature available about the factors influencing the fatigue behaviour of metallic materials [135,136], it is known that not only the mean stress, but several factors would be expected to affect the fatigue strength of cellular meta-materials. Among them, of prime importance are the issues of environment, temperature, variable amplitude and multiaxial loading. Unfortunately, to the best of the authors' knowledge, environmental effects have only been addressed in the very recent literature, the main objective of which was to develop fatigue-resistant biocompatible cellular materials for biodegradable implants [118,137]. For this purpose, the experimental testing apparatus, illustrated in Fig. 18A, was designed [118]. It basically consists of an environmental chamber where the cellular specimen is immersed in a simulated body fluid (r-SBF), maintained via a thermostat at constant temperature and refreshed using a peristaltic pump. Fig. 18B shows a comparison of the S/N curves of samples with diamond unit cells made up of pure iron tested in air and r-SBF, which illustrates the detrimental environmental effects associated with the synergism of fatigue and corrosion phenomena. Additional investigations are still needed to obtain a comprehensive understanding of the corrosion-fatigue behaviour of additively manufactured cellular meta-materials, especially if they are intended to be exposed to aggressive and high-temperature environments, like those experienced by aircraft components [135]. In this regard, it is worth mentioning that preliminary tests undertaken in [138] on additively manufactured Ti-6Al-4 V structural alloy clearly demonstrated faster rates of fatigue crack growth in NaCl solution than in air.

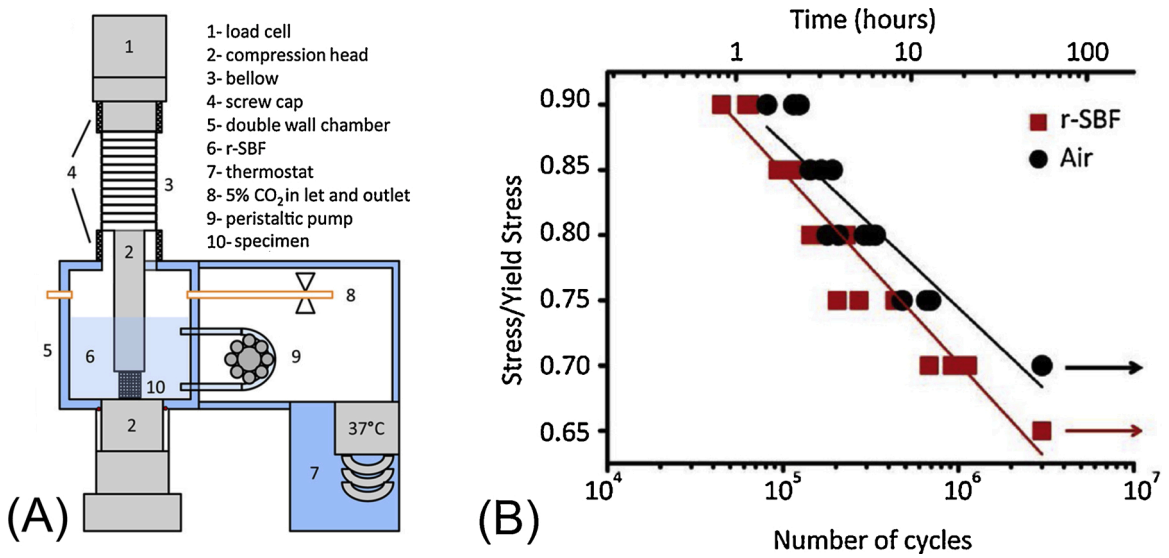

Fig. 18. (A) Testing apparatus for compression-compression fatigue experiments in simulated body fluid (r-SBF). (B) Comparison between SN curves of samples with diamond cells made up of pure iron in air and r-SBF. Images are taken from [118].

There is still ample opportunity for further experimental fatigue analyses of cellular materials. In this regard, there is a growing awareness that when these meta-materials are used in biomedical implants, they are exposed to complicated physiological stress-states that are invariably multiaxial [139], but until now research studies on these materials have been limited to uniaxial loading and quasi-static torsion [139,140]. Refai et al. [132] developed a computational framework to predict the multiaxial fatigue strength of various cell architectures, but experimental validation was obtained only for uniaxial loading. Variable-amplitude fatigue loading is another critical fatigue-related issue that still has not been addressed for cellular lattice materials.

4. Experimental assessment of fatigue-related issues

The discussion up to this point has highlighted the importance of manufacturing quality of the cellular material. There are multiple competing contributions to the fatigue performance of cellular structures, which we have discussed so far in terms of designed porosity and architecture of the lattice structure. However, in addition, differences in manufacturing are a major source of variability between different studies and even between samples in the same study. This variability is well known in bulk materials manufactured by metal additive manufacturing, and largely relates to the *quality* of the materials in terms of their nano/microstructure. In this context, much progress is being made in improving the reliability of additive manufacturing to improve the fatigue properties and reduce the scatter in results for bulk materials [31,40,41,141–146]. These improvements are mainly through optimized process parameters, well developed workflows, stringent quality control, appropriate post-processing and extensive mechanical testing.

While the same is needed for cellular lattice structures, the impact of the same manufacturing defects may have different contributions to their measured mechanical properties. For example, surface depressions due to the rough as-built surface likely play a much larger role in fatigue performance than in bulk materials, due to the size of the effective "micro-notch" compared to the strut diameter.

As mentioned above, extensive investigations have been performed on the quasi-static mechanical properties of cellular structures, but far less on cyclic fatigue. This is unfortunate as fatigue is invariably the most important degradation mechanism limiting the mechanical performance of structural materials and components. Accordingly, the role of defects and microstructural imperfections on fatigue performance in cellular materials urgently needs further investigation to unravel the different contributions of defect types and to discern ways to mitigate or overcome these through design, process quality improvement or post-processing. In the following section, we discuss the experimental evaluation of different morphological and microstructural issues that affect fatigue performance of cellular lattice structures.

4.1. Surface morphology and its measurement

As-built surfaces in metal additive manufacturing have relatively high roughness. This roughness varies with changes in process parameters and orientation (or inclination angle) relative to the build platform [26,147]. This is especially important for cellular structures as they have relatively high surface areas and typically many different surface orientations. Upward-facing (upskin) surfaces typically are quite smooth relative to other surfaces, but individual tracks may be visible. Side surfaces are usually rougher and downward-facing (downskin) surfaces are typically very rough with excess melted material (dross formation). At surfaces oriented at an angle, both downskin and upskin surfaces also contain stair-step effects [147] due to the individual layers, which affects the roughness and depends mainly on the layer height setting. Process parameters leading to balling and lack of fusion create irregular tracks and imperfect melting which leads to a rougher surface; this typically occurs at high scan speed or low laser power. At slower scan speed or higher laser power, the surface quality improves but, in excess, this can lead to a much larger meltpool size and higher local temperatures. The larger meltpool causes larger tracks with associated larger surface features; higher temperatures result in more particles being attached to the surface. In addition, high temperature can create higher thermally-induced stress leading to microcracks, which may form on the surface and further add to their poor surface quality.

Typical L-PBF systems have focussed laser spot sizes of 50−100 μm and single-track widths of 100−200 μm. This creates a fundamental minimum size limit, limiting the best possible geometrical accuracy [25]. With cellular structures (struts or walls) near the size of single tracks, the individual melted layers may require only one or a few tracks adjacent to one another, which may cause either thinner or thicker features by variations of less than one track width as the exact dimension cannot be achieved with the fixed track width (typically 0.1 – 0.2 mm). Similarly, cellular structures often require only short scan trajectories to produce thin struts – individual layers comprise of very short scan tracks. The accuracy of the start-stop cycling of the system influences the accuracy and regularity of the single track, as does the meltpool

conditions in these short exposures – the melting and solidification are different in short scan tracks compared to long continuous tracks optimized for solid parts. A similar issue occurs with some systems that do not use continuous tracks but rather a point scanning strategy, but here the problem is exaggerated due to the small feature sizes. Another related issue is the typical hatch-contour scan strategy (see Fig. 4D) used, which becomes problematic at the scale of thin lattice struts. It might not be possible to use contouring and hatching together – if both are used the structure may be too large, or if only contouring is used some locations might remain unmelted. An example of an extreme case of a single manufactured strut nearing the size limit is shown in Fig. 19.

In addition to the scan strategy, local high temperatures may cause residual stress and warping or cracking. Due to the lack of support structures on horizontal or diagonal struts, these may particularly warp upwards causing build failure; they may hit the scraper damaging it or may create a problem for powder delivery on the next layer by blocking the powder delivered. Slight warping or cracking may go unnoticed without build failure and have a negative effect on the mechanical properties. The residual stress itself may also affect the mechanical properties. In addition, horizontal and diagonal struts which are unsupported are typically built thicker than vertical struts, due to the dross formation on the downskin surfaces and penetration of the meltpool into underlying layers [149,150]. Horizontally-built struts show poor mechanical properties as shown in [151]. The diagonal struts also have the additional stair-step effect which depends on the selected layer thickness and strongly affects the roughness and the manufacturability [147,152]. Diagonal and vertical struts may also have a layered effect where individual layers show a “pancaking” effect. Imperfect process parameters leading to balling effect may result in molten balls on the ends of scan tracks which adds to the roughness, or partially melted particles may be attached to the surface. In all the above cases the effect on the surface may create irregular notch-like surface defects which would significantly degrade mechanical performance, especially under cyclic loading.

The effect of surface roughness, imperfections and notches on fatigue failure has already been well established [153]. The roughness directly affects the fatigue strength of the material [154], the local roughness act similar to designed notches for crack initiation [155] with the fatigue strength depending on notch depth [156] and varying roughness due to different surface orientations [157,158]. The competition between surface roughness, porosity, microstructure and residual stress is also complex and depends on the geometry of the part in question, as discussed in [41]. It can be expected that lattice structures, with their high surface area and low material fraction, are generally more sensitive to surface imperfections and roughness compared to other factors. It is therefore important to understand and measure this roughness and moreover find ways to improve it.

Measurement of the roughness of flat additively manufactured surfaces is generally performed using a profilometer according to ISO Standard 4287:1997 [159]. It is also possible to evaluate additive surfaces based on non-contact methods, as outlined in [160]. However, cellular structures are particularly challenging in this regard as no flat surface is available and the roughness varies locally depending on the surface orientation. It is therefore recommended to evaluate accessible surfaces as far as practically possible, depending on the cellular design and to evaluate different orientations of surfaces (*e.g.*, not only upwards-facing surfaces).

X-ray CT allows the evaluation of the surface roughness of lattice structures due to all surfaces being accessible in the acquired data [161]. There are some advantages to this method for evaluating the roughness as it may reveal notches and undercut features. For example, it has been demonstrated that CT reveals deeper roughness notches than an optical profilometer in a study correlating roughness with fatigue life [142]. The characterization of lattice structures by CT was first demonstrated in [162]; subsequently, a method was devised by the same group to also evaluate the surface roughness of lattices from CT scans [163,164].

4.2. Geometrical inaccuracies and CT scans

In addition to the roughness of the surface, it is well known that there can be a considerable deviation between the as-designed geometry (CAD) and the as-built geometry for AM parts and this issue is particularly relevant in parts with fine details such as cellular lattices [91]. Ultimately, the accuracy of L-PBF is determined by the size of the melt pool; the bigger it is, the more difficult it becomes to reproduce fine details. The size of the melt pool is determined by the local thermal properties of the powder/solid system and by the energy provided by the scanning laser. If a large amount of heat is provided and/or it is not carried away quickly, a large melt pool will form; otherwise, a smaller melt pool is obtained. The energy input provided by the laser is determined by the process parameters such as the laser spot size, laser power, the scanning speed, the layer thickness and the hatch distance [58,165,166].

The local heat transfer properties of the solid/powder system are a

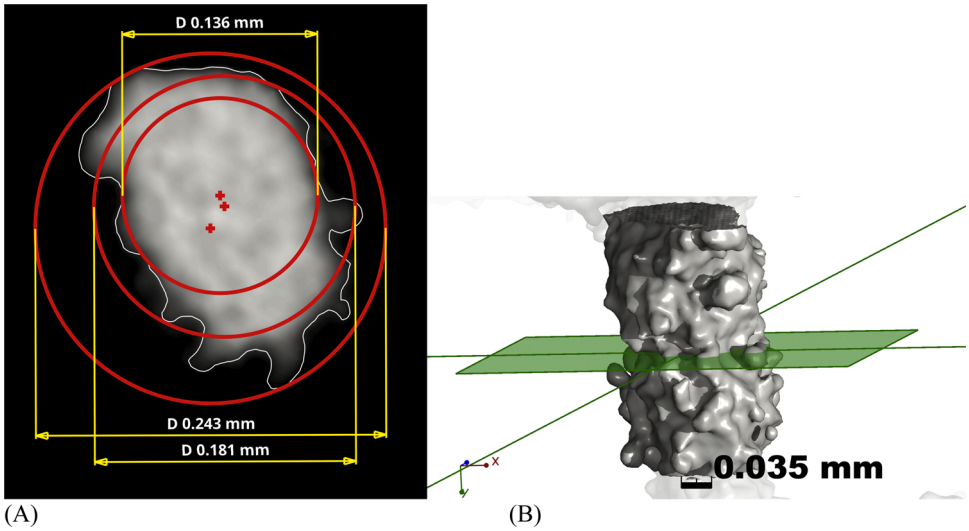

Fig. 19. Example of an individual strut with diameter ~0.2 mm, showing its irregular surface morphology and attached particles (B). Taken from micro-CT scan of a larger structure, from a study reported in [148]. (A) fitted circles are shown with different fitting methods - largest inscribed circle, smallest circumscribed circle, and gaussian least-squares best fit. This emphasizes the effect of irregular surface morphology on strut effective diameter.

complex issue, but they mainly depend on the spatial orientation of the already solid material, on the quantity of solid with respect to the powder and on the packing density of the powder (Fig. 20A). The powder, regardless of its packing density, is less conductive than the solid, and so heat will be mainly carried away by the already solidified part. For instance, a horizontal strut is supported only by the less conductive powder below and thus the melt pool will tend to be large [162,163]. Moreover, due to gravitational and capillary effects, the melt will tend to flow into the powder, leading to an oversized strut with an irregular surface, particularly on the lower side where many loose particles are found [38,166]. On the other hand, in the case of a vertical strut, the melt pool is supported only by solid material and it is thus smaller, leading to a much more faithful reproduction of the CAD. In other words, the morphological quality of a horizontal strut is the lowest and it progressively improves with increasing angle [121,167]. This phenomenon is not limited to the struts of cellular lattices but is a characteristic of any overhanging part [150,168]. Inclined struts can show the so called "staircase effect" (Fig. 20C), which is caused by the strut being made of small layers welded one to the other with a small axial offset due to the inclination [38,163]. The complexity of the as-built/as-designed mismatch issue is increased by material shrinkage during solidification and cooling [169]. The aspects discussed above are responsible for the as-built/as-designed mismatch, which can be decomposed into several contributions, useful mainly for modelling purposes [35,94,170]:

- Strut waviness. The centroid of the cross-sections along the length of the strut do not typically lie on the nominal axis but there is some degree of offset which produces a wavy effect (Fig. 21A) [35,162].
- Strut section irregularity. The as-built shape of the cross-section tends to deviate from the designed shape due to the irregular distribution of material (Fig. 21A) [35,167].
- Strut thickness variation. The average thickness (or diameter, depending on the geometry of the cross-section) of the cross-section can be higher or lower than the as-designed value depending on the inclination of the struts to the printing direction and the process parameters [57,58,121,162]. The thickness of struts with large angles relative to the building direction (horizontal struts) tend to be considerably thicker than struts parallel to the printing direction (vertical struts) (Fig. 20B) [85,121].
- Alteration of the local node geometry. Excess material is added to the struts during the printing process due to the excessive local melting and bonding of partially melted particles [171]. The distribution of the excess material depends on the inclination to the printing direction. In general, the material tends to accumulate below the struts (with respect to the printing direction). The most affected are the horizontal struts, the least affected are the vertical struts, as shown in Fig. 21B. The main fatigue-related consequence of this geometrical imperfection is that, if the nodes are intentionally filleted to reduce the stress concentration, the beneficial effect of this design measure is diminished by the reduction in the actual fillet radius in the downfacing surfaces of the node because of the accumulation of excess material. This is evident looking at Fig. 21C, which reports the results of the image analysis aimed at identifying and measuring the main features of Fig. 21B [171]. Specifically, fillets are interpolated with circles.

The effect of geometrical imperfection on the static mechanical properties has been widely investigated in the literature [35,134,170]. In essence, strut waviness greatly affects the elastic modulus, especially of stretching-dominated lattices, because such structures are very stiff given that the struts are loaded only axially; waviness introduces bending moments that cause a drop in the stiffness of the strut promoting in fact a transition to a quasi-bending-dominated behaviour. The deviation of the cross-section shape and size for the design also has a strong effect on the elastic modulus both in the case of stretching- and bending-dominated structures because it changes the moment of inertia and the load-bearing area of the struts. The effect can both be to increase or decrease the modulus, depending on whether the section is bigger or smaller. In this context, the load bearing cross-sectional area is often smaller than the measured area due to the irregular surface condition and attached particles, most of which does not carry load (Fig. 19). Strut waviness decreases strength, although to a lesser extent than the elastic modulus. Variations in the shape and size of the cross-section strongly

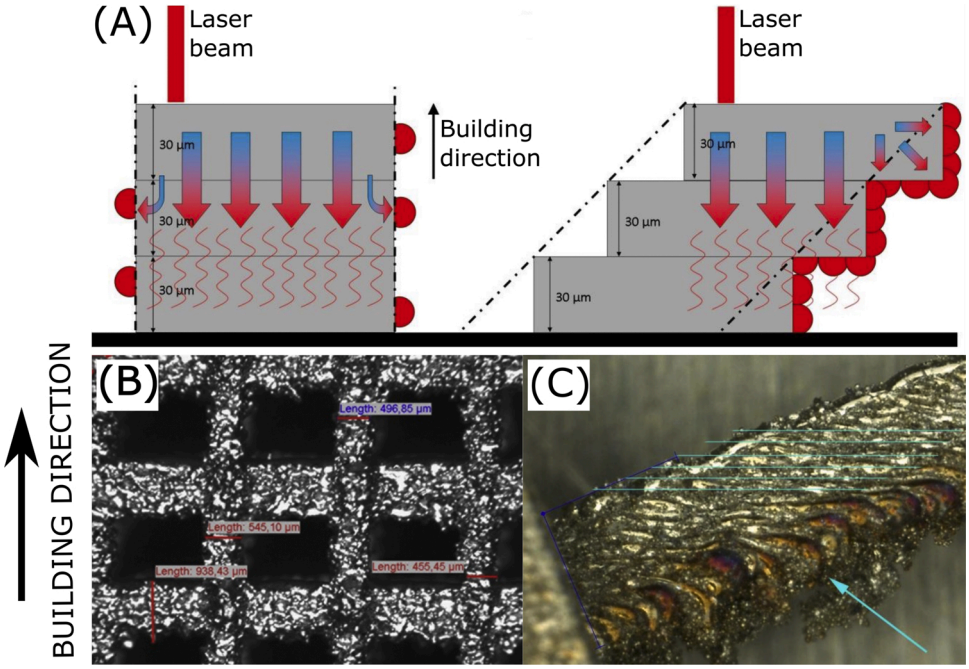

Fig. 20. Effect of strut orientation on strut morphology: (A) heat (arrows) is carried away more efficiently by vertical struts then horizontal struts, improving the surface appearance and geometrical accuracy compared to (B) horizontal and (C) inclined struts. The formation of the staircase effect is shown in (A) and (C) [(A) [163]; (B) [85]; (C) [167]].

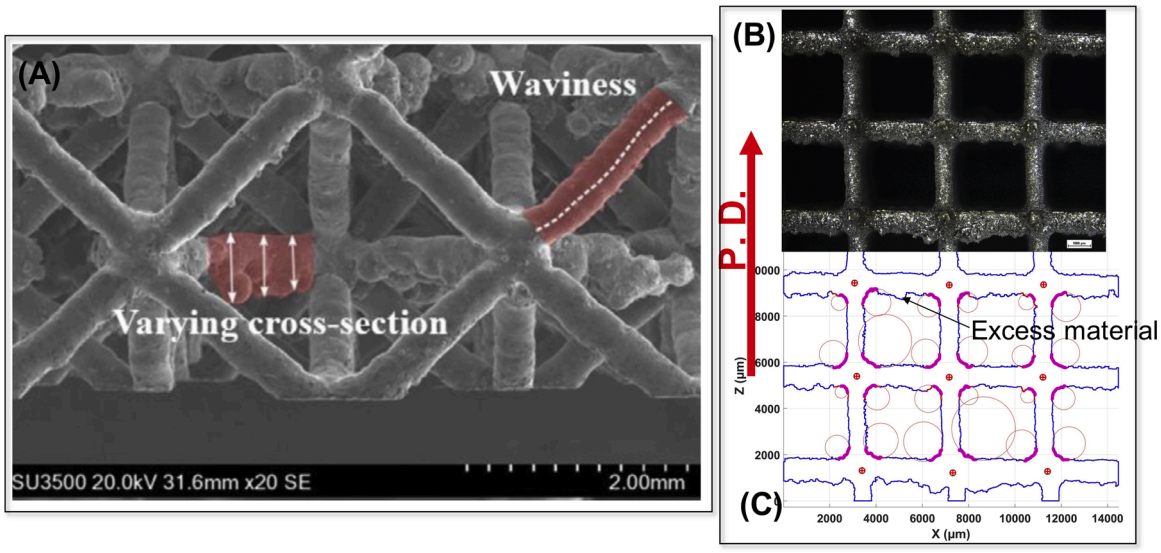

Fig. 21. (A) Examples of geometrical irregularities in an L-PBF lattice: strut waviness and strut cross-section variation on a horizontal strut [35]. (B) Example of filleted cubic lattice showing excess material accumulated on the downfacing surface of the horizontal struts. (C) Output of the image analysis that identifies and measures the main features of each picture (strut thickness, fillet radii and unit cell distortion) [171]. P.D. denotes the printing (building) direction.

affect strength, increasing it or decreasing it depending on whether the as-built section is bigger or smaller than the designed section [35,58]. For these reasons, the possibility of compensating, at least partially, some of these geometrical imperfections has been extensively investigated by the scientific community [121]. The beneficial effect of compensation in terms of better reproducibility of the expected properties of the lattice materials has been proven for geometric and static mechanical properties [121,162], but this has yet to be carried out for fatigue resistance.

The effect of manufacturing defects is commonly to decrease the fatigue performance of the lattice, although it is difficult to identify general trends and the effect of defects should be analysed case by case. Since fatigue, contrary to the elastic modulus and other monotonic properties, is a highly localized phenomenon, it is very hard to devise analytical models able to predict the effect of geometrical inaccuracy on the fatigue strength. Local detailed inspections are therefore necessary to identify fatigue critical spots in the lattice materials. For this purpose, X-ray CT scanning is useful for checking the fidelity of the manufactured lattice structure by comparison to the design; this could be achieved, for example, by measuring the strut thicknesses, checking for warping or even identifying additional unmolten or partially molten material inside the lattice structure [161]. It is possible for unmelted powder to get stuck inside lattice structures, especially when the pore spaces are small, and post-process heat treatment might partially sinter this material making it impossible to remove; this can readily be identified, however, through micro-CT imaging. In addition to checking the manufactured part quality, micro-CT images can be used as a basis for simulations such as shown in Fig. 22. In this example, the stress concentrations from notch-like surface irregularities are highlighted. Such simulations using image-based inputs to model the real geometry, are useful for taking manufacturing irregularities into account in predictions of mechanical properties of lattice structures. For example, using multiscale X-ray CT and finite element modelling (FEM), the compression of lattice structures has been studied by incorporating the internal strut pores into the simulation [172]. Similarly, it has been shown how strut surface irregularities affect failure using CT scans during *in situ* compression testing [35]. In a detailed CT study of lattice structures, different forms of defects relating to the designed cubic geometry were identified and used to improve FEM models for predicting the mechanical behaviour [173]. In subsequent work by the same authors, the fatigue performance was studied, including the role of rounded corners; in this study, poor properties were found specifically due to surface irregularities even for

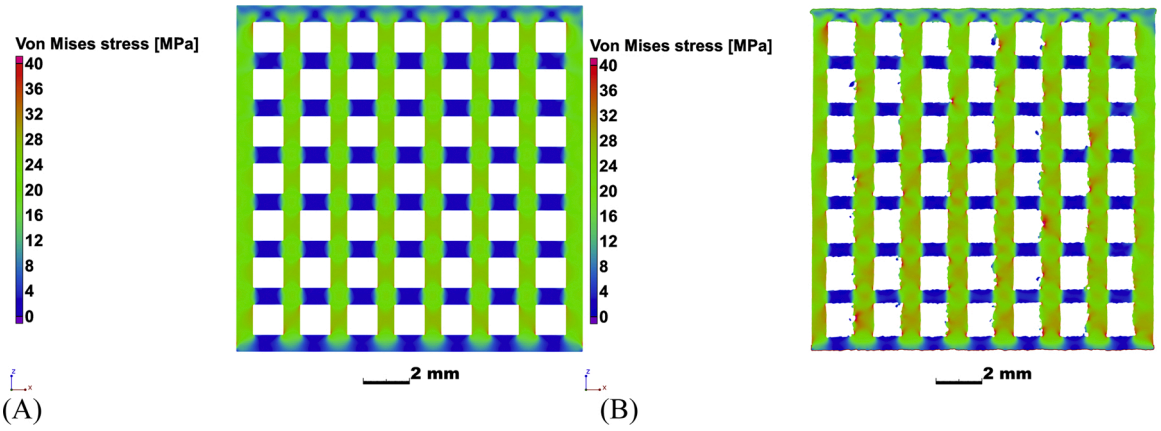

Fig. 22. Compressive load simulation applied to a cube-design lattice structure in (A) ideal geometry, and (B) as-built geometry from micro-CT scan. This highlights the local high stress concentrations in as-built surfaces, emphasizing the importance of the surface quality for lattice structures. Simulations were performed with identical parameters [172].

hot-isostatically pressed (HIP) samples [36].

The geometrical errors associated with roughness, described above and in the previous section, may play varying roles in the fatigue properties – some of the details of this issue have been studied using numerical methods to investigate the relative effects of surface irregularities, design and other factors on the fatigue strength and the fatigue power-law slope [97,174]. Specifically, it was found in these studies that such geometric errors, *e.g.*, irregular thickness of the struts, can markedly affect the fatigue strength. A computational approach to fatigue property prediction was used in [98]. This work revealed a strong influence of surface irregularities especially at low stresses (high-cycle fatigue); in particular, catastrophic failure was found to occur in diagonal shear failure after only 1% of struts had failed. This was as extension of previous work in the same group where surface irregularities were incorporated into the FEM models [94]. More recently, CT scans were utilized as an efficient modelling tool to predict mechanical properties; this approach modelled irregular struts as ellipses with varying diameter at a central location along strut direction, [175]. A similar concept employing CT scan inputs was used to incorporate actual node geometries and node defects into an efficient simulation approach [176].

4.3. Internal defects, CT scans and fractographic inspections

In addition to surface roughness and geometric errors, internal defects inside struts may occur. These include mainly pores, but microcracks and inclusions are also possible depending on the material and process parameters. Porosity may occur due to many different reasons, and it is important to realize that the formation of porosity is interrelated with the issues of surface roughness and build quality discussed in

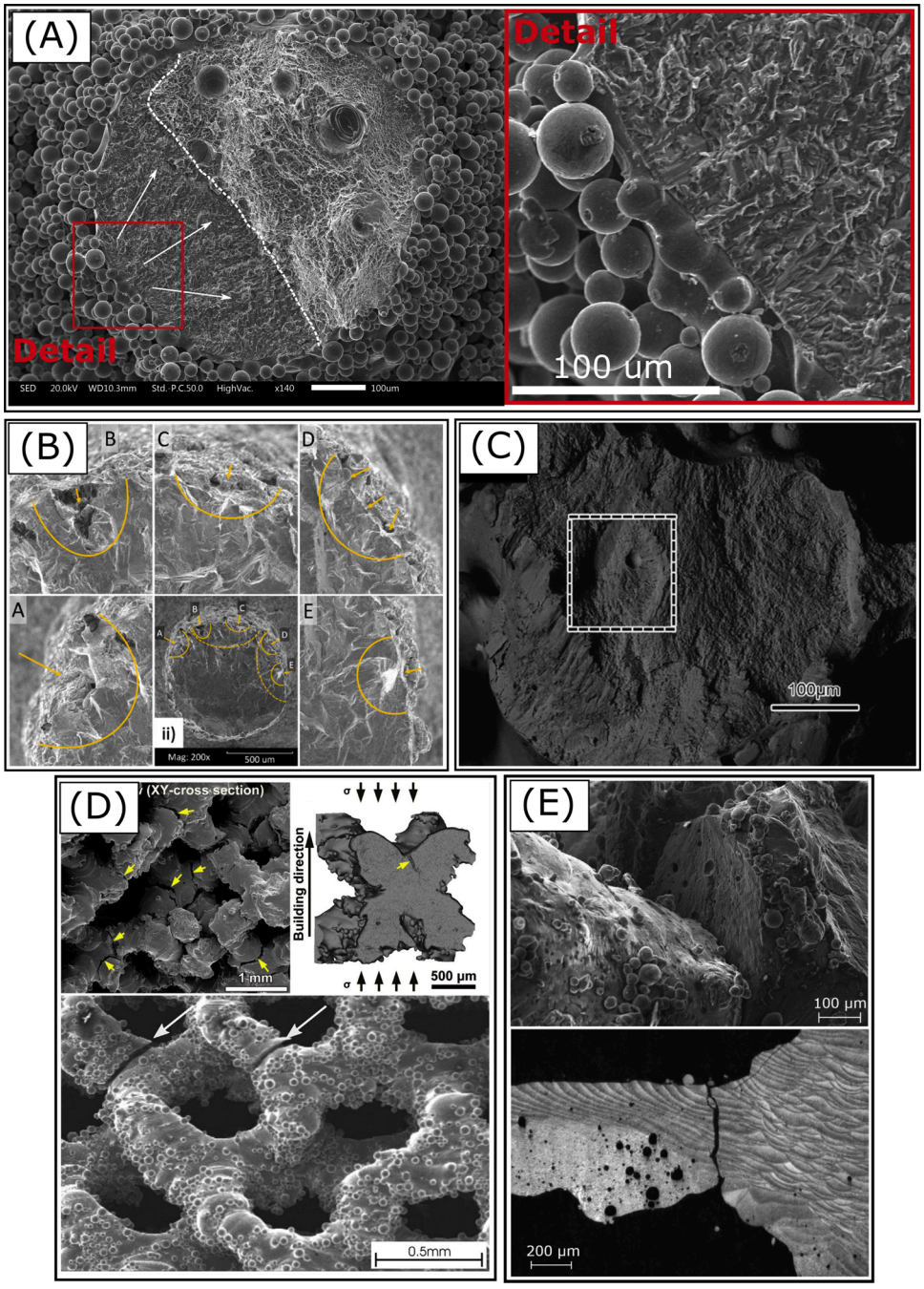

Fig. 23. Experimental investigations on the role of internal defects on the fatigue behaviour of lattice materials. (A) fatigue crack nucleated from surface defects, internal flaws are visible only on the final ductile fracture surface [37]. White arrows indicate crack growth direction, the dashed line separates the fatigue fracture surface from the final fracture. (B) Multiple surface crack initiation observed in Inconel BCC lattice materials followed by crack coalescence [184]. (C) Internal defect triggering fatigue crack initiation. Final fatigue fracture, however, is dominated by a surface main crack [128]. (D) Multiple crack initiation on several lattice nodes. The top part of the figure compares SEM and CT inspections of the same lattice node [119]. The bottom part reports similar SEM observations on diamond lattice materials [110]. (E) SEM (top) and optical (bottom) micrographs showing surface crack initiation regardless of the presence of internal porosity in the immediate vicinity [123].

the previous sections.

One major cause of porosity is improper process parameters [177–179]. Keyhole porosity occurs due to high laser power relative to scan speed resulting in an unstable vapour cavity which collapses and leaves rounded pores in the solidified material. Too low laser power, high scan speed, too large layer height setting or too large hatch spacing all can create lack of fusion porosity. Lack of fusion porosity is irregularly shaped and is known to be more detrimental especially to fatigue properties, as for example shown in a recent study of gyroid lattices [180]. Optimized parameters are available for minimizing porosity in most materials, but the local meltpool conditions during the building of lattice structures can vary from those in bulk solid parts, which may require additional or separate optimization processes. The optimal process parameters for lattice structures may therefore be different from that for bulk material and may depend on the lattice geometry [181]. Process parameters are not the only reason for porosity; the overlap of contour and hatch tracks is often a source of porosity that leads to subsurface porosity near the edges of parts, an issue that might become problematic in lattice structures, especially when only short hatch tracks are used. This type of porosity was observed in sheet based gyroid lattices in a study by Kelly et al. [106]. In their work, the process parameters were specifically optimized to improve this, resulting in better fatigue performance for the specially optimized parameters. Additionally, the powder feedstock may contain pores which are entrapped into the solidified material during melting. A variety of other unexpected errors may also create unexpected porosity, despite the best efforts at optimized parameters. Overall, the effects of pores on mechanical properties are such that near-surface pores are most detrimental to fatigue performance [182,183]. It is pertinent to note in this regard that in cellular structures, all pores are effectively near-surface.

The main experimental technique to investigate the role of defects on fatigue damage is post-mortem SEM inspections. Fig. 23 illustrates some notable examples of the fracture surfaces of cellular lattice materials tested under fatigue loading. Looking at Fig. 23A, it is evident that crack initiation originated from the outer surface of the struts of the cubic cells [37] due to the irregular and rough surface morphology. Internal porosity is clearly visible but only on the final ductile fracture of the strut cross-section. Fig. 23B [184] shows the fracture surface observed in a BCC Inconel lattice structure. Surface defects here led to multiple crack nucleation, followed by coalescence into a single main crack. Zhao et al. [128] are among the few to report fatigue crack initiation at an internal defect (Fig. 23C), even though the main crack leading to eventual fracture nucleated on the surface. The micrographs collated in Fig. 23D (top image taken from [119], bottom part published in [110]) indicate that the lattice nodes predominantly represent the critical locations for the fatigue of lattice cellular materials. Note that in [119], CT scans and SEM observations of the same critical fatigue location were combined to reveal fatigue cracks emanating from the strut junction, as shown in the top part of Fig. 23D. This outcome was further confirmed by fractographic inspections (Fig. 23E) on $AlSi_7Mg$ cubic lattice structures [123], where crack initiation was found to occur on the strut surface regardless the presence of internal porosity in the immediate vicinity.

4.4. Residual stresses

Residual stress is a concern in metal additive manufacturing due to the fast heating and cooling during melting and solidification by a fast-moving laser source. Compressive and tensile residual stresses may form in different locations, which is difficult to predict, especially in complex geometries [185]. Residual stresses may be reduced by appropriate scanning strategies, for example using island or stripe strategies. These strategies act to melt regions, by jumping to different locations on the layer, in order to allow a solidified region to cool down before continued melting and solidification takes place alongside it. This helps to prevent excess heat accumulation. Another strategy is to use bed pre-heating which reduces residual stress, as is employed *in vacuo* with E-PBF. However, as many studies [36,37,129], on the properties of lattice structures make use of as-built samples, this makes it difficult to separate the possible effects of residual stress from other factors.

Post-process heat treatment has been used with great success to eliminate most stresses. For Ti6Al4V alloys for example, this requires the platform with parts to be heat treated at ~600 °C for 2−3 hours in an argon or vacuum environment, prior to cutting them from the baseplate. This leads to parts with excellent performance, as demonstrated in [186].

The measurement of residual stress in additively manufactured metals is usually performed by X-ray diffraction [185] but this is difficult to realize in complex lattice structures due to the size of the features. To our knowledge, neither X-ray nor neutron diffraction has been applied to date to evaluate the residual stresses in lattice structures. However, the residual stresses in a lattice structure has been measured using traditional micro-hole drilling techniques, coupled with digital image correlation (DIC) in an SEM [36]. This method is not widely used as it is limited to areas that can be probed and is partially destructive. Nevertheless, the work demonstrated that some tensile residual stress can be retained even in stress-relieved specimens.

As residual stress depends on thermal conditions during the manufacturing process, the lattice geometry likely plays a role in the build-up of such stresses. For example, thicker struts would dissipate excess heat more easily to the baseplate than thinner struts, but at the same time, thinner struts are less likely to build up the same amount of heat. Thermal build simulations may play a key role here in understanding the importance of lattice design to minimize these stresses. Another key factor here is the solid-lattice interface which creates a possible discontinuity; building a solid part above a lattice might result in excess heat which cannot be dissipated efficiently, leading to residual stress and warping.

4.5. Microstructure

The nature of the L-PBF process, with its fast cooling rates, results in fine-grained microstructures with elongated grains oriented along the build direction. The manufacturing of lattices may influence this grain structure, as discussed in [187], with grains attempting to follow the lattice struts at nodes. However, vertically oriented grains likely intersect diagonal or horizontal strut edges more often, causing possible fatigue crack initiation and poorer performance for these struts compared to vertical struts. In the context of vertical struts, it should be noted that a comparison of lattices with and without additional vertical pillars (*e.g.*, BCC and BCC-Z) were studied in [74], where the addition of Z-pillars to the architecture was found to result in stretch-dominated mechanical behaviour, with increased elastic modulus and yield strength.

For Ti6Al4V lattice structures, heat treatment, HIP and chemical etching were studied in [110] in an attempt to improve fatigue performance. It was found that brittle fracture occurred in all samples but the fatigue properties were improved to a comparable degree after both heat treatment and HIP, as compared to the as-built state, which could be due to the α 'phase being transformed to $\alpha+\beta$. In the chemical etched samples (after HIP), further improvements were attributed to the smoother surface.

A recent study, comparing CP-Ti and Ti6Al4V for two designs of cellular structures, showed superior fatigue behaviour in the topology optimized design and better performance by the CP-Ti [108]. The improved fatigue properties of CP-Ti, compared to Ti6Al4V, was attributed to its higher ductility; the superior fatigue properties of the topology optimized design was simply attributed to improved design.

The beneficial fatigue properties achieved following HIP processing can be attributed to the improved ductility as well as the reduction of porosity. This effect was demonstrated in work on lattice structures where the reported normalized fatigue strength was 0.65 [188]. Fig. 24 illustrates a cube-design lattice structure, which was manufactured by L-PBF in two build orientations as indicated by the red arrows [189]. The

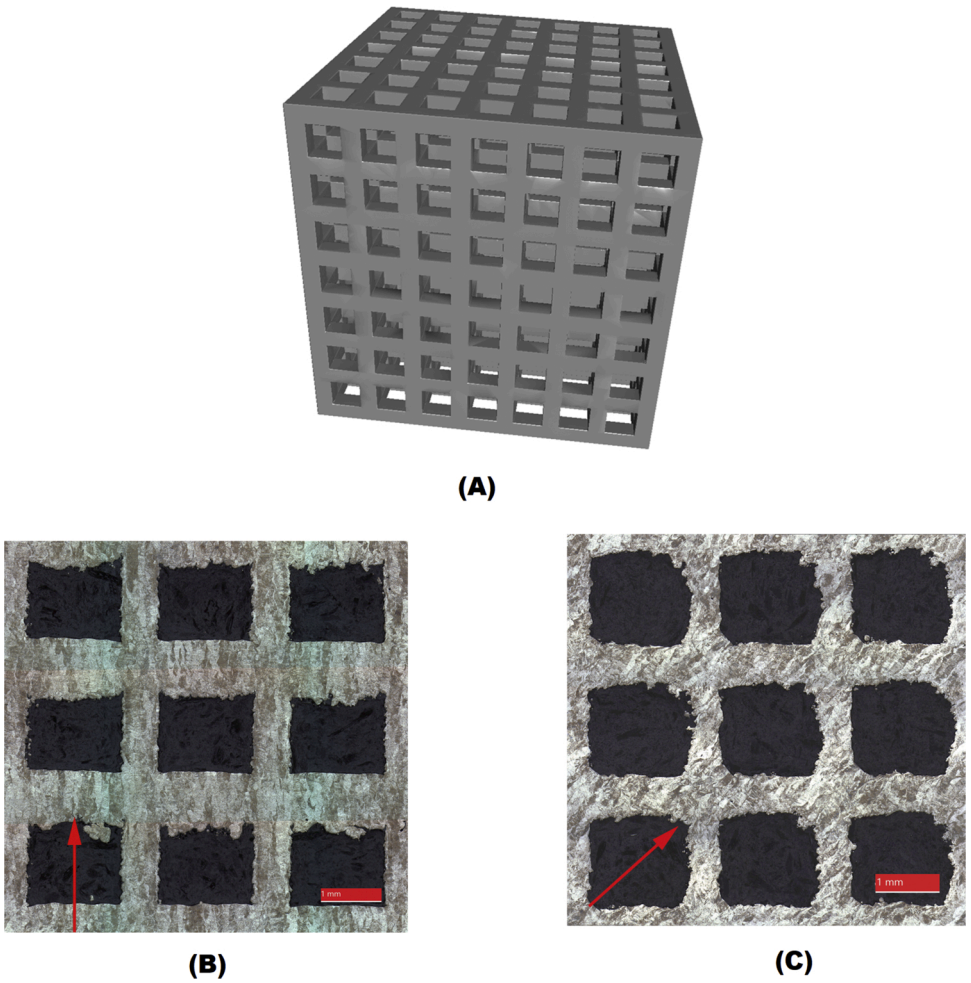

Fig. 24. Cube-design lattice structure shown in (A), manufactured in Ti6Al4V and shown with physical cross sections indicating the microstructure in vertically built (B) and diagonally built (C) samples. There is grain growth along the build direction (indicated by red arrows) [189]. (For interpretation of the references to colour in this figure legend, the reader is referred to the web version of this article).

microstructural grains are oriented along the build direction, which may affect the mechanical properties of the structure when loaded along the vertical direction in the image.

5. Design and technological measures to improve the fatigue behaviour

All the manufacturing errors and imperfections in the metal additive manufacturing process conceivably play a role in reduced mechanical performance and especially in reliability of the structures produced. For this reason, it is crucial to find ways to mitigate these errors, improve the quality of the parts produced, and to design parts to limit the influence of the manufacturing errors. This section highlights some ways to improve quality to specifically enhance fatigue performance.

5.1. Process parameters for lattice materials

As is known from the additive manufacturing of bulk material, the process parameters for L-PBF must be optimized and refined to produce the best quality defect-free parts. Despite the understanding of this concept and the availability of optimal process parameters for specific materials, even small variations in the build conditions can influence the meltpool conditions; for example, a locally increased temperature may create a deeper penetration, but stronger meltpool dynamics, to cause more entrapped pores and more spatter formation. As shown in [190], the formation of porosity varies with process parameters and never truly reaches absolute zero – some small pores are always present even in the most optimized case.

As lattice structures typically require only a few tracks alongside one another in individual layers to be melted, this can create significantly different conditions from the bulk manufacturing situation. In addition, since less material is typically present below the solidified material, thermal energy may be more difficult to dissipate, which entirely changes the local thermal properties for the next layer; this then affects the residual stresses, microstructure development and the possible formation of small porosity. For these reasons, a detailed analysis of lattice structures is essential, and process parameters, compared to bulk manufacturing, may need modification for the generation of lattices.

An example of this was presented by Kelly et al. (Fig. 25) who showed with micro-CT scans the presence of extensive porosity inside the walls of sheet-based TPMS cellular structures. By refining the process parameters, these authors demonstrated far less such porosity in the walls of samples produced using the refined parameters. Indeed, their optimized parts displayed improved mechanical properties, with a specific improvement for samples with thicker walls in both static and fatigue tests; thin-wall samples, however, showed no difference, likely due to the overriding effect of their surface condition [106].

In addition to optimized process parameters, the use of contour tracks can serve to improve the surface quality. This was studied and optimized by process parameter variations for the contour tracks, independently of the hatch tracks, in [142]; this work demonstrated the realization of improved fatigue properties as a consequence. The

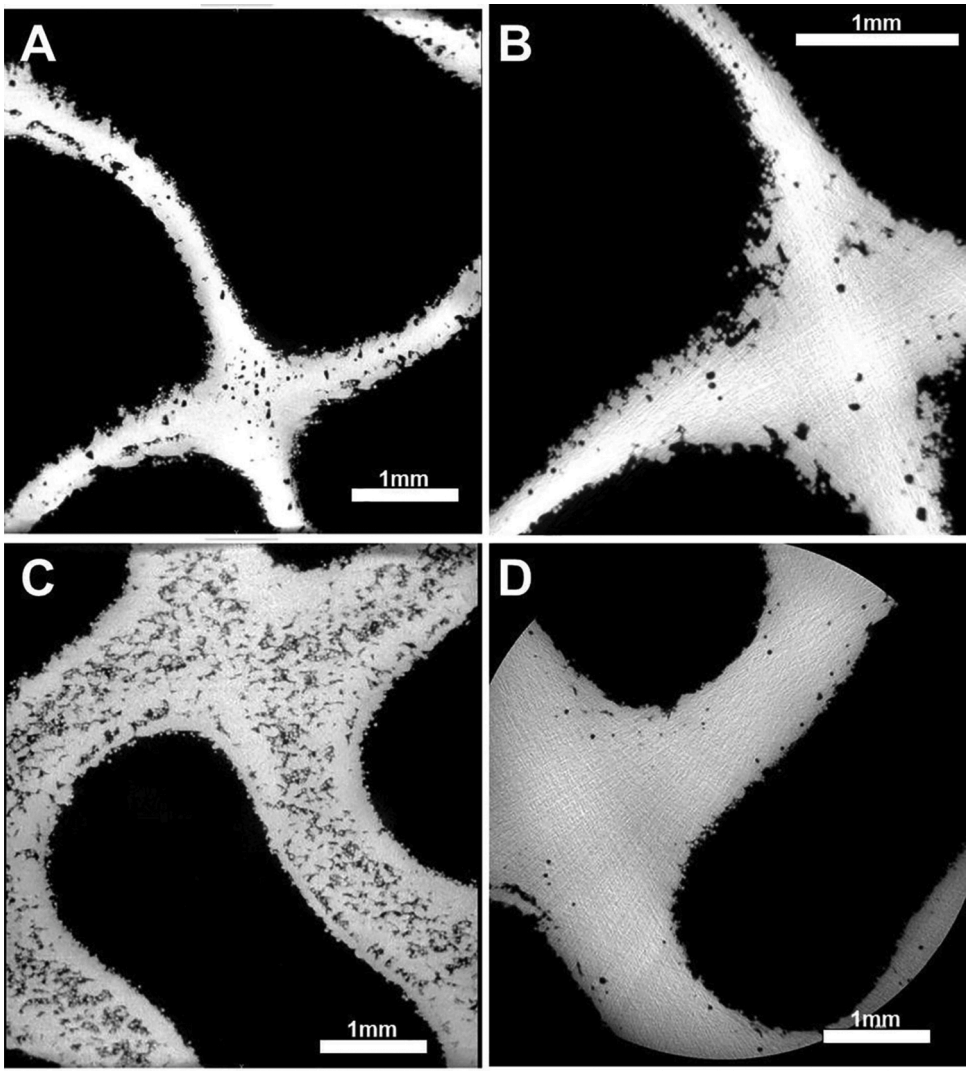

Fig. 25. Porosity in struts of gyroid sheet lattices in the 2019 study by Kelly et al. [106]. Imaging by micro-CT cross sections reveal that the effect of porosity can result in much reduced fatigue strength and enhanced fatigue life scatter, depending on the location of the porosity in the structure.

influence of process parameters, contour scans and skywriting strategies were also studied in relation to upskin and downskin surface roughness on inclined surfaces in [189]. In a recent study of gyroid lattice structures, one set of parts was manufactured without contour tracks, resulting in poorer mechanical properties [180] due to the rougher surface resulting from not employing contour tracks.

5.2. Improving geometrical accuracy

From the discussion presented in Section 4.2, it is clear that ideally the lattice should be manufactured as close as possible to that of the design and the surface quality should be carefully considered. In part, this translates to a design problem; specifically, the manufacturability of the design and the associated design rules must be kept in mind [191]. For example, long slender struts may easily trigger manufacturing errors or may require supports, defeating the purpose of using a cellular design (as support structures cannot be removed from inside a lattice structure). For these reasons, self-supporting lattice structures are particularly of interest [15]. One category of lattices which have emerged with these properties is the class of triply periodic minimal surfaces (TPMS), see Fig. 6B and C.In a comparison study of the morphologies of sheet-based and strut-based TPMS lattice structures reported in [190], it was shown how mean sheet thicknesses of 150−250 μm correlate to strut thicknesses of 300–700 μm for equivalent structures (at the same density). In a different study comparing sheet based and strut based lattices [192], poor fatigue performance of the sheet-based designs was attributed to notch-like surface defects prevalent in the sheet structures, but failure still occurred at nodes and junctions in both sheet and strut based designs.

Other design rules would be avoid the minimum feature size of the system by selecting thicker struts that can be manufactured with better geometrical accuracy. Since the mechanical properties (stiffness and strength) of metamaterials depend on the ratio between characteristic dimensions of the unit cell, an increment in strut thickness can be obtained without altering the design properties of the metamaterial only by upscaling the unit cell, *i.e.*, with a larger unit cell with the same density would have a thicker strut. In a recent investigation, Dallago et al. [37] compared the fatigue strength of cellular lattice specimens made up of filleted cubic cells with different cell sizes. Strut thickness and fillet radius were adapted to obtain the same apparent density and resulting elastic modulus of 3 GPa. The results are shown in Fig. 26. Increasing the cell size from 1.5 mm to 3 mm resulted in an improved manufacturing accuracy of the lattice and consequently in a significant fatigue strength enhancement (by a factor of 2). Another difference for this improvement in fatigue performance was presumed to be the different building direction used to fabricate the thinnest struts

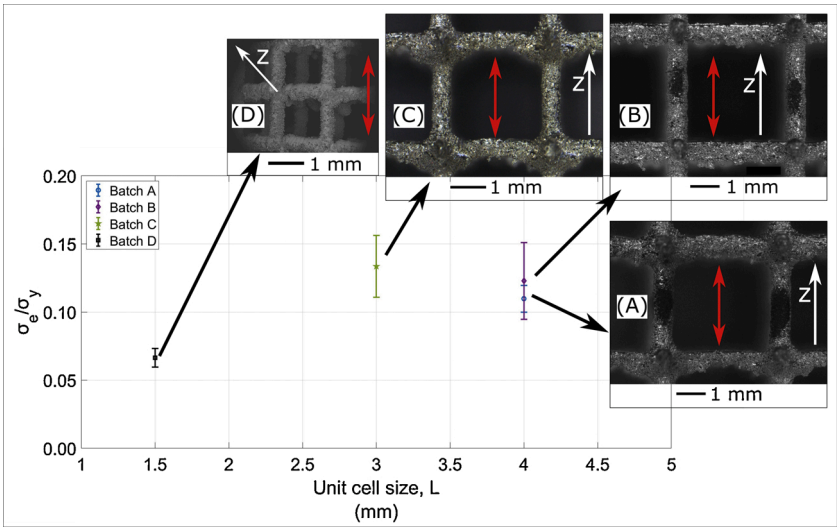

Fig. 26. Effect of cell size on the normalized fatigue strength of cellular lattice specimens made up of filleted cubic cells [37,129]. White arrows indicate the building direction, red arrows the fully-reversed fatigue loading direction. σ_e is the fully-reversed fatigue strength at 10^6 cycles, σ_y the yield strength. (For interpretation of the references to colour in this figure legend, the reader is referred to the web version of this article).

(indicated by white arrow in Fig. 26). Although more work is still needed to fully understand this behaviour, we can argue the existence of a manufacturability threshold, below which the fatigue properties declines considerably. For an acceptable fatigue design, it is therefore essential to identify whether such manufacturability threshold exists for each selected cell topology and AM process/material.

Moreover, the orientation of the struts has to be taken into account; struts oriented in the direction of the applied load provide a higher contribution to the overall mechanical performance of the lattice. In other words, the defects on these struts have a stronger influence than those affecting struts that carry a lower fraction of the load [137]. As a general rule, struts laying in the building plane (horizontal struts) should be avoided because, especially if they are oriented in the loading direction, they can considerably alter the mechanical properties of the lattice [151]. This is, however, not straightforward, as different cell topologies have different amounts of vertical features and even different strut or wall thicknesses for the same total density of the structure. As a rule of thumb, the fatigue designer should opt for cell architectures that allow all the struts to be manufactured at a sufficiently high angle (>30° [38]) with respect to the printing direction. For instance, this occurs in cubic (if printed along the cell diagonal) and diamond cells [130]. If the required type of unit cell does not apply to this building criterion, it is of paramount importance to quantify the fatigue strength of the struts as a function of their orientation with respect to the building plane. In this regard, Persenot et al. [193] investigated the effect of the building direction on the fatigue strength of single struts, and showed that geometrical inaccuracies mainly affected the struts built parallel to the printing plane, leading to a dramatic reduction in fatigue strength. The building direction dependent fatigue characteristics of the single struts were then incorporated by Burr et al. [133] into a numerical framework which provides a means to predict the fatigue strength of a complex lattice structure composed of octet-truss unit cells.

5.3. Filleted nodes

Nodal regions at which struts intersect in strut-based lattice materials are known to be critical locations that can dictate their structural integrity. Indeed, in the vicinity of the nodes, stresses are the highest because of two concomitant effects: (i) the axial loads transmitted through the struts must be transmitted through nodes where the load bearing area is lower because of the overlapping strut volume; (ii) changes in cross-section at strut intersections invariably lead to local stress concentrations, especially when the struts are loaded in tension [95]. For these reasons, the majority of investigations carried out on the fatigue of lattice metamaterials (and reviewed in Section 4.3) attested that fatigue crack initiation occurred at, or near, strut intersections. In particular, the conclusions of ref. [123], which are summarized in Fig. 27, are of note. Fatigue cracks were found to nucleate close to lattice nodes on the outer surface of horizontal struts (Fig. 27A, B, C), which, as discussed in Section 4.2, are more severely affected by geometrical imperfections. From the FEM simulations shown in Fig. 27D on the base of a CT reconstruction of the real geometry, it can be argued that the stress concentration effect at the nodes acts synergistically with local geometrical imperfections, such as reentrant notch-like corners, surface roughness and satellite powder particles [123,129,130,133,194]. Conversely, internal defects, even if located in the nodal regions, play a marginal role in triggering the fatigue damage [123,129,133,173], but nevertheless they still might play a role in changing the local stress distribution.

From the above discussion, it is clear that design measures able to mitigate the stress concentration near nodes are of paramount importance to devise fatigue resistant cellular materials. An effective way to achieve this goal is to employ gradual transitions in strut cross-section area, such as those obtained with the use of fillets to eliminate discontinuities in the tangent along the cell's outer boundary surfaces that lead to stress singularities [195]. By estimating the stress concentration factor in planar square cell lattices as a function of the fillet radius at the nodes, Dallago et al. [196] showed the attenuation of the stress peak near the lattice nodes with increasing fillet radius. Further investigations by Dallago et al. [197], Refai et al. [198], Savio et al. [199] and Latture et al. [95] demonstrated that the presence of filleted and spherical nodes increases the nodal stiffness and therefore affects the orthotropic elastic constants of the metamaterial. The resulting stiffening effect must be then included in the design of the cellular materials, not only to achieve the highest fatigue strength but also to satisfy stiffness requirements [196]. Khalil Abad et al. [200] observed that fillets, which remove the discontinuity in the outer surface tangent (surface first derivative), but not that in the curvature (surface second derivative), are affected by stress peaks at the location of the curvature discontinuity. Therefore, these authors devised continuous curvature hexagonal and square lattices with improved fatigue strength with respect to lattice counterparts with conventional circular fillets. Unfortunately, no experimental validation has as yet been provided to confirm their design solution.

Fig. 28 shows the outcomes of a recent fatigue testing program

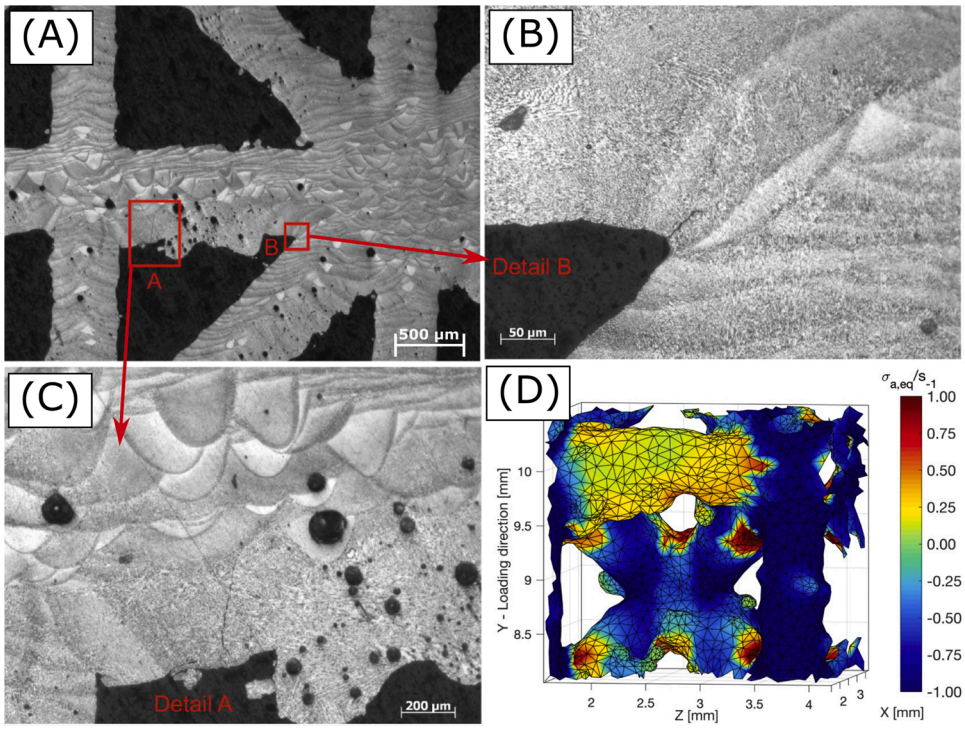

Fig. 27. Fatigue cracks in FCC lattices made of $AlSi_7Mg$ [123]. (A), (B), (C) Optical micrograph showing crack initiation in a horizontal strut at a geometrical imperfection located in the vicinity of the node. (D) stress distribution estimated from FEM simulations of the real lattice geometry reconstructed via CT scans. Hot spots (red coloured regions) are located in the vicinity of lattice nodes. (For interpretation of the references to colour in this figure legend, the reader is referred to the web version of this article).

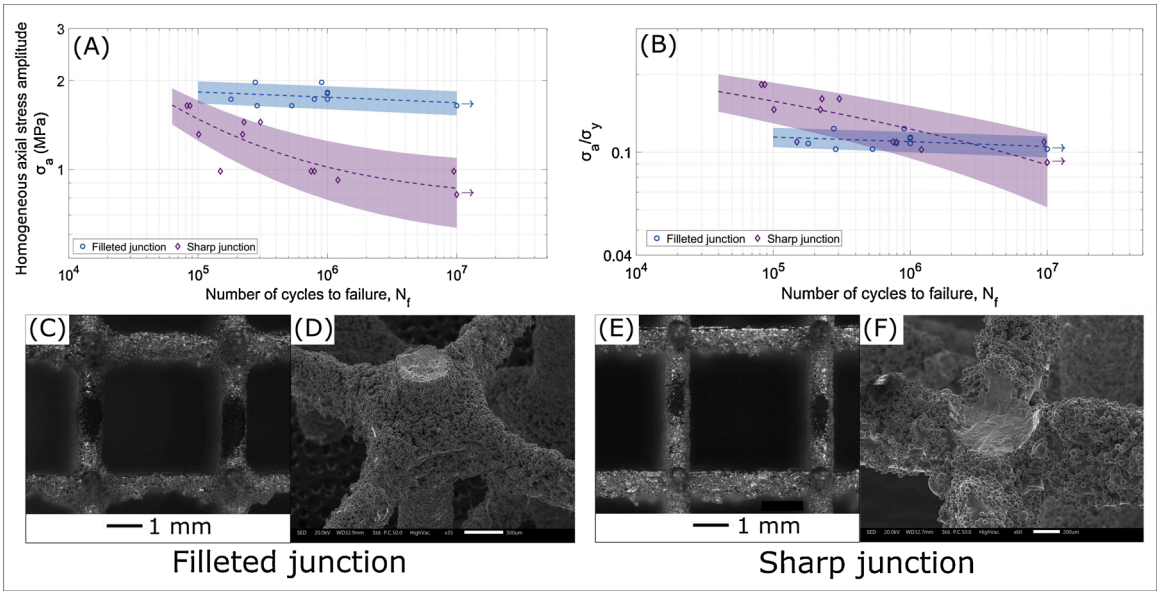

Fig. 28. Results of fatigue experiments performed on cubic lattice materials designed with filleted (C) and sharp (E) strut junctions. S/N curves are expressed in terms of homogeneous (A) and (B) normalized axial stress. The fatigue fracture surface near the filleted junction (D) and at the sharp edge between intersecting struts (F) [37].

carried out on cubic lattice materials, which were designed either with (Fig. 28C) or without (Fig. 28E) filleted strut junctions [37]. The resulting S/N curves are compared in Fig. 28A in terms of the homogeneous (global) axial stress where a marked beneficial effect of introducing filleted nodes is evident; in fact, the high fatigue strength is improved by a factor of nearly 2. As noted above, fatigue crack initiation occurred near, but not at, the node in the case of filleted nodes (Fig. 28D), presumably at the point of curvature discontinuity, whereas with the sharp junctions, fatigue cracks nucleated at the location of the sharp edge between intersecting struts (Fig. 28F). Interestingly, if the S/N curves are normalized with respect to the yield stress of the lattice material, the two curves nearly overlap. This suggests that filleted nodes are not only beneficial to the fatigue strength but also to the monotonic mechanical properties such as the strength [95].

Very recently, Savio et al. [201,202], applied a subdivision surface modelling approach based on Catmull and Clark's recursive algorithm [203] to generate cubic lattice structures with continuous shape variation as the limit of a sequence of successive refinements of a mesh. Fig. 29A compares three different node topologies at the intersection among circular struts: non-filleted node (CY), node with conventional fillet surfaces (CYF, surface continuity class C1), and node obtained after 3 iterations of the Catmull-Clark subdivision scheme (CC, asymptotic

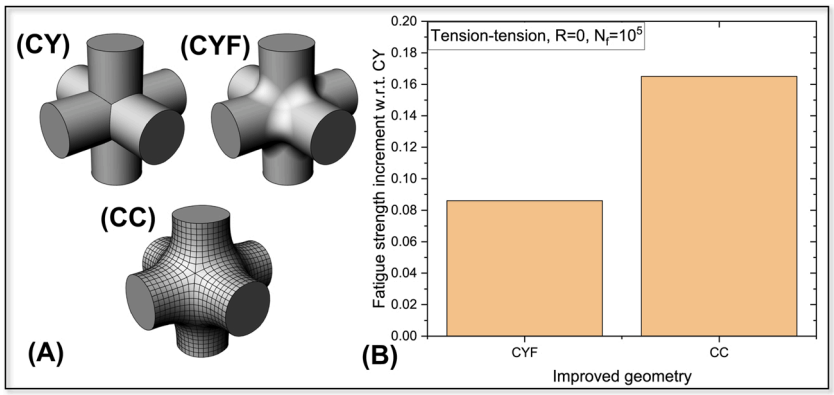

Fig. 29. (A) Cubic unit cells without fillet (CY), with conventional fillet (CYF) and with continuous shape variation (CC) [202]. (B) The increment in tension-tension fatigue strength with respect to the CY node topology. The fatigue strength data were taken from [202], where the cellular lattice samples with cell topologies indicated in (A) were AMed using polyamide.

surface continuity class C2). In [202], cellular lattice specimens with the above-mentioned three cell topologies were fabricated by AM of a polyamide polymeric material in order to conduct tension-tension fatigue tests. The results are summarized in Fig. 29B in terms of the improvement in fatigue strength (defined at 10^5 cycles to failure) with respect to that of the non-filleted cell architecture CY. The beneficial effect of conventional fillets (CYF) is here confirmed (8% fatigue strength increment). Interestingly, the cell topology with the continuous shape variation (CC) outperforms the CYF, with a two-fold fatigue strength increment (nearly 16 %). However, further investigations are needed to assess the beneficial effect of this design strategy on the fatigue strength of metallic materials, as fatigue and ductility properties of metals are entirely different from those of the polyamide material investigated in [202].

Triply periodic minimal surface (TPMS) designs can be considered an extension of the concept of continuous curvature nodes introduced above. They are however designed mathematically in either skeletal (cellular) or sheet-based varieties (Fig. 6, [77]). The skeletal versions, such as the skeletal gyroid, resemble strut-based lattices with continuous curves. The curvature of these structures serves to improve their manufacturability and hence their conformance to CAD design, surface quality and fatigue performance. An example of a skeletal gyroid manufactured in Ti6Al4V by L-PBF is shown in Fig. 30 in a cropped micro-CT view of one unit cell of a larger structure. The colour-coding shows the local stress distribution in a linear elastic compression loading simulation on the actual geometry. Stresses are highest between "nodes" on the down-facing surfaces. Sheet-based structures have been studied extensively due to their potential for implant applications, as reported in [49,106]. Despite their potential, the minimum sheet thickness is a practical manufacturing issue for sheet-based TPMS designs. For example, comparing skeletal and sheet-based gyroids, for the same density structures with the same unit cell sizes, the sheet thickness is much lower than the skeletal gyroid "strut thickness", as pointed out in [190]. In this latter work, the measurement of pore sizes and strut thickness is also discussed in detail - it is important to realize that pore sizes and strut thickness varies within a structure and multiple pore sizes and strut thicknesses exist depending on the geometry. However, the TPMS designs (both sheet and skeletal) show more homogeneous thickness distributions, compared to strut-based designs.

5.4. *Topology and simulation optimized lattices*

Regular repeated unit cells of fixed size, which are tessellated to fill a given 3D design space, represent a simple solution to lattice generation, although it is not always be the optimal solution. If one considers real objects with complex curved geometries, latticing specific regions will lead to edge effects whereby parts of the lattice unit are "cut off" arbitrarily at the ends. This leads to unexpected and unwanted edge effects, which can be overcome by creating lattices with varied sizes to fit the space, *e.g.*, conformal lattice geometries stretched to match the exterior

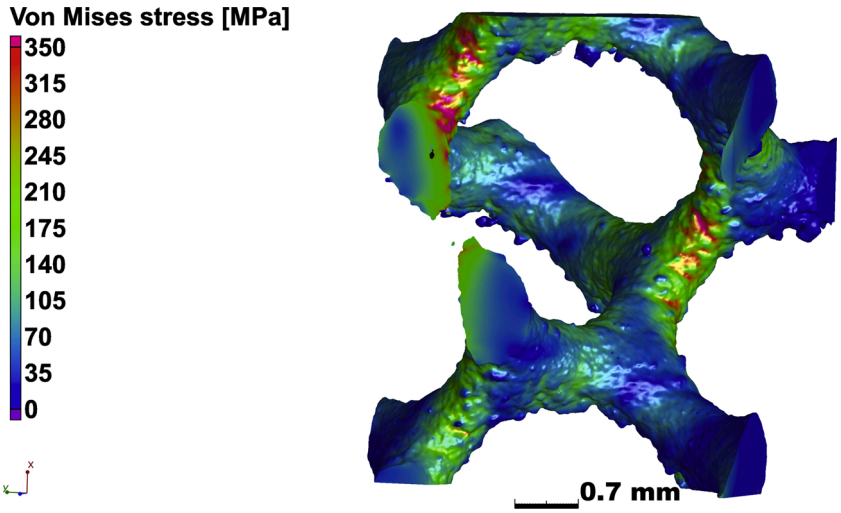

Fig. 30. Micro-CT image of real geometry of skeletal gyroid lattice with compression load simulation, showing the highest stresses in downward facing surfaces with irregular morphology, between "nodes".

geometry. Conformal lattice generation is possible by stretching unit cells near the edges to match the geometry or topology of the exterior of the part. Related to this is the concept of gradient lattices which vary their density locally across the structure; these have been investigated widely recently for their potential application in implants [204].

Topology optimization (also termed "generative design") in general refers to simulation-driven design of the optimal material distribution for a structure, assuming specific load cases. This method is now popular in additive manufacturing to provide lightweight parts with optimized stiffness, as discussed in detail in [12,13,205]. What is not widely utilized yet is the capability to design lattice structures using the same concepts. Using a given set of loads and boundary constraints, a target mass fraction and a design set of strut thicknesses and length ranges, it is possible to design an arbitrary simulation-optimized lattice structure. This has the potential to further implement manufacturing constraints such as specific build angle limits and slenderness ratios (*e.g.*, too long and thin struts excluded from the possibilities). Topology optimization itself may also be used in the design of the unit cells of lattice structures, and has been implemented with some success, as described in [206–208]. All the above-mentioned optimized designs implement some form of reduction of stress concentration, which should lead to improved fatigue performance.

5.5. Thermo- chemo- mechanical treatments

Section 4 showed that metallic cellular metamaterials fabricated by powder bed fusion processes are affected by a fine and anisotropic microstructure (resulting from the high cooling rate, especially in L-PBF), high surface roughness, internal porosity and residual stresses [28,209]. All these factors can adversely impact ductility and fatigue strength [30]. Post-build treatments are often necessary to mitigate or eliminate such detrimental effects [28,30,146], to achieve final application readiness.

In general, a post-heat treatment is necessary to relieve residual stresses, prevent distortions and restore a minimum material ductility. This is generally performed at low temperatures to not affect the fine microstructure, which is acicular martensitic in non-austenitic steels [210] and α and α+β Ti-alloys [146]. In case the microstructure is not suitable for the final application, post-heat treatments are carried out at higher temperatures to recrystallize and homogenise the microstructure as well as to eliminate dendritic structures [211]; this very often results in a noticeable increment in material ductility [212]. For aluminium alloys [213] and maraging steels [214], the post-build solution treatment can be then accompanied by an ageing treatment to promote precipitation hardening and improve the mechanical properties. In general, post heat treatments resulting in a ductility increment are beneficial to the fatigue strength as well [146,215], even though the heat treatments aimed at maximizing the fatigue strength must in general achieve the highest possible gain in ductility without excessive loss in tensile strength [216].

Hot isostatic pressing (HIP) is a powerful thermo-mechanical treatment aimed at closing internal pores and improving the microstructure of parts [217,218], significantly improving the fatigue properties of fully solid AMed components [40,146]. Although this process usually does not affect the surface, it was recently shown that when near-surface porosity is present, this may be exposed by the HIP process, leaving effectively deep notches in the surface [219], which can negatively affect fatigue performance. The best solution to prevent this is to ensure defect-free manufacturing parameters, using HIP only to eliminate the few remaining pores and to improve the microstructure. The effects of surface roughness and porosity in combination with HIP and other post processing is discussed in [220] with respect to fatigue properties. The effectiveness of such treatments in improving the fatigue strength of AMed cellular metamaterials will be discussed in the following sections.

Other popular forms of post-processing which may affect the surface quality includes mechanical machining or polishing, laser shock peening or shot peening, and chemical treatment. Mechanical processing is simplest and offers the best improvement in the surface condition [40] but is not possible in complex geometries such as cellular structures. Shot peening and laser shock peening has the effect of introducing a surface compressive stress and surface smoothing, both of which are good for fatigue properties [146,221,222], but this requires direct line of sight access for processing, which is not possible inside cellular structures. Conversely, sand-blasting, employing a very fine abrasive medium proved to be quite effective in improving the fatigue strength of cellular lattice samples [116], sometimes in combination with a preliminary HIP post treatment [181]. Chemical treatment provides an alternative [146] and has been demonstrated with some success in cellular structures [163,223], with the only disadvantage being the removal of material. It is possible to take this into consideration in the design phase and manufacture the lattices with thicker struts, but the material removal must be further investigated [110]. The influence of roughness and its correlation with fatigue properties improvement by chemical etching in lattice structures was recently reported in [223] using X-ray tomography evaluation of the surfaces. Chemical etching may, however, vary in efficiency depending on the lattice geometry and its permeability properties. It proved to be particularly effective in enhancing the fatigue strength of cellular metamaterials when applied in combination with a HIP post treatment [116,181]. Another surface finishing possibility is abrasive flow machining, demonstrated to improve the surface inside conformal cooling channels in [224], but this has not yet been applied to lattice structures.

To provide the reader with a quantitative assessment of the fatigue strength improvement made possible by the aforementioned post-build treatments, Fig. 31E summarizes the average fatigue strength increment with respect to the as-built condition reported in the literature for several post treatments applied to cellular metamaterials made up of Ti-6Al-4 V [103,110,111,116,181]. Heat treatments below β-transus (~1000 °C, HTsub) enhance the fatigue strength by about 15 %. The majority of AMed materials are operated in service in this condition. A higher fatigue increment is achieved by heat treatments above β-transus (HTsup) [215]. Sand-blasting (SB) alone induces a fatigue strength comparable to HTsub, which can be mainly ascribed to the removal of satellite powder particles (compare Fig. 31A with B). Interestingly, HIP treatments allow for average fatigue increments comparable to those induced by thermal treatments only. This relatively modest increment in fatigue strength, in comparison with HIPed fully solid components [40,217,220], confirms the observations made in Section 5.3 about the predominant role played by surface geometrical imperfections in dictating the fatigue strength of cellular metamaterials. Consequently, the beneficial effect exerted by HIP is ascribable mostly to the improvement in microstructure and ductility and only marginally to the elimination of internal porosity. This latter beneficial effect is evident only if HIP is accompanied by a surface treatment, like sandblasting or chemical etching (CE), as shown in Fig. 31C, E. Chemical etching in particular is able to improve the surface quality of struts and nodes and to eliminate brittle α-case [36], which is sometimes caused by HIP due to inevitable oxygen contamination of the argon atmosphere in which the treatment is conducted (see white arrows in Fig. 31D).

5.6. Novel materials

Before concluding this section devoted to design measures aimed at improving the fatigue strength of cellular metamaterials, it is worth emphasizing that the important role played by the base material should not be overlooked and needs to be further investigated. This is particularly evident looking at Fig. 15, *viz.* the very different normalized fatigue strengths displayed by metamaterials with nominally identical cell architecture and porosity but with a different base material. Interestingly, the lower band of the plot is occupied by the cellular metamaterials made of the metallic alloy that is so far the most investigated in the literature for this application, namely Ti-6Al-4 V. Accordingly, the

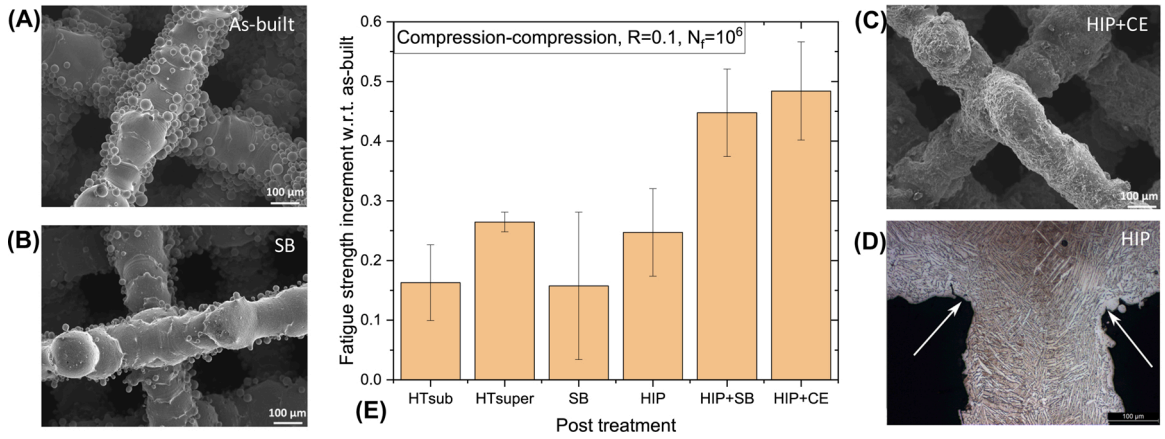

Fig. 31. Effect of post-build treatments on the 10^6 cycles compression-compression fatigue strength of cellular metamaterials made of Ti-6Al-4 V. SEM micrographs of (A) as-built, (B) sand-blasted and (C) HIPed and chemical etched diamond lattice [116]. (D) Optimal micrograph of the microstructure of HIPed cubic lattice; arrows indicate brittle α-case [36]. (E) increment in fatigue strength with respect to the as-built conditions. HTsub: heat treatment below β-transus (~1000 °C). HTsuper: heat treatment above β-transus. SB: sand blasting. HIP: hot isostatic pressing. HIP + SB: HIP followed by sand blasting. HIP + CE: HIP followed by chemical etching. Error bands refer to 1 standard deviation.

normalized fatigue strength is well below 0.4, a threshold that is typical of fully-solid metallic materials [135]. For bulk Ti-6Al-4 V, this threshold is even higher, ~0.6 [225]. The reason for this dramatic reduction in normalized fatigue strength is not fully clear as yet, but it can be argued that Ti-6Al-4 V suffers from limited ductility when fabricated via PBF and this impacts detrimentally on the fatigue strength of cellular metamaterials carrying a plethora of stress raisers. Another explanation is related to a lower geometrical error and surface condition, which may affect cellular materials more than the bulk material, especially in this material. For these reasons, the scientific community is now researching alternative metallic materials with improved ductility and manufacturability. Pure metals in general tend to display higher ductility than their alloyed counterparts [68]. Indeed, looking at Fig. 15, cellular metamaterials made of pure metals generally exhibit superior normalized fatigue strength. A careful reader might object that pure metals display also a lower yield strength and this fact must be taken into account when looking at the absolute values of the fatigue strength. Nevertheless, Wauthle et al. [68] demonstrated that pure titanium metamaterials show higher high-cycle fatigue strength than their Ti-6Al-4 V counterparts, which conversely display higher static and low-cycle fatigue properties. Popular metal alloys that can be manufactured by additive manufacturing and which have high ductility are Co-Cr [114,226], stainless steel [38] and Inconel [74]. These can be good candidates for manufacturing fatigue-resistant metamaterials, but the existing literature is very limited, even though the preliminary results plotted in Fig. 15 are quite promising. Ni-Ti (Nitinol) deserves also to be mentioned, even though lattice cellular specimens made of this material displayed a fatigue strength on the lower band of the plot reported in Fig. 15. This alloy is very prominent in the biomedical filed due to its superelastic properties and exceptional corrosion resistance. Its fatigue behaviour, however, is complex due to the *in situ* presence of a stress-induced phase transformation from a tetragonal to monoclinic structure, both of which have differing fatigue properties [227]. Perhaps a better comprehension of the fatigue mechanisms along with an improvement in the fabrication accuracy of the cellular lattice material might lead to a significant enhancement in their fatigue strength [228]. Finally, high-entropy alloys (HEA) are a new generation of metallic alloys, some of which have unprecedented mechanical properties [229,230]. Investigations on their manufacturability via PBF are still underway [231–233]. Cellular metamaterials made of HEAs have not been reported in the literature yet, but we are sure they will belong to the metamaterials of the future. Auxetic lattices [234,235], are another emerging class of metamaterials with the appealing characteristic of displaying a negative Poisson's ratio conferred by the particular cell architecture (Fig. 6). Preliminary investigations suggest a beneficial effect of such elastic properties on their fatigue performance [236].

6. Fatigue verification and design of architected cellular lattice materials

In previous sections, the common lattice architectures and the experimental aspect of fatigue analysis of cellular structures were reviewed and discussed. As a successful tool to gain a better understanding of fatigue failure mechanisms and to incorporate the key influencing factors in design against fatigue, theoretical and numerical techniques can be utilized. In conventional manufacturing technologies, a given material with specific and well-known material properties is often used for subtractive production of the mechanical parts. In this scenario, given the known material properties, the mechanical behaviour of the part can be evaluated using the available theoretical models in the literature. In contrast, while using AM as the manufacturing technology, the material properties depend highly on the fabrication process and the input geometry of the part. AM parts may contain specific small porosities, can be anisotropic, and have inherent rough surfaces, all related to the underlying fabrication strategy, which in turn depends on the geometry of the part. In this scenario, designers can face a dilemma. On the one hand, AM technology is able to produce parts with complex geometries which were previously not possible to produce. On the other hand, the processes are complex, often resulting in poorly known material properties of AM parts, making their failure prediction under complex loading conditions a difficult task.

To develop a theoretical interpretation of structural integrity of these geometrically complex components under monotonic and cyclic loading conditions is then a fundamental step for taking advantage of AM technology in structural components. Until now, few design protocols have been proposed in the literature, taking into account accurate microstructural features as well as specific mechanical behaviour as a function of the input geometry and fabrication routine. Hence, as a strategic point, it is important to fill this knowledge gap to allow future designers and customers to take full advantage of the unique characteristics of AM, making it an integrated every-day manufacturing technique.

Although the majority of engineering structures are subjected to the loads which result in elastic stress/strains under normal conditions, the presence of geometrical discontinuities can lead to local yielding of the material under cyclic loading. Hence, a cyclic load will invariably have a detrimental effect on the mechanical resistance of a lattice structure. Various factors such as alternating and mean stress, loading frequency,

environmental conditions, and the macroscopic and microscopic morphology of the structure, specifically the overall geometry of the lattice part and the geometry of its unit cell, all govern fatigue failure [200]. Performing fatigue tests are usually time consuming and costly; accordingly, through consideration of the various key factors in defining the outcome of the design, such as relative density and cell size, numerous fatigue tests should be performed to develop a clear understanding of the designed lattice structure. In this regard, supplementing these experimental measurements with a theoretical/numerical package to evaluate the fatigue behaviour of lattice structures prior to fabrication is undoubtedly beneficial.

6.1. Fatigue prediction methodologies

Numerous efforts since the 1950s have been made to predict mechanical behaviour of lattice structures under monotonic loading [237]. The prediction of mechanical behaviour has been recently improved by adoption of advanced finite element (FE) methods. Despite the significant number of proposed methodologies for failure prediction under monotonic loading, limited corresponding efforts have been made to evaluate the structural integrity of these structures under cyclic loading. This is possibly due to the rather large number of participating factors which will make systematic fatigue analysis of lattice structures expensive and time-consuming. However, since fatigue is invariably the most prominent degradation mechanism in actual structures and components, this is a situation that must be rectified. To this end, several fatigue prediction techniques have been proposed for lattice structures. These can be categorized into four main groups which are described below.

6.1.1. Global failure

Dealing with the compression fatigue loading condition, McCullough et al. [238] proposed a simple model based on the creep model of Gibson and Ashby [47] which takes into account the accumulation of ratcheting strain during fatigue loading (Eq. (6)). Using the material properties of the base material and global stress applied to the lattice, this model proposes that the fatigue life of a porous structure can be predicted using the expression given below [238]:

$$\frac{1}{N_f} = \frac{C_3(1-R)^p}{\varepsilon_y}\frac{0.6}{n+2}\left[\frac{1.7(2n+1)}{n}\frac{|\sigma|_{\max}}{\sigma_0}\right]^n\left(\frac{\rho}{\rho_0}\right)^{\frac{(3n+1)}{2}} \tag{6}$$

where N_f is the fatigue life, C_3, p, and σ_0 are material constants, R is the stress ratio, $|\sigma|_{\max}$ is the maximum loading stress (*i.e.*, the fatigue strength), and ε_y is the monotonic yield strain. By combining the previous equations for a given number of cycles, it is then possible to obtain relationships between the fatigue strength, relative density, and modulus of the porous structure. Since the proposed formulation is based on plastic deformation accumulation at an early stage of fatigue cycling prior to fatigue crack propagation, it is expected to provide more accurate results when the fatigue mechanism of the lattice structure is dominated by cyclic ratcheting during cyclic deformation [105]. Indeed, Eq. (6) has been shown to successfully predict the fatigue life of certain AM porous structures [65].

Li et al. [109] performed experimental analysis on Ti-6Al-4 V lattice structures produced by electron beam powder bed fusion and reported that both cyclic ratcheting of the lattice struts and fatigue crack initiation and propagation through the struts play important roles in the fatigue damage of the structure. Following the suggestions of Lemaitre et al. [239] for cyclic damage, dD/dN, based on cyclic ratcheting strain, ε_c, and cyclic plastic strain, ε_p, they reported the following equation for fatigue life prediction in AM lattice structures as:

$$\frac{dD}{dN} = \frac{1}{\varepsilon_f}\left\{C_3(1-R)^p\frac{0.6}{n+2}\left[\frac{1.7(2n+1)}{n}\frac{|\sigma|_{\max}}{\sigma_0}\right]^n\left(\frac{\rho}{\rho_0}\right)^{\frac{(3n+1)}{2}} + C_4\varepsilon_y\left(\frac{\rho^2}{|\sigma|_{\max}\rho_0^2}\right)^{-\alpha/\beta}\right\} \tag{7}$$

in which ε_f is the ductility of the material, and C_4, α, and β are material constants. The mentioned formulas provide an estimation of fatigue life based on the overall mechanical properties and loading condition. However, they do not specifically consider the sole influence of geometrical discontinuities in their formulation. In this regard, Yang et al. [103] suggested replacing the maximum loading stress in Eq. (7) with the local maximum stress $|\sigma|_{\max}$, thus converting the analysis more toward a local evaluation of fatigue with the help of numerical analysis.

6.1.2. Local failure (stress and strain)

Due to the local nature of fatigue failure, especially in geometrically complex components, numerous fatigue failure approaches have been presented in the literature for fatigue prediction by means of local evaluation of a key parameter (*e.g.*, stress, strain, strain energy, etc.) at the notch root [240]. Getting inspiration from these classic fatigue assessment techniques, researchers in this field have evaluated the stress/strain distribution in the lattice model using numerical techniques such as FEM. The local stress and strain values at the vicinity of stress concentration were then considered as input for fatigue assessment based on stress-life approaches such as the Basquin S/N [120] and strain-life approaches such as Coffin-Manson law [102] to predict the fatigue failure in the high-cycle fatigue (HCF) and low-cycle fatigue (LCF) regimes. The overall approach presumes that the fatigue life of cellular structures can then be predicted based on the mechanical properties of the base material.

Numerous research studies have evaluated the geometry of connections (local notches) in lattice structures to reduce the stress concentration in the area close to the junctions, with the objective of improving the fatigue life of the designed lattice [200,241,242]. In these studies, minimizing the linear elastic stress at the notch root was the goal. Furthermore, the use of a gradient of unit cell porosity within the lattice structure was reported to improve its overall stiffness compatibility in the case of biomedical applications [243].

On the question of lifetime prediction, Lipinski et al. [122] reported more accurate estimations of fatigue life by incorporating a stress gradient in their fatigue analysis. They performed theoretical and numerical analysis on porous implant models and reported notch sensitivity relations as a function of the lattice geometry. Peng et al. [244] performed parametric analysis on four different architectures of lattice structures. Following the procedure shown in Fig. 32, they obtained stress-life curves of the studied structures through the use of the Brown-Miller theory [245] (Eq. (8)). According to approach, the maximum fatigue damage is modelled to occur on the plane which experiences the maximum shear strain amplitude, such that:

$$\frac{\Delta\gamma_{\max}}{2} + \frac{\Delta\varepsilon_n}{2} = 1.65\frac{\sigma_f^{'}}{E}(2N_f)^b + 1.75\varepsilon_f^{'}(2N_f)^c \tag{8}$$

where $\Delta\gamma_{\max}$ is the maximum range of the shear strain, $\Delta\varepsilon_n$ is the maximum range of the normal strain, $\sigma_f^{'}$ is the fatigue strength coefficient, $\varepsilon_f^{'}$ is the fatigue ductility coefficient, b is the fatigue strength exponent, c is the fatigue ductility exponent, and $2N_f$ is the endurance in terms of stress reversals. In addition to a comparative study of different architectures, by performing more than 400 analyses, the detailed dependency of the fatigue behaviour to the scale, presence of geometrical imperfections, and relative density of the lattice structures was evaluated [244].

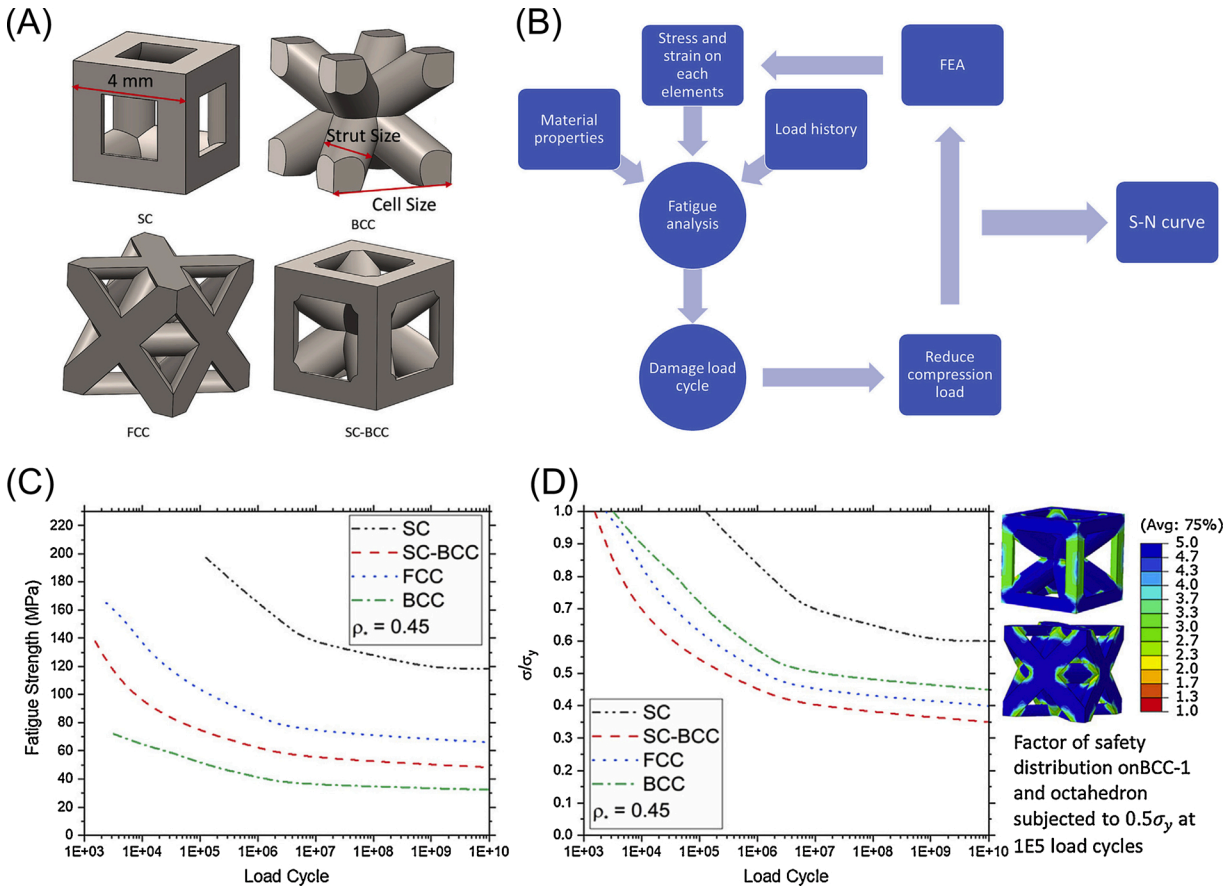

Fig. 32. An overview of the research in [244]; (A) Geometries of Simple Cubic (SC), Body Centered Cubic (BCC), Simple Cubic Body Centred Cubic (SCBCC) and Face Centred Cubic (FCC) lattice unit cells; (B) Numerical algorithm to determine the S/N curve; (C) S/N curve for different lattice structures with a relative density of 0.45; (D) Normalized S/N curve for different lattice structures with a relative density of 0.45.

With respect to the issue of the effect of mean stress effect on the fatigue life of lattice structures, Jamshidinia et al. [246] performed experimental and numerical analyses on a dental implant produced by EB-PBF. According to their numerical results, the Soderberg model provided more accurate predictions of fatigue life compared to Goodman and Gerber models. See Section 2.3 for more information about these mean-stress models.

6.1.3. Fatigue crack growth life

According to fracture mechanics approach, the fatigue failure of lattice structures can be divided into two stages of microcracking and macrocrack propagation, characterized by continuous reduction of stiffness of cellular structures [107,123,246]. Under cyclic loading, the material deterioration results in creation of microcracks in the struts of the structure. Propagation of these microcracks follows the equation also known as the Paris law. According to the Paris law, the fatigue crack growth rate, da/dN, of microcracks can be expressed as [247]:

$$\frac{da}{dN} = A\left(\frac{1.683\Delta Pl\sqrt{\pi a}}{t^2}\right)^m \tag{9}$$

in which A and m are empirical material constants, ΔP is the cyclic concentrated force range per unit thickness of the strut, l and t are the length and thickness of the strut, and a is the length of microcrack.

Propagation of the microcracks in the weakest strut will eventually result in its failure. At this point, the fatigue crack is presumed to propagate to the neighbouring cell with the growth rate of this microcrack, of a length equal to the width of the cell, a^*, can be written as:

$$\frac{da^*}{dN^*} = A_1^*\left(\Delta K_1^*\right)^m \tag{10}$$

in which A_1^* is a function of strut length and relative density of the cellular structure and $\Delta K_1^* = \Delta\sigma^*\sqrt{\pi a^*}$ ($\Delta\sigma^*$ is the cyclic stress range on cellular structure). The same formulation was then extended for the case of high-cycle and low-cycle fatigue failure of 2D lattice structures by use of the Basquin equation and the Coffin-Manson law, respectively [247]. Using this formulation, Huang et al. evaluated the fatigue behaviour of periodic cellular solids (honeycombs and foams) under uniaxial [247], in-plane multiaxial [248] and general multiaxial [249] loading conditions. Based on the proposed methodology, the fatigue behaviour of cellular material with a desired density can be predicted if experimental data on the fatigue of one particular density of the cellular structure with the same cell architecture and the same bulk material is known. They reported a dependency of fatigue crack growth behaviour to the cyclic stress-intensity range, the cell geometry, relative density of cellular material, and fatigue properties of the bulk material. In these studies, the cell walls were assumed to bend similar to a beam. However, according to Simone and Gibson [250], since beam elements cannot accurately capture the real stress distribution in the lattice wall, their application (instead of continuum elements) can lead to unrealistic results that possibly will limit the use of these methods for fatigue design.

6.1.4. Damage accumulation

Another strategy in theoretical fatigue prediction of lattice structures consists of using the stress-life curve for single struts to predict the overall fatigue behaviour including the chronology of local failures occurring in the lattice structure. In this scenario, the progressive stress redistribution within the unbroken struts of the lattice and the local damage in each strut during the whole cyclic process should be taken into account. From this perspective, some research studies have relied

on a damage-mechanics approach, such as using a damage accumulation relationship based on Miner's rule [251].

According to Miner's rule [251,252], applying n_i cycles with a stress amplitude $S_{a,i}$ and corresponding fatigue life of N_i is equivalent to consuming a portion of $D_i = n_i/N_i$ of the total fatigue life. Fatigue failure occurs when 100 % of the fatigue life is consumed (Eq. (11)), or some fraction of it based on the use of a safety factor. Restricting this analysis to the fatigue crack initiation life of small specimens, Miner proposed the mentioned rule by the assumption that the total fatigue life until failure is approximately the same as the fatigue crack initiation life [34]. This relationship was later further modified to consider non-linear damage function and challenging loading conditions such as the effect of periodic overloads [253–255].

$$\sum D_i = \sum \frac{n_i}{N_i} = 1 \tag{11}$$

To apply Miner's rule specifically for lattice structures, one approach is to sum the resulting damage within the struts at the different applied stress levels to provide an estimation of the total fatigue life.

Hedayati et al. [98,256], analysed the fatigue resistance of three different elementary cells namely diamond, rhombic dodecahedron, and truncated cuboctahedron by considering the stiffness drop due to damage in the struts prior to fatigue failure. Using the material properties (*i.e.*, monotonic elastic-plastic constitutive law and S/N data) of the parent material (and not the struts), they proposed an iterative algorithm (Fig. 33) in which each FE simulation cycle represented a number of loading-unloading cycles, Δn_i. This increment of cycles evolves depending on the failure events occurring during cycling. To account for the effect of stress concentrations, a single stress concentration factor, k_f, was used for each type of lattice structure. This stress concentration factor was obtained using trial-and-error correction to obtain numerical fatigue life close to the experimental data. The effect of stiffness reduction in the model was then taken into account through the use of the following relationship:

$$E_{i,j}=E(1-D_{i,j}) \tag{12}$$

where $E_{i,j}$is the elastic modulus of strut i and $D_{i,j}$ is the accumulated damage to strut i obtained from Miner's rule (both corresponding to the simulation cycle j). The elements with a larger damage value than unity were removed from the model during the numerical simulation. Comparison of the numerical results, with and without stiffness degradation, revealed that the models with a stiffness degradation present a smoother change in the maximum displacement model as well as the elastic modulus of the lattice structure during cyclic loading. In this case, the damage process started earlier and ended later than the model without stiffness degradation resulting in longer predicted fatigue lives. Further studies are required to evaluate the accuracy of these two procedures in simulating the progressive damage in the lattice structures. However, the proposed methodology by Hedayati et al. [98,256], does result in acceptable failure predictions when the load level does not exceeding 60 % of the yield strength.

By neglecting the stiffness change due to damage and considering the progressive fatigue damage to be governed solely by a series of successive failures in struts, Zargarian et al. [97,174], proposed a numerical method through the use of a linear elastic FE analysis to predict the fatigue life of lattice structures (Fig. 34). These authors used the material properties of single struts from experimental data in the literature and claimed that by doing so their model is capable of taking into account residual stress, crystalline grain size variations, and stress concentration. The geometrical irregularities in the AM lattice structures were modelled by assigning a random cross-section to each element of the strut along its length (Fig. 34B). Using Basquin's equation applied to single struts and considering the mean stress correction formula, they were able to simulate fatigue failure under a specific cyclic macro-stress (*i.e.*, stress applied to the whole lattice structure). Unlike the relatively continuous damaging process in the work of Hedayati et al. [98,256]. Zargarian et al. considered a discontinuous damage process that is only updated once a strut has failed (*i.e.*, the strut reaches its fatigue life under a given maximum stress). Using an iterative algorithm, the strut(s) with the lowest fatigue life was removed in each simulation cycle and the induced damage due to failure of that strut was implemented in fatigue calculations using Miner's rule. Summation of the fatigue lives of the weakest struts after cyclic simulation was then introduced as the total fatigue life of the lattice structure. It is worth mentioning that a similar simulation procedure was previously proposed by Demiray et al. [257] for open-cell foams.

In the aforementioned damage accumulation techniques, a unique S/N curve of the constitutive material was used for the fatigue behaviour at the scale of individual struts, meaning that all the struts had identical fatigue properties. However, due to geometrical and microstructural inconsistencies of AM parts, a relatively large scatter has been reported for the experimental fatigue results of single struts [133]. To study the effect of scatter in the S/N data and the spread of strut radius size distribution on the accuracy of life predictions, Burr et al. [133] used the methodology proposed by Zargarian et al. [97,174]. They assigned a radius and an S/N curve to every strut of the lattice structure and performed statistical analysis on the effect of these two key parameters on the fatigue life. According to their findings, for their studied as-built cases, the radius distribution seems to have a larger impact on the accuracy of the fatigue life predictions compared to the S/N curve distribution (*i.e.*, the scatter in fatigue data). An increase in both strut radius size distribution and dispersion of the S/N curve distribution resulted in a fatigue life reduction [133]. Although the fatigue predictions using these analyses were in relatively good agreement with experimental results, the effect of radius variation along the strut length, possible bending contribution to stress in struts, and geometrical singularities were not accurately taken into account in their method and must therefore be considered as possible sources of error.

As mentioned earlier, damage accumulation leads to stress redistribution in the lattice structure up to the moment of final failure. By utilizing a functionally graded lattice structure, one can in principle control the damage propagation and postpone the fatigue failure and consequently increase the fatigue life of the lattice structure. Zhao et al. [105] reported superior fatigue properties for functionally graded Ti-6Al-4 V lattice structures compared to ordinary uniform lattice structures. According to their findings, the crack propagation in lattices with higher strength was retarded by the stress redistribution in lattices with lower strength. This eventually resulted in a variation in the cyclic ratcheting rate in the lattice structure. They qualitatively correlated the damage accumulation to their experimental observations. Further studies should be performed to evaluate the applicability of the available fatigue prediction methodologies for functionally graded lattice structures.

7. Advanced fatigue design of AM cellular lattice materials

Closer inspection of the literature on lattice materials shows that the majority of the fatigue design methods rely on experiments, which are customized to handle selected lattice architectures and materials. This is time-consuming and often expensive. The available theoretical approaches, on the other hand, seem to lack accuracy, mainly because of their simplified methodology which might fail to capture the real stress distribution in the lattice structure [200]. In the absence of residual stresses, the sources of variability that may affect the fatigue behaviour of lattice structures can be categorized as surface roughness, geometrical accuracy, and local microstructure [132]. The surface roughness of AM parts involves a large number of local defects (also known as micro-notches) which act as stress raisers and are considered as potential locations for fatigue crack initiation. To incorporate a more detailed topology of the lattice structures in the fatigue prediction routine, inspection techniques such as X-ray tomography can be used.

In this framework, FE analysis has been recently used on the real

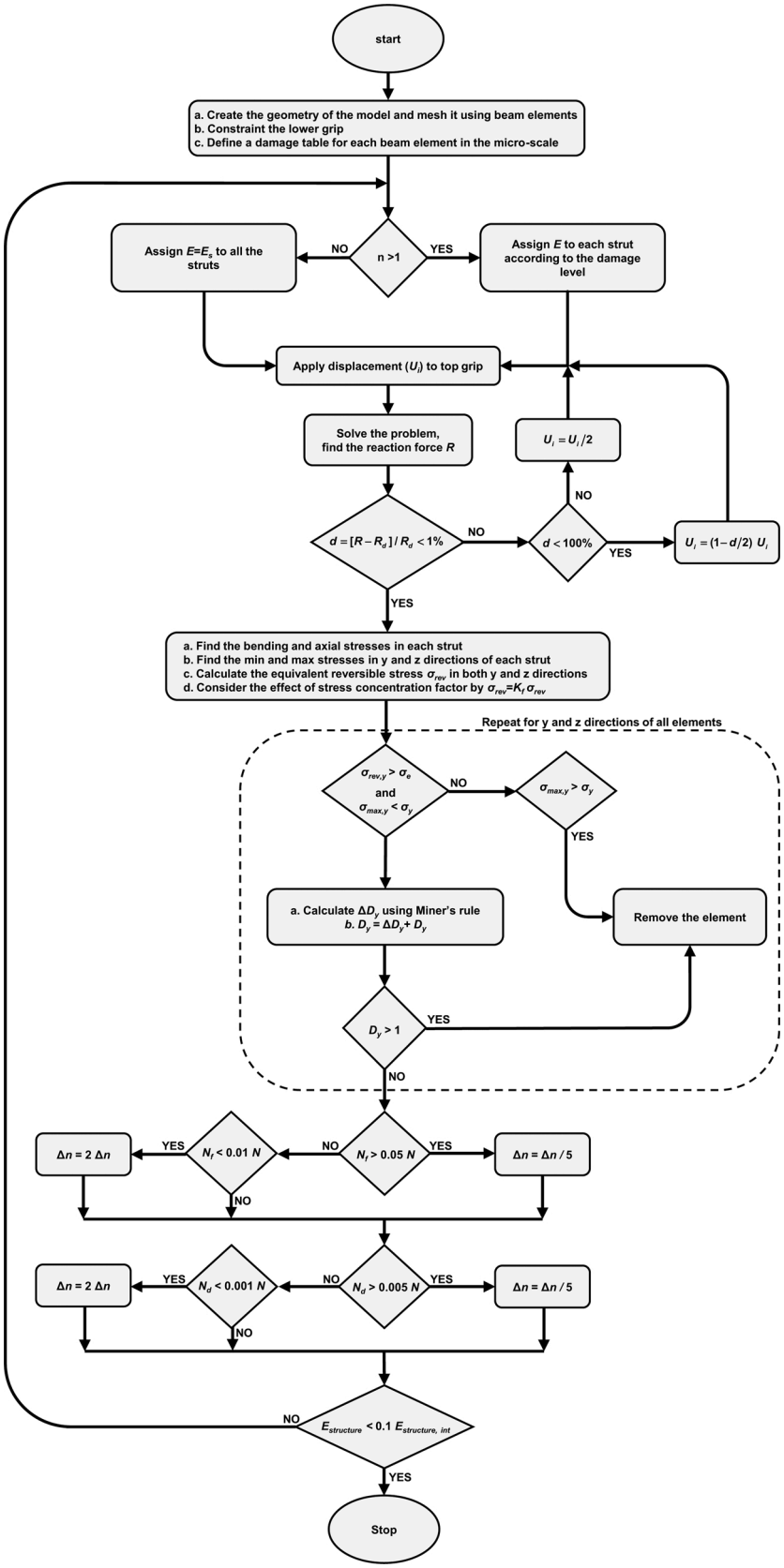

Fig. 33. The numerical algorithm proposed in [254,255], for micro-scale fatigue assessment of lattice structures.

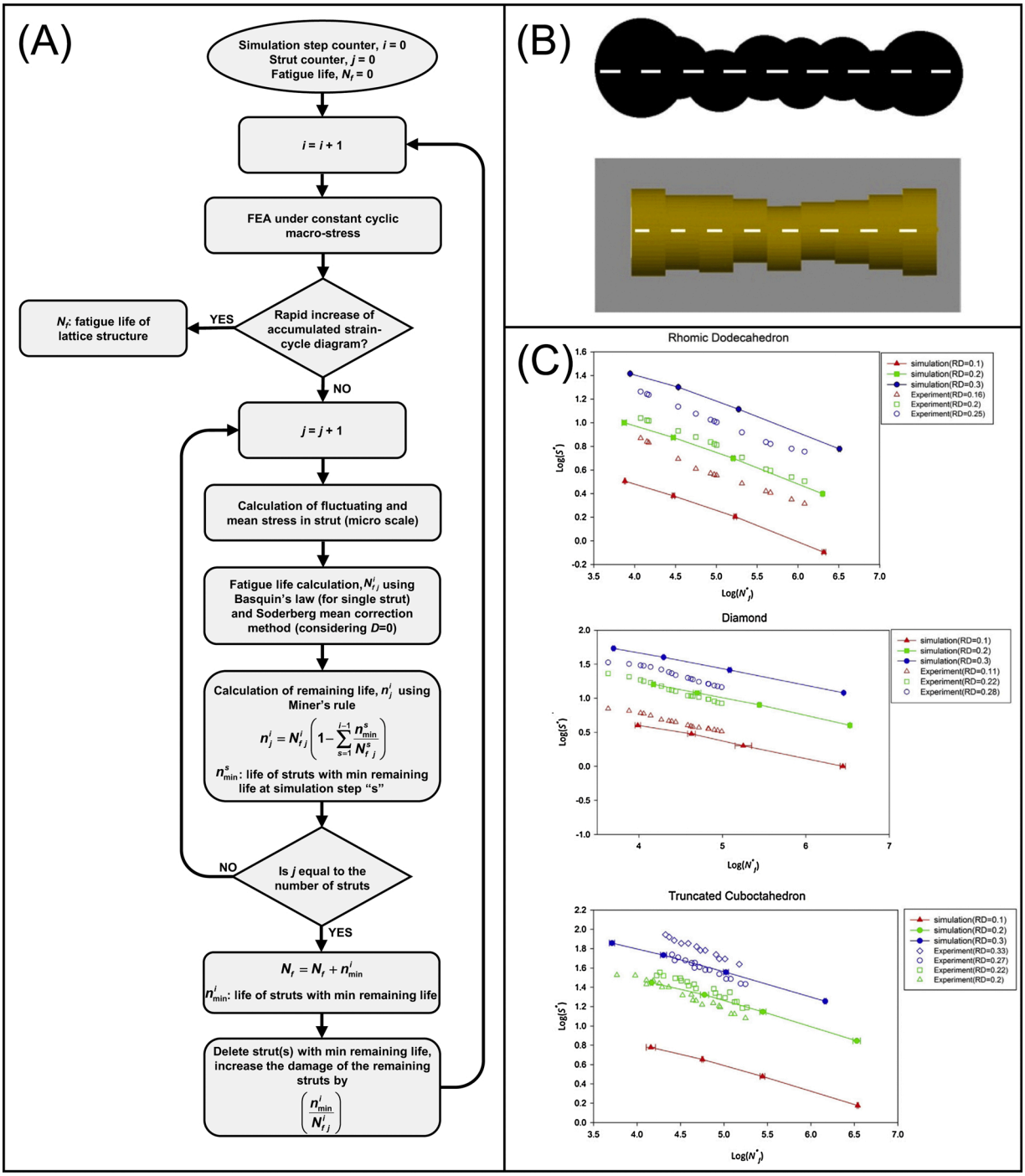

Fig. 34. (A) Numerical algorithm proposed in [97,174], (B) Details of the meshing in single struts with variable radius along the strut length, (C) Comparative fatigue data obtained from numerical simulation and experiments.

geometry of a lattice structure to compare the stress-state in real and the nominal CAD geometries in order to qualitatively correlate the numerical results to the experimental fatigue data [112,139]. FE analyses of stress distributions at the strut junctions revealed higher stress concentration in the model with the as-built geometry acquired with a micro-CT scan of a specimen; however, these values were still lower than the expected stress concentration from the experiments (see Fig. 35 for the FE models) [36]. This was reported to be due to the smoothening procedure, performed for meshing the FE model, that resulted in decreased severity (to a certain degree) of the surface notches, although the presence of residual stresses in the structure, even after stress relief heat treatment, could also markedly influence the accuracy of the numerical analyses [36].

Under uniaxial fatigue loading, the presence of localized stresses in the struts will result in a multiaxial, non-symmetric, and non-uniform state of stress in the lattice. Therefore, a fatigue criterion that is capable of addressing stress multiaxiality in the presence of a mean stress and a stress gradient should be employed for these complex structures [123]. The primary results of a fatigue prediction strategy addressing these specific points was reported by Boniotti et al. [123]. After performing stress analysis on the FE model constructed by a micro-CT scan of the lattice, the theory of critical distance (TCD) was employed for fatigue life prediction. In order to address the multiaxiality, the stress amplitudes were calculated based on the equivalent

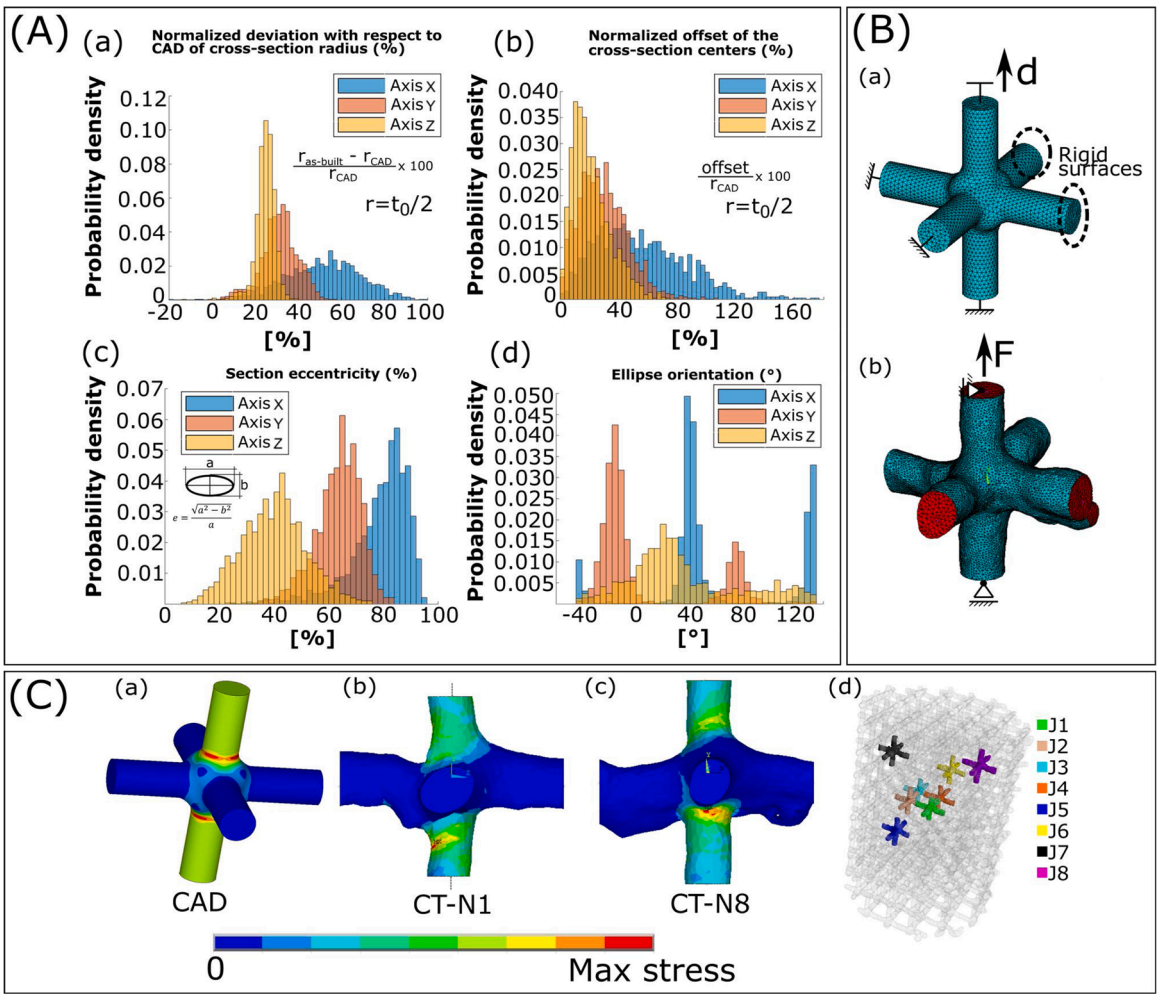

Fig. 35. (A) Results of statistical analysis on the point cloud obtained by a micro-CT scan of a regular cubic cellular lattice produced by L-PBF (t_0: strut diameter), (B) FE models based on nominal CAD and real geometries, (C) von Mises contour plots obtained from the FE analyses. The FE mesh was chosen to be close to that of the resolution of the micro-CT spatial. The unit cell FE models based on real geometry were selected randomly from the micro-CT scan of the lattice [36].

von Mises stress proposed by Sines [258]. In this scenario, for each node, the average equivalent stress amplitude was determined in a spherical control volume around it. The radius of the control volume was set to El-Haddad's size parameter [259] obtained from fatigue assessment of the same material [260]. Fatigue crack initiation was then expected to occur in the FE model when the local equivalent stress amplitude is greater than the fatigue strength of the material. Using this methodology, successful fatigue life, and failure location prediction were reported.

In general, the size effect has been recognized to be mainly related to the geometrical scale (*e.g.*, specimen thickness/diameter) and the microstructural scale (*e.g.*, grain or phase size in the material) [261–265]. In order to address a combined effect of these two scales, an aspect ratio (t/d) of the specimen thickness/diameter, t, to the grain size, d, can be introduced. This ratio was proven to have a significant impact on the mechanical properties when the values of t and d are in the same order [266]. The scale and thickness effect on mechanical behaviour of conventional materials has been previously studied using experimental and theoretical studies [267–269]. The experimental results on conventionally fabricated metallic materials show that when $t/d \gg 1$, both LCF and HCF strengths are controlled by the grain size d. When $3 < t/d < 25$, the fatigue life depends on the crack propagation life, while for $t/d < 3$ it depends on the crack initiation life. For small scale specimens ($20\ \mu m < t < 200\ \mu m$), both the LCF and HCF strengths are governed by the specimen thickness and independent of t/d. However, there is still a knowledge gap in this regard in the field of AM components. In AM parts, the microstructure, internal defects, and surface condition are dependent on both process parameters and the geometry and scale of the part. To the best of the authors' knowledge, the studies on this aspect are only limited to the experimental aspect of scale effect on microstructures [270–275], tensile properties [274,275], and fatigue properties [154, 275]. By considering the mentioned factors, the scale and build thickness effect may not follow the rule derived from conventional materials and still needs to be elucidated.

An appropriate fatigue prediction methodology should be capable of addressing intrinsic factors associated with microstructures (t, d, t/d) but also the extrinsic factors related to defects (internal defects and surface roughness) [269]. To capture the effect of intrinsic factors, microstructure-sensitive fatigue models (*e.g.*, multiscale fatigue model [276,277]) can be used. As for the extrinsic factors, defect-sensitive fatigue models such as the $\sqrt{area}$ (the square root of the equivalent defect area projected onto the loading plane) model and Kitagawa-Takahashi diagram have been shown to successfully predict the fatigue life of certain AM parts [220,278,279].

In general, it is still a difficult task to incorporate all the aforementioned models together in a suitable fatigue model to capture material, geometry, and scale-dependent properties of AM components. Hence, a more practical fatigue prediction methodology can rely on the combination of a large amount of experimental data, theoretical computations, and machine learning [269].

Finally, it is noteworthy that over the last decade, a large amount of literature has emerged in the context of machine learning algorithms and data driven approaches [280]. Modern machine learning algorithms are able to learn highly complex nonlinear relationships between predictor and target variables, even in highly stochastic environments. Very recent applications of machine learning to additive manufacturing have been developed focusing on different aspects, such as quality detection during or post-manufacturing, optimisation problems around build process parameters and final design assessment [281–285]. Data-driven approaches and their applications to fracture mechanics problems are nowadays a hot research topic which is being investigated by top researchers in the field [286–291] and is beginning to show an impressive potential for future applications. This immense knowledge currently under intense development will be surely useful in the future to better correlate and assess the fatigue performances based on process parameters, geometrical desired features and topological optimization. Data driven approaches will take advantages of the recent developments and findings on the influence of defects and porosities on the fatigue strength [292–299]. This will be coupled with the full understanding of three-dimensional effects in presence of geometrical discontinuities [300–304] and the application of proper local advanced fatigue criteria which is nowadays a field of active research with continuous progress [305–316]. This will allow to create the appropriate domain knowledge for a proper and efficient application of data-driven approaches.

8. Summary and outlook

AM processes are now increasingly employed in different strategic fields such as aerospace, automotive and medical industries because of many unique possibilities of producing value added components that could not be easily produced by traditional manufacturing processing. There are several synergistic factors for the expansion and continuous growth and development of additive manufacturing processes. Among these factors there is the continuous improvement of computational means and the valuable knowledge of metallurgy and fusion welding. However, several technological challenges are now affecting AM products quality and costs. This includes defects in parts such as pores, lack of fusion, poor surface finish, residual stresses and distortion. These challenges need to be addressed to allow the commercial employment of AM at large scale. The full control of the mechanical properties both under static and cyclic loading is the key of the future success. This requires a deep understanding of AM processes and the final impact on the produced parts. A substantial progress for better understanding the interaction between AM processes and the final structural integrity of the realized parts will be the key to avoid common defects and to tailor the structure and the desired final properties. In addition an increased level of standardization and control will be required to assure repeatable processes and to fabricate parts with consistent properties.

The rapid growth in advanced manufacturing processes has led to the emergence of mechanical metamaterial lattice structures. These light and high-performing structures have quickly spread out in several leading industrial sectors, and their full-scale employment is only a matter of time. Speeding up their use in real applications requires an intelligible understanding of their relevant parameters and the development of advanced approaches that allow to assess their mechanical properties and their failure response under different loading conditions. In fact, the functionality of the lattice structures is profoundly affected by process-induced defects. Optimization of the process parameters and post-heat treatments can highly improve the microstructure and the mechanical performances.

The many advantages of additive manufacturing and the control that it provides for economically creating metamaterial lattice structures with optimal shapes for specific components, coupled with such properties as lightweight, stiffness, and strength, etc., is undeniable, but fatigue is invariably the prime degradation mechanism in the vast majority of critical structures, oftentimes coupled with high temperatures (creep-fatigue) or adverse environments (corrosion fatigue). Unlike the *global* properties of stiffness and strength, premature fatigue failure is driven by *local* factors like defects, microstructural imperfections, surface roughness, and as this review has highlighted strut junctions in lattice structures; thus designing and manufacturing these materials with adequate fatigue resistance and with the ability to reliably predict their safe lifetimes represents a grand challenge.

The present critical review has summarised a significant amount of lattice structure-based literature in order to identify the potential and main limitations of these structures with specific emphasis on when they are subjected to cyclic fatigue loading. Our intent is to contribute to "filling the void" in the overall understanding of this critical feature in lattice structures – how fatigue can severely degrade their overall structural integrity and to provide a complete and updated state-of-the-art on how this problem can be addressed. The manufacturing of lattice structures using conventional manufacturing methods seems to be very prohibitive and accordingly, AM can play a fundamental role in this field. Lattice structures can be designed or tailored for achieving specific structural functionality and performance requirements. They are quite attractive because of their large surface area, low mass, regular repeated structure and open interconnected pore spaces. The advantage of additively manufactured lattice structures is the full and accurate control of the micro-architecture or even multi-scale structure. However, defects and imperfections cannot be completely removed and eliminated. Fatigue life can be significantly increased with *ad-hoc* post-heat treatments of the lattices due to the homogenization of the surfaces and the possibility of improving the ductility of their structure.

This review has also shown that substantial improvements have been achieved to better understand the structural behaviour of lattice structures, their overall properties and the possibilities of building final parts for real-life applications. This growing knowledge will allow to produce parts free of defects and reproducible at large scale. The capacity of fully assessing with precision the lifetime of lattice structures will be a fundamental step. The current rapid developments of data-driven approaches and the possibility of easily managing a large quantity of data in a structured way together with the capacity of topological optimizing a structure almost in real-time will lead to new possibilities and to a wide diffusion of AM lattice structures for the fabrication of commercial products.

Author Contribution

The authors equally contributed to the development of the present review paper.

Declaration of Competing Interest

The authors declare that they have no known competing financial interests or personal relationships that could have appeared to influence the work reported in this paper.

Acknowledgements

AdP acknowledges support from the South African Collaborative Program in Additive Manufacturing (CPAM), an initiative of the Department of Science and Innovation.

FB acknowledges the support for dissemination provided by the twinning program in the frame of SIRAMM project.

References

[1] A. Fuganti, L. Lorenzi, A. Grønsund, M. Langseth, Adv. Eng. Mater. 2 (4) (2000) 200–204, https://doi.org/10.1002/(SICI)1527-2648(200004)2:4<200::AID-ADEM200>3.3.CO;2-U.

[2] Y. Fujimori, S. Guo, K. Kitazono, J. Japan Inst. Light Met. 70 (8) (2020) 333–338, https://doi.org/10.2464/jilm.70.333.

[3] J.C. Najmon, J. DeHart, Z. Wood, A. Tovar, SAE Int. J. Transp. Saf. 6 (3) (2018), https://doi.org/10.4271/2018-01-1057, pp. 2018-01–1057.
[4] L.E. Murr, et al., Philos. Trans. R. Soc. A Math. Phys. Eng. Sci. 368 (1917) (2010) 1999–2032, https://doi.org/10.1098/rsta.2010.0010.
[5] N.A. Fleck, V.S. Deshpande, M.F. Ashby, Proc. R. Soc. A Math. Phys. Eng. Sci. 466 (2121) (2010) 2495–2516, https://doi.org/10.1098/rspa.2010.0215.
[6] M. Ashby, Philos. Trans. R. Soc. A Math. Phys. Eng. Sci. 364 (1838) (2006) 15–30, https://doi.org/10.1098/rsta.2005.1678.
[7] A. Vigliotti, D. Pasini, Comput. Methods Appl. Mech. Eng. 229–232 (2012) 27–43, https://doi.org/10.1016/j.cma.2012.03.018.
[8] L.J. Gibson, Annu. Rev. Mater. Sci. 30 (1) (2000) 191–227, https://doi.org/10.1146/annurev.matsci.30.1.191.
[9] M. Smith, Z. Guan, W.J. Cantwell, Int. J. Mech. Sci. 67 (2013) 28–41, https://doi.org/10.1016/j.ijmecsci.2012.12.004.
[10] X.P. Tan, Y.J. Tan, C.S.L. Chow, S.B. Tor, W.Y. Yeong, Mater. Sci. Eng. C 76 (2017) 1328–1343, https://doi.org/10.1016/j.msec.2017.02.094.
[11] S. Arabnejad, B. Johnston, M. Tanzer, D. Pasini, J. Orthop. Res. 35 (8) (2017) 1774–1783, https://doi.org/10.1002/jor.23445.
[12] A. du Plessis, et al., Addit. Manuf. 27 (2019) 408–427, https://doi.org/10.1016/j.addma.2019.03.033.
[13] M. Orme, I. Madera, M. Gschweitl, M. Ferrari, Designs 2 (4) (2018) 51, https://doi.org/10.3390/designs2040051.
[14] R. Willner, et al., J. Laser Appl. 32 (3) (2020) 032012, https://doi.org/10.2351/7.0000111.
[15] J. Plocher, A. Panesar, Mater. Des. 183 (2019) 108164, https://doi.org/10.1016/j.matdes.2019.108164.
[16] T. Vaneker, A. Bernard, G. Moroni, I. Gibson, Y. Zhang, CIRP Ann. Manuf. Technol. 69 (2) (2020) 578–599, https://doi.org/10.1016/j.cirp.2020.05.006.
[17] C. Pan, Y. Han, J. Lu, Appl. Sci. Basel (Basel) 10 (18) (2020) 6374, https://doi.org/10.3390/app10186374.
[18] A. Seharing, A.H. Azman, S. Abdullah, Adv. Mech. Eng. 12 (6) (2020), https://doi.org/10.1177/1687814020916951, p. 168781402091695.
[19] Riddell Partners with Carbon® to Produce First-Ever, 3D Printed Football Helmet Liner – Carbon, 2019. https://www.carbon3d.com/news/riddell-partners-with-carbon-to-produce-next-gen-football-helmet/.
[20] M. Alsulami, M. Mortazavi, S.A. Niknam, D. Li, Int. J. Adv. Manuf. Technol 110 (3–4) (2020) 865–873, https://doi.org/10.1007/s00170-020-05898-3.
[21] S. Catchpole-Smith, R.R.J. Sélo, A.W. Davis, I.A. Ashcroft, C.J. Tuck, A. Clare, Addit. Manuf. 30 (2019) 100846, https://doi.org/10.1016/j.addma.2019.100846.
[22] E. Sacco, S.K. Moon, Int. J. Adv. Manuf. Technol. 105 (10) (2019) 4123–4146, https://doi.org/10.1007/s00170-019-03786-z.
[23] P.R. Gradl, C.S. Protz, Acta Astronaut. 174 (2020) 148–158, https://doi.org/10.1016/j.actaastro.2020.04.067.
[24] T.D. Ngo, A. Kashani, G. Imbalzano, K.T.Q. Nguyen, D. Hui, Compos. Part B Eng. 143 (2018) 172–196, https://doi.org/10.1016/j.compositesb.2018.02.012.
[25] I. Gibson, D. Rosen, B. Stucker, Additive Manufacturing Technologies: 3D Printing, Rapid Prototyping, and Direct Digital Manufacturing, second edition, 2015.
[26] T. Debroy, et al., Prog. Mater. Sci. 92 (2018) 112–224, https://doi.org/10.1016/j.pmatsci.2017.10.001.
[27] A. Nazir, K.M. Abate, A. Kumar, J.Y. Jeng, Int. J. Adv. Manuf. Technol 104 (9–12) (2019) 3489–3510, https://doi.org/10.1007/s00170-019-04085-3.
[28] T. Vilaro, C. Colin, J.D. Bartout, Metall. Mater. Trans. A 42 (10) (2011) 3190–3199, https://doi.org/10.1007/s11661-011-0731-y.
[29] Q.C. Liu, J. Elambasseril, S.J. Sun, M. Leary, M. Brandt, P.K. Sharp, Adv. Mater. Res. 891–892 (2014) 1519–1524, https://doi.org/10.4028/www.scientific.net/AMR.891-892.1519.
[30] G. Kasperovich, J. Hausmann, J. Mater. Process. Technol. 220 (2015) 202–214, https://doi.org/10.1016/j.jmatprotec.2015.01.025.
[31] N. Sanaei, A. Fatemi, Prog. Mater. Sci. 100724 (2020), https://doi.org/10.1016/j.pmatsci.2020.100724.
[32] G. Bergmann, et al., Biomed. Mater. Eng. 20 (2) (2010) 65–75, https://doi.org/10.3233/BME-2010-0616.
[33] A.A. Zadpoor, Acta Biomater. 85 (2019) 41–59, https://doi.org/10.1016/j.actbio.2018.12.038.
[34] J. Schijve, Int. J. Fatigue 25 (8) (2003) 679–702, https://doi.org/10.1016/S0142-1123(03)00051-3.
[35] L. Liu, P. Kamm, F. García-Moreno, J. Banhart, D. Pasini, J. Mech. Phys. Solids 107 (2017) 160–184, https://doi.org/10.1016/j.jmps.2017.07.003.
[36] M. Dallago, B. Winiarski, F. Zanini, S. Carmignato, M. Benedetti, Int. J. Fatigue 124 (2018) 348–360, https://doi.org/10.1016/j.ijfatigue.2019.03.019.
[37] M. Dallago, S. Raghavendra, V. Luchin, G. Zappini, D. Pasini, M. Benedetti, Int. J. Fatigue (2020) 105946, https://doi.org/10.1016/j.ijfatigue.2020.105946.
[38] C. Yan, L. Hao, A. Hussein, P. Young, D. Raymont, Mater. Des. 55 (2014) 533–541, https://doi.org/10.1016/j.matdes.2013.10.027.
[39] T. Maconachie, et al., Mater. Des. 183 (2019) 108137, https://doi.org/10.1016/j.matdes.2019.108137.
[40] R. Molaei, et al., Int. J. Fatigue 132 (2020) 105363, https://doi.org/10.1016/j.ijfatigue.2019.105363.
[41] A. Yadollahi, N. Shamsaei, Int. J. Fatigue 98 (2017) 14–31, https://doi.org/10.1016/j.ijfatigue.2017.01.001.
[42] ASTM F2792-12a, Standard Terminology for Additive Manufacturing Technologies, ASTM International, West Conshohocken, PA, 2012, https://doi.org/10.1520/F2792-10.
[43] T.M. Mower, M.J. Long, Mater. Sci. Eng. A 651 (2016) 198–213, https://doi.org/10.1016/j.msea.2015.10.068.
[44] S.M.J. Razavi, F. Berto, Adv. Eng. Mater. 21 (8) (2019) 1900220, https://doi.org/10.1002/adem.201900220.
[45] A. Aramian, S.M.J. Razavi, Z. Sadeghian, F. Berto, Addit. Manuf 33 (2020) 101130, https://doi.org/10.1016/j.addma.2020.101130.
[46] B. Wysocki, P. Maj, R. Sitek, J. Buhagiar, K. Kurzydłowski, W. Święszkowski, Appl. Sci. Basel (Basel) 7 (7) (2017) 657, https://doi.org/10.3390/app7070657.
[47] L.J. Gibson, M.F. Ashby, Cellular Solids: Structure and Properties, 2nd ed., Cambridge University Press, Cambridge, 1999.
[48] V.S. Deshpande, M.F. Ashby, N.A. Fleck, Acta Mater. 49 (6) (2001) 1035–1040, https://doi.org/10.1016/S1359-6454(00)00379-7.
[49] F.S.L. Bobbert, et al., Acta Biomater. 53 (2017) 572–584, https://doi.org/10.1016/j.actbio.2017.02.024.
[50] M. Afshar, A.P. Anaraki, H. Montazerian, J. Kadkhodapour, J. Mech. Behav. Biomed. Mater. 62 (2016) 481–494, https://doi.org/10.1016/j.jmbbm.2016.05.027.
[51] H.A. Schwarz, Gesammelte Mathematische Abhandlungen, Springer, Berlin Heidelberg, 1890.
[52] K. Michielsen, J.S. Kole, Phys. Rev. B 68 (11) (2003) 115107, https://doi.org/10.1103/PhysRevB.68.115107.
[53] O. Al-Ketan, R.K.A. Al-Rub, R. Rowshan, Int. J. Adv. Mater. Technol. 2 (2) (2017) 1600235, https://doi.org/10.1002/admt.201600235.
[54] M. Leary, in: P. Woodhead, F. Froes, M. Qian (Eds.), Titanium in Medical and Dental Applications, 2018, pp. 203–224.
[55] L. Gibson, M. Ashby, B. Harley, Cellular Materials in Nature and Medicine, 2010.
[56] J. Kadkhodapour, et al., J. Mech. Behav. Biomed. Mater. 50 (2015) 180–191, https://doi.org/10.1016/j.jmbbm.2015.06.012.
[57] S. Ahmadi, et al., Materials (Basel). 8 (4) (2015) 1871–1896, https://doi.org/10.3390/ma8041871.
[58] C. Qiu, et al., Mater. Sci. Eng. A 628 (2015) 188–197, https://doi.org/10.1016/j.msea.2015.01.031.
[59] S. Raghavendra, et al., Proc. Inst. Mech. Eng. Part C J. Mech. Eng. Sci. 234 (16) (2020) 3241–3256, https://doi.org/10.1177/0954406220912786.
[60] Z. Hashin, J. Appl. Mech. 50 (1983) 481–505.
[61] S.J. Hollister, N. Kikuchi, Comput. Mech. 10 (1992) 73–95.
[62] M.M. Shahzamanian, et al., J. Eng. Mater. Technol. 136 (2014) 1–16, https://doi.org/10.1115/1.4025916.
[63] L.J. Gibson, M.F. Ashby, G.S. Schajer, C.I. Robertson, Proc. R. Soc. A Math. Phys. Eng. Sci. 382 (1982) 25–42.
[64] S. Ghouse, S. Babu, R.J. Van Arkel, K. Nai, P.A. Hooper, J.R.T. Jeffers, Mater. Des. 131 (2017) 498–508, https://doi.org/10.1016/j.matdes.2017.06.041.
[65] S. Ghouse, S. Babu, K. Nai, P.A. Hooper, J.R.T. Jeffers, Addit. Manuf. 22 (2018) 290–301, https://doi.org/10.1016/j.addma.2018.05.024.
[66] S. Amin Yavari, et al., Mater. Sci. Eng. C 33 (8) (2013) 4849–4858, https://doi.org/10.1016/j.msec.2013.08.006.
[67] X.Y. Cheng, et al., J. Mech. Behav. Biomed. Mater. 16 (2012) 153–162, https://doi.org/10.1016/j.jmbbm.2012.10.005.
[68] R. Wauthle, et al., Mater. Sci. Eng. C 54 (2015) 94–100, https://doi.org/10.1016/j.msec.2015.05.001.
[69] M. Leary, et al., Mater. Des. 98 (2016) 344–357, https://doi.org/10.1016/j.matdes.2016.02.127.
[70] M. Mazur, M. Leary, S. Sun, M. Vcelka, D. Shidid, M. Brandt, Int. J. Adv. Manuf. Technol. (2015), https://doi.org/10.1007/s00170-015-7655-4.
[71] M. Zhao, F. Liu, G. Fu, D. Zhang, T. Zhang, H. Zhou, Materials (Basel). 11 (12) (2018) 2411, https://doi.org/10.3390/ma11122411.
[72] R. Gümrük, R.A.W. Mines, S. Karadeniz, Mater. Sci. Eng. A 586 (2013) 392–406, https://doi.org/10.1016/j.msea.2013.07.070.
[73] S. Tsopanos, et al., J. Manuf. Sci. Eng. 132 (4) (2010), https://doi.org/10.1115/1.4001743.
[74] M. Leary, et al., Mater. Des. 157 (2018) 179–199, https://doi.org/10.1016/j.matdes.2018.06.010.
[75] S. Campanelli, N. Contuzzi, A. Ludovico, F. Caiazzo, F. Cardaropoli, V. Sergi, Materials (Basel). 7 (6) (2014) 4803–4822, https://doi.org/10.3390/ma7064803.
[76] S. Arabnejad, R. Burnett Johnston, J.A. Pura, B. Singh, M. Tanzer, D. Pasini, Acta Biomater. 30 (2016) 345–356, https://doi.org/10.1016/j.actbio.2015.10.048.
[77] O. Al-Ketan, R. Rowshan, R.K. Abu Al-Rub, Addit. Manuf. 19 (2018) 167–183, https://doi.org/10.1016/j.addma.2017.12.006.
[78] E. Yang, et al., Mater. Des. 184 (2019) 108165, https://doi.org/10.1016/j.matdes.2019.108165.
[79] C. Yan, L. Hao, A. Hussein, P. Young, J. Mech. Behav. Biomed. Mater. 51 (2015) 61–73, https://doi.org/10.1016/j.jmbbm.2015.06.024.
[80] E. Alabort, D. Barba, R.C. Reed, Scr. Mater. 164 (2019) 110–114, https://doi.org/10.1016/j.scriptamat.2019.01.022.
[81] J. Maszybrocka, B. Gapiński, M. Dworak, G. Skrabalak, A. Stwora, Int. J. Adv. Manuf. Technol 105 (7–8) (2019) 3411–3425, https://doi.org/10.1007/s00170-019-04422-6.
[82] S.J. Li, et al., Acta Biomater. 10 (10) (2014) 4537–4547, https://doi.org/10.1016/j.actbio.2014.06.010.
[83] J. Parthasarathy, B. Starly, S. Raman, A. Christensen, J. Mech. Behav. Biomed. Mater. 3 (3) (2010) 249–259, https://doi.org/10.1016/j.jmbbm.2009.10.006.
[84] H. Zaharin, et al., Materials (Basel). 11 (12) (2018) 2402, https://doi.org/10.3390/ma11122402.
[85] A. Cuadrado, A. Yánez, O. Martel, S. Deviaene, D. Monopoli, Mater. Des. 135 (2017) 309–318, https://doi.org/10.1016/j.matdes.2017.09.045.

[86] S.M. Ahmadi, et al., J. Mech. Behav. Biomed. Mater. 34 (2014) 106–115, https://doi.org/10.1016/j.jmbbm.2014.02.003.
[87] R. Hedayati, S. Janbaz, M. Sadighi, M. Mohammadi-Aghdam, A.A. Zadpoor, J. Mech. Behav. Biomed. Mater. 65 (2016) 831–841, https://doi.org/10.1016/j.jmbbm.2016.10.003.
[88] S. Arabnejad, D. Pasini, Int. J. Mech. Sci. 77 (2013) 249–262, https://doi.org/10.1016/j.ijmecsci.2013.10.003.
[89] H.S. Kim, A Morphological Elastic Model of General Hexagonal Columnar Structures, vol. 43, 2001.
[90] W.E. Warren, A.M. Kraynik, Mech. Mater. 6 (1) (1987) 27–37, https://doi.org/10.1016/0167-6636(87)90020-2.
[91] G. Dong, Y. Tang, Y.F. Zhao, J. Mech. Des. 139 (10) (2017), https://doi.org/10.1115/1.4037305.
[92] M.H. Luxner, J. Stampfl, H.E. Pettermann, J. Mater. Sci. 40 (22) (2005) 5859–5866, https://doi.org/10.1007/s10853-005-5020-y.
[93] H.X. Zhu, S.M. Thorpe, A.H. Windle, Int. J. Solids Struct. 43 (5) (2006) 1061–1078, https://doi.org/10.1016/j.ijsolstr.2005.05.008.
[94] G. Campoli, M.S. Borleffs, S. Amin Yavari, R. Wauthle, H. Weinans, A.A. Zadpoor, Mater. Des. 49 (2013) 957–965, https://doi.org/10.1016/J.MATDES.2013.01.071.
[95] R.M. Latture, R.X. Rodriguez, L.R. Holmes, F.W. Zok, Acta Mater. 149 (2018) 78–87, https://doi.org/10.1016/j.actamat.2017.12.060.
[96] M. Alkhader, M. Vural, Int. J. Eng. Sci. 46 (10) (2008) 1035–1051, https://doi.org/10.1016/j.ijengsci.2008.03.012.
[97] A. Zargarian, M. Esfahanian, J. Kadkhodapour, S. Ziaei-Rad, Mater. Sci. Eng. C 60 (2016) 339–347, https://doi.org/10.1016/j.msec.2015.11.054.
[98] R. Hedayati, H. Hosseini-Toudeshky, M. Sadighi, M. Mohammadi-Aghdam, A. A. Zadpoor, Int. J. Fatigue 84 (2016) 67–79, https://doi.org/10.1016/j.ijfatigue.2015.11.017.
[99] C. Veyhl, I.V. Belova, G.E. Murch, T. Fiedler, Mater. Sci. Eng. A 528 (13–14) (2011) 4550–4555, https://doi.org/10.1016/j.msea.2011.02.031.
[100] L. Xiao, et al., J. Impact Eng. 100 (2017) 75–89, https://doi.org/10.1016/j.ijimpeng.2016.10.006.
[101] N.E. Dowling, Mechanical Behavior of Materials, fourth, Pearson, Harlow, 2013.
[102] L.F. Coffin, J. Mater. 6 (2) (1971) 388–402.
[103] L. Yang, et al., Acta Mater. 181 (2019) 49–66, https://doi.org/10.1016/j.actamat.2019.09.042.
[104] M. Speirs, B. Van Hooreweder, J. Van Humbeeck, J.P. Kruth, J. Mech. Behav. Biomed. Mater. 70 (2016) 53–59, https://doi.org/10.1016/j.jmbbm.2017.01.016.
[105] S. Zhao, et al., Acta Mater. 150 (2018) 1–15, https://doi.org/10.1016/j.actamat.2018.02.060.
[106] C.N. Kelly, et al., Acta Biomater. 94 (2019) 610–626, https://doi.org/10.1016/j.actbio.2019.05.046.
[107] M.W. Wu, J.K. Chen, B.H. Lin, P.H. Chiang, M.K. Tsai, Mater. Sci. Eng. A 790 (2020) 139695, https://doi.org/10.1016/j.msea.2020.139695.
[108] Y.J. Liu, D.C. Ren, S.J. Li, H. Wang, L.C. Zhang, T.B. Sercombe, Addit. Manuf. 32 (2019), https://doi.org/10.1016/j.addma.2020.101060.
[109] S.J. Li, et al., Acta Mater. 60 (3) (2012) 793–802, https://doi.org/10.1016/j.actamat.2011.10.051.
[110] B. Van Hooreweder, Y. Apers, K. Lietaert, J.P. Kruth, Acta Biomater. 47 (2017) 193–202, https://doi.org/10.1016/j.actbio.2016.10.005.
[111] W. Yuan, et al., J. Mater. Sci. Technol. 34 (7) (2018) 1127–1131, https://doi.org/10.1016/j.jmst.2017.12.003.
[112] A. Yánez, M.P. Fiorucci, A. Cuadrado, O. Martel, D. Monopoli, Int. J. Fatigue 138 (2020) 105702, https://doi.org/10.1016/j.ijfatigue.2020.105702.
[113] S. Amin Yavari, et al., J. Mech. Behav. Biomed. Mater. 43 (2015) 91–100, https://doi.org/10.1016/j.jmbbm.2014.12.015.
[114] S.M. Ahmadi, et al., Acta Biomater. 65 (2018) 292–304, https://doi.org/10.1016/j.actbio.2017.11.014.
[115] N.W. Hrabe, P. Heinl, B. Flinn, C. Körner, R.K. Bordia, J. Biomed. Mater. Res. - Part B Appl. Biomater. 99 B (2) (2011) 313–320, https://doi.org/10.1002/jbm.b.31901.
[116] S.M. Ahmadi, et al., Acta Biomater. 83 (2019) 153–166, https://doi.org/10.1016/j.actbio.2018.10.043.
[117] J. de Krijger, C. Rans, B. Van Hooreweder, K. Lietaert, B. Pouran, A.A. Zadpoor, J. Mech. Behav. Biomed. Mater. 70 (2017) 7–16, https://doi.org/10.1016/j.jmbbm.2016.11.022.
[118] Y. Li, et al., Corros. Sci. 156 (2019) 106–116, https://doi.org/10.1016/j.corsci.2019.05.003.
[119] Y.J. Liu, et al., Acta Mater. 126 (2017) 58–66, https://doi.org/10.1016/j.actamat.2016.12.052.
[120] O.H. Basquin, Soc. Test. Mater. Proc. 10 (1910) 625–630.
[121] Z.S. Bagheri, D. Melancon, L. Liu, R.B. Johnston, D. Pasini, J. Mech. Behav. Biomed. Mater. 70 (2017) 17–27, https://doi.org/10.1016/j.jmbbm.2016.04.041.
[122] P. Lipinski, A. Barbas, A.S. Bonnet, J. Mech. Behav. Biomed. Mater. 28 (2013) 274–290, https://doi.org/10.1016/j.jmbbm.2013.08.011.
[123] L. Boniotti, S. Beretta, L. Patriarca, L. Rigoni, S. Foletti, Int. J. Fatigue 128 (2019) 105181, https://doi.org/10.1016/j.ijfatigue.2019.06.041.
[124] L.P. Lefebvre, E. Baril, M.N. Bureau, Sci. Mater. Med. 20 (11) (2009) 2223–2233, https://doi.org/10.1007/s10856-009-3798-x.
[125] S. Özbilen, D. Liebert, T. Beck, M. Bram, Mater. Sci. Eng. C 60 (2016) 446–457, https://doi.org/10.1016/j.msec.2015.11.050.
[126] M. Ashby, et al., Appl. Mech. Rev. 54 (6) (2001) B105–B106, https://doi.org/10.1115/1.1421119.
[127] Y. Sugimura, A. Rabiei, A. Evans, A. Harte, N. Fleck, Mater. Sci. Eng. A 269 (1–2) (1999) 38–48, https://doi.org/10.1016/S0921-5093(99)00147-1.
[128] S. Zhao, S.J. Li, W.T. Hou, Y.L. Hao, R. Yang, R.D.K. Misra, J. Mech. Behav. Biomed. Mater. 59 (2016) 251–264, https://doi.org/10.1016/j.jmbbm.2016.01.034.
[129] M. Dallago, et al., J. Mech. Behav. Biomed. Mater. 78 (2018) 381–394, https://doi.org/10.1016/j.jmbbm.2017.11.044.
[130] K. Lietaert, A. Cutolo, D. Boey, B. Van Hooreweder, Sci. Rep. 8 (1) (2018) 1–9, https://doi.org/10.1038/s41598-018-23414-2.
[131] N. Soro, N. Saintier, J. Merzeau, M. Veidt, M.S. Dargusch, Addit. Manuf. (2020) 101653, https://doi.org/10.1016/j.addma.2020.101653.
[132] K. Refai, C. Brugger, M. Montemurro, N. Saintier, Int. J. Fatigue 138 (2020) 105623, https://doi.org/10.1016/j.ijfatigue.2020.105623.
[133] A. Burr, et al., Int. J. Fatigue 139 (2020) 105769, https://doi.org/10.1016/j.ijfatigue.2020.105769.
[134] W. Ronan, V.S. Deshpande, N.A. Fleck, Int. J. Solids Struct. 102–103 (2016) 200–213, https://doi.org/10.1016/j.ijsolstr.2016.10.004.
[135] J. Schijve (Ed.), Fatigue of Structures and Materials, Springer Netherlands, Dordrecht, 2009.
[136] S. Suresh, Fatigue of Materials, Cambridge University Press, 1998.
[137] Y. Li, et al., Acta Biomater. 106 (2020) 439–449, https://doi.org/10.1016/j.actbio.2020.02.001.
[138] L.P. Borrego, J. De Jesus, J.A.M. Ferreira, J.D. Costa, C. Capela, Procedia Struct. Integr. 17 (2019) 562–567, https://doi.org/10.1016/j.prostr.2019.08.075.
[139] A. Pérez-Sánchez, A. Yánez, A. Cuadrado, O. Martel, N. Nuño, Mater. Des. 155 (2018) 106–115, https://doi.org/10.1016/j.matdes.2018.05.066.
[140] T. Imwinkelried, J. Biomed. Mater. Res. Part B Appl. Biomater. 81A (4) (2007) 964–970, https://doi.org/10.1002/jbm.a.31118.
[141] A. Fatemi, et al., Fatigue Fract. Eng. Mater. Struct. 42 (5) (2019) 991–1009, https://doi.org/10.1111/ffe.13000.
[142] J. Gockel, L. Sheridan, B. Koerper, B. Whip, Int. J. Fatigue 124 (2019) 380–388, https://doi.org/10.1016/j.ijfatigue.2019.03.025.
[143] J.W. Pegues, et al., Int. J. Fatigue 132 (2020) 105358, https://doi.org/10.1016/j.ijfatigue.2019.105358.
[144] S.M.J. Razavi, A. Avanzini, G. Cornacchia, L. Giorleo, F. Berto, Int. J. Fatigue 142 (2021) 105926, https://doi.org/10.1016/j.ijfatigue.2020.105926.
[145] M. Benedetti, V. Fontanari, M. Bandini, F. Zanini, S. Carmignato, J. Chronic Fatigue Syndr. 107 (2018) 96–109, https://doi.org/10.1016/j.ijfatigue.2017.10.021.
[146] M. Benedetti, et al., J. Mech. Behav. Biomed. Mater. 71 (2017) 295–306, https://doi.org/10.1016/j.jmbbm.2017.03.024.
[147] G. Strano, L. Hao, R.M. Everson, K.E. Evans, Proc. IEEE Int. Symp. Signal Proc. Inf. Tech. 213 (4) (2013) 589–597, https://doi.org/10.1016/j.jmatprotec.2012.11.011.
[148] A. Du Plessis, et al., Materials 11 (9) (2018) 1663, https://doi.org/10.3390/MA11091663.
[149] D. Wang, Y. Yang, Z. Yi, X. Su, Int. J. Adv. Manuf. Technol 65 (9–12) (2013) 1471–1484, https://doi.org/10.1007/s00170-012-4271-4.
[150] F. Calignano, Mater. Des. 64 (2014) 203–213, https://doi.org/10.1016/j.matdes.2014.07.043.
[151] R. Wauthle, et al., Addit. Manuf. 5 (2015) 77–84, https://doi.org/10.1016/J.ADDMA.2014.12.008.
[152] E.E. Covarrubias, M. Eshraghi, JOM 70 (3) (2018) 336–342, https://doi.org/10.1007/s11837-017-2706-y.
[153] Y. Murakami, C. Klinger, M. Madia, U. Zerbst, D. Bettge, Eng. Fail. Anal. 97 (2019) 759–776, https://doi.org/10.1016/j.engfailanal.2019.01.034.
[154] J. Pegues, M. Roach, R. Scott Williamson, N. Shamsaei, Int. J. Fatigue 116 (2018) 543–552, https://doi.org/10.1016/j.ijfatigue.2018.07.013.
[155] K. Solberg, F. Berto, Int. J. Fatigue 134 (2020) 105428, https://doi.org/10.1016/j.ijfatigue.2019.105428.
[156] M. Benedetti, C. Santus, Int. J. Fatigue 121 (2019) 281–292, https://doi.org/10.1016/j.ijfatigue.2018.12.020.
[157] G. Nicoletto, R. Konečná, M. Frkáň, E. Riva, J. Chronic Fatigue Syndr. 116 (2018) 140–148, https://doi.org/10.1016/j.ijfatigue.2018.06.011.
[158] A. du Plessis, S. Beretta, Addit. Manuf 35 (2020) 101424, https://doi.org/10.1016/j.addma.2020.101424.
[159] ISO - ISO 4287, Geometrical Product Specifications (GPS) — Surface Texture: Profile Method — Terms, Definitions and Surface Texture Parameters, 1997.
[160] A. Townsend, N. Senin, L. Blunt, R.K. Leach, J.S. Taylor, Precis. Eng. 46 (2016) 34–47, https://doi.org/10.1016/J.PRECISIONENG.2016.06.001.
[161] A. du Plessis, I. Yadroitsev, I. Yadroitsava, S.G. le Roux, 3D Print. Addit. Manuf. 5 (3) (2018) 227–247, https://doi.org/10.1089/3dp.2018.0060.
[162] S. Van Bael, G. Kerckhofs, M. Moesen, G. Pyka, J. Schrooten, J.P. Kruth, Mater. Sci. Eng. A 528 (24) (2011) 7423–7431, https://doi.org/10.1016/J.MSEA.2011.06.045.
[163] G. Pyka, G. Kerckhofs, I. Papantoniou, M. Speirs, J. Schrooten, M. Wevers, Materials (Basel). 6 (12) (2013) 4737–4757, https://doi.org/10.3390/ma6104737.
[164] G. Kerckhofs, G. Pyka, M. Moesen, S. Van Bael, J. Schrooten, M. Wevers, Adv. Eng. Mater. 15 (3) (2013) 153–158, https://doi.org/10.1002/adem.201200156.
[165] S.L. Sing, F.E. Wiria, W.Y. Yeong, Robot. Comput. Manuf. 49 (2018) 170–180, https://doi.org/10.1016/j.rcim.2017.06.006.
[166] L. Mullen, R.C. Stamp, P. Fox, E. Jones, C. Ngo, C.J. Sutcliffe, J. Biomed. Mater. Res. Part B Appl. Biomater. 92B (1) (2010) 178–188, https://doi.org/10.1002/jbm.b.31504.

[167] J. Kessler, N. Balc, A. Gebhardt, K. Abbas, MATEC Web Conf., vol. 137, 2017, p. 02005, https://doi.org/10.1051/matecconf/201713702005.
[168] J. Kranz, D. Herzog, C. Emmelmann, J. Laser Appl. 27 (S1) (2015) S14001, https://doi.org/10.2351/1.4885235.
[169] Z. Zhu, N. Anwer, L. Mathieu, Procedia Cirp 60 (2017) 211–216, https://doi.org/10.1016/j.procir.2017.01.023.
[170] C. Chen, T.J. Lu, N.A. Fleck, J. Mech. Phys. Solids 47 (11) (1999) 2235–2272, https://doi.org/10.1016/S0022-5096(99)00030-7.
[171] M. Dallago, S. Raghavendra, V. Luchin, G. Zappini, D. Pasini, M. Benedetti, Mater. Today Proc. 7 (2019) 353–361, https://doi.org/10.1016/j.matpr.2018.11.096.
[172] Y. Amani, S. Dancette, P. Delroisse, A. Simar, E. Maire, Acta Mater. 159 (2018) 395–407, https://doi.org/10.1016/j.actamat.2018.08.030.
[173] M. Dallago, F. Zanini, S. Carmignato, D. Pasini, M. Benedetti, Procedia Struct. Integr. 13 (2018) 161–167, https://doi.org/10.1016/j.prostr.2018.12.027.
[174] A. Zargarian, M. Esfahanian, J. Kadkhodapour, S. Ziaei-Rad, D. Zamani, Theor. Appl. Fract. Mech 100 (2019) 225–232, https://doi.org/10.1016/j.tafmec.2019.01.012.
[175] B. Lozanovski, et al., Mater. Des. 171 (2019) 107671, https://doi.org/10.1016/j.matdes.2019.107671.
[176] B. Lozanovski, et al., Addit. Manuf. 36 (2020) 101593, https://doi.org/10.1016/j.addma.2020.101593.
[177] A. du Plessis, Addit. Manuf. 30 (2019) 100871, https://doi.org/10.1016/j.addma.2019.100871.
[178] E. Malekipour, H. El-Mounayri, Int. J. Adv. Manuf. Technol 95 (1–4) (2018) 527–550, https://doi.org/10.1007/s00170-017-1172-6.
[179] N. Sanaei, A. Fatemi, N. Phan, Mater. Des. 182 (2019) 108091, https://doi.org/10.1016/j.matdes.2019.108091.
[180] A. du Plessis, S.M.J. Razavi, F. Berto, Mater. Des. 194 (2020) 108899, https://doi.org/10.1016/j.matdes.2020.108899.
[181] K. Karami, et al., Addit. Manuf. 36 (2020) 101433, https://doi.org/10.1016/j.addma.2020.101433.
[182] U. Zerbst, M. Madia, C. Klinger, D. Bettge, Y. Murakami, Eng. Fail. Anal. 97 (2019) 777–792, https://doi.org/10.1016/j.engfailanal.2019.01.055.
[183] A. du Plessis, I. Yadroitsava, I. Yadroitsev, Mater. Des. 187 (2020), https://doi.org/10.1016/j.matdes.2019.108385.
[184] L. Huynh, J. Rotella, M.D. Sangid, Mater. Des. 105 (2016) 278–289, https://doi.org/10.1016/j.matdes.2016.05.032.
[185] J.L. Bartlett, X. Li, Addit. Manuf. 27 (2019) 131–149, https://doi.org/10.1016/j.addma.2019.02.020.
[186] I. Yadroitsev, P. Krakhmalev, I. Yadroitsava, A. Du Plessis, JOM 70 (3) (2018) 372–377, https://doi.org/10.1007/s11837-017-2655-5.
[187] T. Niendorf, F. Brenne, M. Schaper, Mater. Trans. B Process Metall. Mater. Process. Sci. 45 (4) (2014) 1181–1185, https://doi.org/10.1007/s11663-014-0086-z.
[188] M.W. Wu, J.K. Chen, B.H. Lin, P.H. Chiang, Mater. Des. 134 (2017) 163–170, https://doi.org/10.1016/j.matdes.2017.08.048.
[189] Y. Tian, D. Tomus, P. Rometsch, X. Wu, Addit. Manuf. 13 (2017) 103–112, https://doi.org/10.1016/J.ADDMA.2016.10.010.
[190] A. du Plessis, I. Yadroitsava, I. Yadroitsev, S. le Roux, D. Blaine, Virtual Phys. Prototyp. (2018) 1–16, https://doi.org/10.1080/17452759.2018.1491713.
[191] M. Leary, Design for Additive Manufacturing, 1st ed., Elsevier, 2019.
[192] P. Köhnen, C. Haase, J. Bültmann, S. Ziegler, J.H. Schleifenbaum, W. Bleck, Mater. Des. 145 (2018) 205–217, https://doi.org/10.1016/j.matdes.2018.02.062.
[193] T. Persenot, A. Burr, G. Martin, J.Y. Buffiere, R. Dendievel, E. Maire, J. Chronic Fatigue Syndr. 118 (2019) 65–76, https://doi.org/10.1016/j.ijfatigue.2018.08.006.
[194] D. Ashouri, et al., Int. J. Fatigue 134 (2020) 105503, https://doi.org/10.1016/j.ijfatigue.2020.105503.
[195] W.D. Pilkey, D.F. Pilkey, B. Zhuming, Peterson's Stress Concentration Factors, John Wiley & Sons, Hoboken NJ, 2020.
[196] M. Dallago, S. Raghavendra, V. Fontanari, M. Benedetti, Mater. Des. Process. Commun. 2 (2) (2020) 1–8, https://doi.org/10.1002/mdp2.98.
[197] M. Dallago, M. Benedetti, V. Luchin, V. Fontanari, Int. J. Mech. Sci 122 (2017) 63–78, https://doi.org/10.1016/j.ijmecsci.2016.12.026.
[198] K. Refai, M. Montemurro, C. Brugger, N. Saintier, Mech. Adv. Mater. Struct. 0 (0) (2019) 1–14, https://doi.org/10.1080/15376494.2018.1536816.
[199] G. Savio, A. Curtarello, S. Rosso, R. Meneghello, G. Concheri, Int. J. Interact. Des. Manuf. 13 (1) (2019) 263–276, https://doi.org/10.1007/s12008-019-00543-0.
[200] E. Masoumi Khalil Abad, S. Arabnejad Khanoki, D. Pasini, Int. J. Fatigue 47 (2013) 126–136, https://doi.org/10.1016/j.ijfatigue.2012.08.003.
[201] G. Savio, R. Meneghello, G. Concheri, Rapid Prototyp. J. 24 (2) (2018) 351–360, https://doi.org/10.1108/RPJ-07-2016-0122.
[202] G. Savio, S. Rosso, A. Curtarello, R. Meneghello, G. Concheri, Addit. Manuf. 25 (2019) 50–58, https://doi.org/10.1016/j.addma.2018.10.047.
[203] E. Catmull, J. Clark, Comput. Des. 10 (6) (1978) 350–355, https://doi.org/10.1016/0010-4485(78)90110-0.
[204] D. Mahmoud, M. Elbestawi, J. Manuf. Mater. Process 1 (2) (2017) 13, https://doi.org/10.3390/jmmp1020013.
[205] I. Ferguson, M. Frecker, T.W. Simpson, C.J. Dickman. Proc. ASME 2016 Int. Des. Eng. Tech. Conf. Comput. Inf. Eng. Conf., 2016, pp. 1–11.
[206] A.M. Vilardell, et al., Mater. Sci. Eng. A 766 (2019) 138330, https://doi.org/10.1016/j.msea.2019.138330.
[207] V.N. Hoang, P. Tran, V.T. Vu, H. Nguyen-Xuan, Compos. Struct. 252 (2020) 112718, https://doi.org/10.1016/j.compstruct.2020.112718.
[208] X. Wang, et al., Biomaterials 83 (2016) 127–141, https://doi.org/10.1016/j.biomaterials.2016.01.012.
[209] L.E. Murr, et al., J. Mech. Behav. Biomed. Mater. 2 (1) (2009) 20–32, https://doi.org/10.1016/j.jmbbm.2008.05.004.
[210] P. Bajaj, A. Hariharan, A. Kini, P. Kürnsteiner, D. Raabe, E.A. Jägle, Mater. Sci. Eng. A 772 (2020) 138633, https://doi.org/10.1016/j.msea.2019.138633.
[211] S. Cheruvathur, E.A. Lass, C.E. Campbell, JOM 68 (3) (2016) 930–942, https://doi.org/10.1007/s11837-015-1754-4.
[212] L. Facchini, E. Magalini, P. Robotti, A. Molinari, S. Höges, K. Wissenbach, Rapid Prototyp. J. 16 (6) (2010) 450–459, https://doi.org/10.1108/13552541011083371.
[213] L. Zhou, A. Mehta, E. Schulz, B. McWilliams, K. Cho, Y. Sohn, Mater. Charact. 143 (2018) 5–17, https://doi.org/10.1016/j.matchar.2018.04.022.
[214] J. Mutua, S. Nakata, T. Onda, Z.-C. Chen, Mater. Des. 139 (2018) 486–497, https://doi.org/10.1016/j.matdes.2017.11.042.
[215] S. Leuders, et al., Int. J. Fatigue 48 (2013) 300–307, https://doi.org/10.1016/j.ijfatigue.2012.11.011.
[216] S. Leuders, T. Lieneke, S. Lammers, T. Tröster, T. Niendorf, J. Mater. Res. 29 (17) (2014) 1911–1919, https://doi.org/10.1557/jmr.2014.157.
[217] M. Ahlfors, F. Bahbou, A. Eklund, Mater. Res. Proc. 10 (2019) 1–10, https://doi.org/10.21741/9781644900031-1.
[218] H.V. Atkinson, S. Davies, Mater. Trans. A Phys. Metall. Mater. Sci. 31 (12) (2000) 2981–3000, https://doi.org/10.1007/s11661-000-0078-2.
[219] A. du Plessis, E. Macdonald, Addit. Manuf. 34 (2020) 101191, https://doi.org/10.1016/j.addma.2020.101191.
[220] H. Masuo, et al., Procedia Struct. Integr. 7 (2017) 19–26, https://doi.org/10.1016/j.prostr.2017.11.055.
[221] N.E. Uzan, S. Ramati, R. Shneck, N. Frage, O. Yeheskel, Addit. Manuf. 21 (2018) 458–464, https://doi.org/10.1016/j.addma.2018.03.030.
[222] L. Hackel, J.R. Rankin, A. Rubenchik, W.E. King, M. Matthews, Addit. Manuf. 24 (2018) 67–75, https://doi.org/10.1016/j.addma.2018.09.013.
[223] T. Persenot, et al., Materialia 9 (2020) 100589, https://doi.org/10.1016/j.mtla.2020.100589.
[224] S. Han, F. Salvatore, J. Rech, J. Bajolet, Precis. Eng. 64 (2020) 20–33, https://doi.org/10.1016/j.precisioneng.2020.03.006.
[225] G. Lütjering, Mater. Sci. Eng. A 243 (1–2) (1998) 32–45, https://doi.org/10.1016/S0921-5093(97)00778-8.
[226] G. Barucca, et al., Mater. Sci. Eng. C 48 (2015) 263–269, https://doi.org/10.1016/j.msec.2014.12.009.
[227] M.J. Mahtabi, N. Shamsaei, M.R. Mitchell, J. Mech. Behav. Biomed. Mater. 50 (2015) 228–254, https://doi.org/10.1016/j.jmbbm.2015.06.010.
[228] H. Cao, M.H. Wu, F. Zhou, R.M. McMeeking, R.O. Ritchie, J. Mech. Phys. Solids 143 (2020) 104057, https://doi.org/10.1016/j.jmps.2020.104057.
[229] Z. Li, K.G. Pradeep, Y. Deng, D. Raabe, C.C. Tasan, Nature 534 (7606) (2016) 227–230, https://doi.org/10.1038/nature17981.
[230] Z. Zhang, et al., Nat. Commun. 6 (1) (2015) 10143, https://doi.org/10.1038/ncomms10143.
[231] V. Ocelík, N. Janssen, S.N. Smith, J.T.M. De Hosson, JOM 68 (7) (2016) 1810–1818, https://doi.org/10.1007/s11837-016-1888-z.
[232] P. Sarswat, T. Smith, S. Sarkar, A. Murali, M. Free, Materials Basel (Basel) 13 (13) (2020) 3001, https://doi.org/10.3390/ma13133001.
[233] S. Luo, C. Zhao, Y. Su, Q. Liu, Z. Wang, Addit. Manuf 31 (2020) 100925, https://doi.org/10.1016/j.addma.2019.100925.
[234] H.M.A. Kolken, A.A. Zadpoor, RSC Adv. 7 (9) (2017) 5111–5129, https://doi.org/10.1039/C6RA27333E.
[235] X. Ren, R. Das, P. Tran, T.D. Ngo, Y.M. Xie, Smart Mater. Struct. 27 (2) (2018) 023001, https://doi.org/10.1088/1361-665X/aaa61c.
[236] L. Francesconi, A. Baldi, G. Dominguez, M. Taylor, Exp. Mech. 60 (1) (2020) 93–107, https://doi.org/10.1007/s11340-019-00539-7.
[237] M.R. Karamooz Ravari, M. Kadkhodaei, M. Badrossamay, R. Rezaei, J. Mech. Sci. 88 (2014) 154–161, https://doi.org/10.1016/j.ijmecsci.2014.08.009.
[238] McCullough, Fleck, Fract. Eng. Mater. Struct. 23 (3) (2000) 199–208, https://doi.org/10.1046/j.1460-2695.2000.00261.x.
[239] J. Lemaitre, A. Plumtree, J. Eng. Mater. Technol. 101 (3) (1979) 284–292, https://doi.org/10.1115/1.3443689.
[240] E. Santecchia, et al., Adv. Mater. Sci. Eng. Int. J. 2016 (2016) 1–26, https://doi.org/10.1155/2016/9573524.
[241] P. Lohmuller, J. Favre, B. Piotrowski, S. Kenzari, P. Laheurte, Materials (Basel). 11 (7) (2018) 1–12, https://doi.org/10.3390/ma11071146.
[242] S. Rosso, R. Meneghello, G. Concheri, G. Savio, Scale and Shape Effects on the Fatigue Behaviour of Additively Manufactured SS316L Structures: A Preliminary Study, 2020, pp. 879–890.
[243] S. Arabnejad Khanoki, D. Pasini, J. Mech. Behav. Biomed. Mater. 22 (2013) 65–83, https://doi.org/10.1016/j.jmbbm.2013.03.002.
[244] C. Peng, P. Tran, H. Nguyen-Xuan, A.J.M. Ferreira, Compos. Struct. 235 (2020) 111821, https://doi.org/10.1016/j.compstruct.2019.111821.
[245] M.W. Brown, K.J. Miller, Inst. Mech. Eng. 187 (1) (1973) 745–755, https://doi.org/10.1243/PIME_PROC_1973_187_069_02.
[246] M. Jamshidinia, L. Wang, W. Tong, R. Ajlouni, R. Kovacevic, Proc. IEEE Int. Symp. Signal Proc. Inf. Tech. 226 (2015) 255–263, https://doi.org/10.1016/j.jmatprotec.2015.07.013.
[247] J.S. Huang, J.Y. Lin, Acta Mater. 44 (1) (1996) 289–296, https://doi.org/10.1016/1359-6454(95)00170-4.
[248] J.-S. Huang, S.-Y. Liu, Mater. Sci. Eng. A 308 (1–2) (2001) 45–52, https://doi.org/10.1016/S0921-5093(00)01996-1.

[249] J. Huang, Int. J. Fatigue 23 (3) (2001) 233–240, https://doi.org/10.1016/S0142-1123(00)00096-7.
[250] A.E. Simone, L.J. Gibson, Acta Mater. 46 (6) (1998) 2139–2150, https://doi.org/10.1016/S1359-6454(97)00421-7.
[251] M.A. Miner, J. Appl. Mech. 12 (1945) A159–A164.
[252] A. Palmgren, Ball Bear. J. 034 (1937), pp. 34–34.
[253] J. Schijve. Minutes 4th Conference of the Int Committee on Aero Fatigue (ICAF), 1956 p. Paper 2.
[254] K. Heyer, Multi-step Tests on Structural Elements, 1943.
[255] C.R. Smith, Proc. Soc. Exp. Stress Anal. 16 (1) (1958) 9.
[256] R. Hedayati, H. Hosseini-Toudeshky, M. Sadighi, M. Mohammadi-Aghdam, A. A. Zadpoor, J. Chronic Fatigue Syndr. 113 (2018) 416–427, https://doi.org/10.1016/j.ijfatigue.2018.05.006.
[257] S. Demiray, W. Becker, J. Hohe, Mater. Sci. Eng. A 504 (1–2) (2009) 141–149, https://doi.org/10.1016/j.msea.2008.10.036.
[258] G. Sines, J.L. Waisman, T.J. Dolan, Metal Fatigue, McGraw-Hill University, New York, 1959.
[259] M.H. El Haddad, T.H. Topper, K.N. Smith, Eng. Fract. Mech. 11 (3) (1979) 573–584, https://doi.org/10.1016/0013-7944(79)90081-X.
[260] S. Romano, A. Brückner-Foit, A. Brandão, J. Gumpinger, T. Ghidini, S. Beretta, Eng. Fract. Mech. 187 (2018) 165–189, https://doi.org/10.1016/j.engfracmech.2017.11.002.
[261] E. Arzt, Acta Mater. 46 (16) (1998) 5611–5626, https://doi.org/10.1016/S1359-6454(98)00231-6.
[262] G.P. Zhang, C.A. Volkert, R. Schwaiger, P. Wellner, E. Arzt, O. Kraft, Acta Mater. 54 (11) (2006) 3127–3139, https://doi.org/10.1016/j.actamat.2006.03.013.
[263] Q. Yu, et al., Nature 463 (7279) (2010) 335–338, https://doi.org/10.1038/nature08692.
[264] J.R. Greer, W.C. Oliver, W.D. Nix, Acta Mater. 53 (6) (2005) 1821–1830, https://doi.org/10.1016/j.actamat.2004.12.031.
[265] M.D. Uchic, Science (80-.) 305 (5686) (2004) 986–989, https://doi.org/10.1126/science.1098993.
[266] C. Keller, E. Hug, X. Feaugas, J. Plast. 27 (4) (2011) 635–654, https://doi.org/10.1016/j.ijplas.2010.08.002.
[267] E.O. Hall, Phys. Soc. Sect. B 64 (9) (1951) 747–753, https://doi.org/10.1088/0370-1301/64/9/303.
[268] N.J. Petch, J. Iron Steel Inst. 174 (1953) 25–28.
[269] H.Y. Wan, G.F. Chen, C.P. Li, X.B. Qi, G.P. Zhang, J. Mater. Sci. Technol. 35 (6) (2019) 1137–1146, https://doi.org/10.1016/j.jmst.2018.12.011.
[270] Y.H. Kok, X.P. Tan, N.H. Loh, S.B. Tor, C.K. Chua, Virtual Phys. Prototyp. 11 (3) (2016) 183–191, https://doi.org/10.1080/17452759.2016.1210483.
[271] X. Tan, et al., Sci. Rep. 6 (1) (2016) 26039, https://doi.org/10.1038/srep26039.
[272] P. Wang, X. Tan, M.L.S. Nai, S.B. Tor, J. Wei, Mater. Des. 95 (2016) 287–295, https://doi.org/10.1016/j.matdes.2016.01.093.
[273] X. Tan, et al., J. Alloys. Compd. 646 (2015) 303–309, https://doi.org/10.1016/j.jallcom.2015.05.178.
[274] Z. Dong, X. Zhang, W. Shi, H. Zhou, H. Lei, J. Liang, Materials Basel (Basel) 11 (12) (2018) 2463, https://doi.org/10.3390/ma11122463.
[275] S.M.J. Razavi, B. Van Hooreweder, F. Berto, Addit. Manuf. 36 (2020) 101426, https://doi.org/10.1016/j.addma.2020.101426.
[276] D. McDowell, K. Gall, M. Horstemeyer, J. Fan, Eng. Fract. Mech. 70 (1) (2003) 49–80, https://doi.org/10.1016/S0013-7944(02)00021-8.
[277] Y. Xue, D.L. McDowell, M.F. Horstemeyer, M.H. Dale, J.B. Jordon, Eng. Fract. Mech. 74 (17) (2007) 2810–2823, https://doi.org/10.1016/j.engfracmech.2006.12.031.
[278] Y. Yamashita, T. Murakami, R. Mihara, M. Okada, Y. Murakami, Int. J. Fatigue 117 (2018) 485–495, https://doi.org/10.1016/j.ijfatigue.2018.08.002.
[279] S. Romano, A. Brandão, J. Gumpinger, M. Gschweitl, S. Beretta, Mater. Des. 131 (2017) 32–48, https://doi.org/10.1016/j.matdes.2017.05.091.
[280] M.W. Libbrecht, W.S. Noble, Nat. Rev. Genet. 16 (6) (2015) 321–332, https://doi.org/10.1038/nrg3920.
[281] M. Aminzadeh, T.R. Kurfess, J. Intell. Manuf. 30 (6) (2019) 2505–2523, https://doi.org/10.1007/s10845-018-1412-0.
[282] O. Kwon, et al., J. Intell. Manuf. 31 (2) (2020) 375–386, https://doi.org/10.1007/s10845-018-1451-6.
[283] B. Panda, K. Shankhwar, A. Garg, M.M. Savalani, J. Intell. Manuf. 30 (2) (2019) 809–820, https://doi.org/10.1007/s10845-016-1282-2.
[284] Y. Zhang, A. Bernard, R. Harik, K.P. Karunakaran, J. Intell. Manuf. 28 (6) (2017) 1393–1407, https://doi.org/10.1007/s10845-015-1057-1.
[285] W. Mycroft, et al., J. Intell. Manuf. 31 (7) (2020) 1769–1781, https://doi.org/10.1007/s10845-020-01541-w.
[286] G.X. Gu, C.-T. Chen, D.J. Richmond, M.J. Buehler, Mater. Horizons 5 (5) (2018) 939–945, https://doi.org/10.1039/C8MH00653A.
[287] T. Kirchdoerfer, M. Ortiz, Comput. Methods Appl. Mech. Eng. 304 (2016) 81–101, https://doi.org/10.1016/j.cma.2016.02.001.
[288] S. Conti, S. Müller, M. Ortiz, Arch. Ration. Mech. Anal. 237 (1) (2020) 1–33, https://doi.org/10.1007/s00205-020-01490-x.
[289] T. Kirchdoerfer, M. Ortiz, Int. J. Numer. Methods Eng. 113 (11) (2018) 1697–1710, https://doi.org/10.1002/nme.5716.
[290] T. Kirchdoerfer, M. Ortiz, Comput. Methods Appl. Mech. Eng. 326 (2017) 622–641, https://doi.org/10.1016/j.cma.2017.07.039.
[291] L. Stainier, A. Leygue, M. Ortiz, Comput. Mech. 64 (2) (2019) 381–393, https://doi.org/10.1007/s00466-019-01731-1.
[292] S.M.J. Razavi, P. Ferro, F. Berto, J. Torgersen, Theor. Appl. Fract. Mech. 97 (2018) 376–384, https://doi.org/10.1016/j.tafmec.2017.06.021.
[293] S.M.J. Razavi, P. Ferro, F. Berto, Metals 7 (8) (2017), https://doi.org/10.3390/met7080291 art. 291.
[294] S.M.J. Razavi, G. Bordonaro, P. Ferro, J. Torgersen, F. Berto, Materials 11 (2) (2018), https://doi.org/10.3390/ma11020284 art. 284.
[295] S.M.J. Razavi, G. Bordonaro, P. Ferro, J. Torgersen, F. Berto, Proc. Inst. Mech. Eng. Part C J. Mech. Eng. Sci. (2018), https://doi.org/10.1177/0954406218813384.
[296] T. Borsato, F. Berto, P. Ferro, C. Carollo, Fatigue Fract. Eng. Mater. Struct. 41 (11) (2018) 2231–2238, https://doi.org/10.1111/ffe.12810.
[297] T. Borsato, P. Ferro, F. Berto, Fatigue Fract. Eng. Mater. Struct. 41 (8) (2018) 1746–1757, https://doi.org/10.1111/ffe.12815.
[298] P. Ferro, R. Meneghello, S.M.J. Razavi, F. Berto, G. Savio, Phys. Mesomech. 23 (3) (2020) 256–262, https://doi.org/10.1134/S1029959920030108.
[299] P. Ferro, A. Fabrizi, F. Berto, G. Savio, R. Meneghello, S. Rosso, Theor. Applied Fract. Mech. 108 (2020), https://doi.org/10.1016/j.tafmec.2020.102611 art. 102611.
[300] F. Berto, P. Lazzarin, A. Kotousov, Mech. Materials 43 (6) (2011) 332–341, https://doi.org/10.1016/j.mechmat.2011.03.004.
[301] F. Berto, P. Lazzarin, Int. J. Fatigue 46 (2011) 16–26, https://doi.org/10.1016/j.ijfatigue.2011.12.004.
[302] F. Berto, P. Lazzarin, C.H. Wang, Int. J. Fracture 127 (3) (2004) 265–282, https://doi.org/10.1023/B:FRAC.0000036846.23180.4d.
[303] L.P. Pook, F. Berto, Eng. Fract. Mech. 174 (2017) 2–9, https://doi.org/10.1016/j.engfracmech.2016.10.001.
[304] W. Wu, W. Hu, G. Qian, H. Liao, X. Xu, F. Berto, Mater. Design 180 (2019), 107950, https://doi.org/10.1016/j.matdes.2019.107950.
[305] F. Berto, P. Lazzarin, Mater. Sci. Eng. R 75 (1) (2014) 1–48, https://doi.org/10.1016/j.mser.2013.11.001.
[306] F. Berto, E. Barati, Mater. Design 32 (2) (2011) 822–830, https://doi.org/10.1016/j.matdes.2010.07.017.
[307] A.R. Torabi, A. Campagnolo, F. Berto, Mater. Des. 69 (2015) 22–29, https://doi.org/10.1016/j.matdes.2014.12.037.
[308] F. Berto, P. Gallo, P. Lazzarin, Mater. Design 63 (1) (2014) 609–619, https://doi.org/10.1016/j.matdes.2014.06.048.
[309] M.R. Ayatollahi, M. Rashidi Moghaddam, F. Berto, Theor. Appl. Fract. Mech. 79 (2015) 70–76, https://doi.org/10.1016/j.tafmec.2015.09.004.
[310] S.-P. Zhu, Z.-Y. Yu, J. Correia, A. De Jesus, F. Berto, Int. J. Fatigue 112 (2018) 279–288, https://doi.org/10.1016/j.ijfatigue.2018.03.028.
[311] J. Correia, N. Apetre, A. Arcari, A. De Jesus, M. Muñiz-Calvente, R. Calçada, F. Berto, A. Fernández-Canteli, Int. J. Fatigue 100 (2017) 187–194, https://doi.org/10.1016/j.ijfatigue.2017.03.031.
[312] M. Benedetti, C. Santus, F. Berto, Int. J. Fatigue 126 (2019) 306–318, https://doi.org/10.1016/j.ijfatigue.2019.04.040.
[313] M. Benedetti, F. Berto, L. Le Bone, C. Santus, Int. J. Fatigue 133 (2020), https://doi.org/10.1016/j.ijfatigue.2019.105397 art. 105397.
[314] M. Benedetti, F. Berto, M. Marini, S. Raghavendra, V. Fontanari, Int. J. Fatigue 139 (2020), https://doi.org/10.1016/j.ijfatigue.2020.105728 art. 105728.
[315] D. Liao, S.-P. Zhu, J. Correia, A. De Jesus, F. Berto, Fatigue Fract. Eng. Mater. Struct. 43 (4) (2020) 637–659, https://doi.org/10.1111/ffe.13195.
[316] F. Berto, P. Lazzarin, Theor. Appl. Fract. Mech. 52 (2009) 183–194, https://doi.org/10.1016/j.tafmec.2009.10.001.

Matteo Benedetti is an Associate Professor at the University of Trento, Italy. He has a 20 year experience in the field of mechanics of metallic materials, fatigue and fracture, finite element modelling, surface treatments and residual stresses. He was a visiting researcher at the Technical University Hamburg-Harburg, where he studied the fatigue and fracture mechanisms of titanium alloys. Since 2015 he has been investigating the fatigue-related issues of additively manufactured materials with special focus on lattice cellular biomaterials.

Prof. Anton Du Plessis is an Associate Professor at Stellenbosch University, South Africa and is also affiliated with Nelson Mandela University, South Africa. He is an experienced scholar in the field of additive manufacturing, with specific interests in quality control and process optimization, X-ray tomography and biomimicry applied to additive manufacturing. His interests and expertise range across a wide range of disciplines in the field, and he is an associate editor of the leading journal in the field, Elsevier's Additive Manufacturing journal.

Robert O. Ritchie is the H.T. & Jessie Chua Distinguished Professor of Engineering in the Materials Science & Engineering Department at the University of California Berkeley, and Faculty Senior Scientist at the Lawrence Berkeley National Laboratory. He holds M.A., pH.D. and Sc.D. degrees in physics/materials science from Cambridge University. He is known for his research on the fatigue and fracture mechanics of materials, with current interests on biological and bioinspired materials and fracture in multiple principal-element alloys. He is a Fellow of the U.S. National Academy of Engineering and the U. K. Royal Academy of Engineering, and a Foreign Member of the Royal Society, the Russian Academy of Sciences and the Royal Swedish Academy of Engineering Sciences.

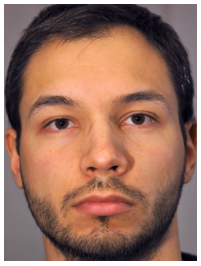

Michele Dallago obtained his PhD in materials engineering from the University of Trento, where he is currently a post-doc researcher, with a thesis on the numerical/experimental investigation of the static and fatigue properties of Ti-6Al-4 V lattices produced via Laser-Powder Bed Fusion. His current work includes the morphological characterization of AM Ti-6Al-4 V cellular materials and the study of the effect of morphological defects on their fatigue and fracture behaviour.

Seyed Mohammad Javad Razavi is an Associate Professor at Norwegian University of Science and Technology (NTNU), Norway. He is currently assistant editor of Material Design & Processing Communications, and has served as editorial board member of Heliyon, and reviewer in more than 65 peer reviewed journals. Since 2011 he has been actively doing experimental and numerical research in the field of fatigue and fracture mechanics of materials and mechanical components. His research interests are on the link between the design, fabrication process and mechanical behaviour with specific interests in the novel fabrication techniques such as additive manufacturing.

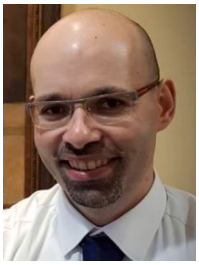

Filippo Berto is international chair in fracture mechanics, fatigue, and structural integrity at the Norwegian University of Science and Technology of Trondheim, Norway, since beginning of 2016. He was professor of machine design at the University of Padua, Italy, between 2006 and 2015. He is chairman of the technical committee ESIS TC15 on Structural Integrity of additive manufactured components of European Structural Integrity Society. Filippo Berto received several awards and distinctions, such as Award of Merit (2018) and Wohler medal (2020) from the European Structural Integrity Society. He has received the Stephen Timoshenko Fellow (2018) given by University of Stanford (USA). Filippo Berto is part of the Top Italian Scientists Engineering (Italy). He is editor-in-chief or Editor of several scientific journals, such as, Fatigue & Fracture of Engineering Materials & Structures, Material Design & Processing Communications and Materials. In addition, he belongs to the editorial board of several leading scientific journals in the area of fatigue, fracture and structural integrity, such as, Materials & Design, International Journal of Fatigue, Safety Science, Theoretical and Applied Fracture Mechanics, Materials Science and Engineering: A, Advanced Engineering Materials, Polymer Testing, Strength of Materials, among others. Filippo Berto is also voting member of ASTM F42 on Additive Manufacturing Technologies and ASTM E08 on Metal Fatigue and Fracture. As technical Chair of TC15 is also the founder of the series of European conferences on additive manufacturing ESIAM. In 2020 he has been one of the founders of TC18 of ESIS dedicated to the structural integrity of welded structures. Filippo Berto has a major role in the Italian Group of Fracture being vice-president since 2019 and co-editor in chief of the associated journal.